COLLECTIVE PHENOMENA IN STRONGLY COUPLED DUSTY PLASMA MEDIUM

By

Vikram Singh Dharodi

PHYS06201004004

Institute for Plasma Research, Gandhinagar

A thesis submitted to the
Board of Studies in Physical Sciences

In partial fulfillment of the requirements

For the Degree of

DOCTOR OF PHILOSOPHY

of

HOMI BHABHA NATIONAL INSTITUTE

June 2016

Homi Bhabha National Institute

Recommendations of the Viva Voce Committee

As members of the Viva Voce Committee, we certify that we have read the dissertation prepared by **Vikram Singh Dharodi** entitled "Collective phenomena in strongly coupled dusty plasma medium" and recommend that it may be accepted as fulfilling the thesis requirement for the award of Degree of Doctor of Philosophy.

PKaw

______________________________ **Date : 24/08/2016**

Chairman : Prof. Predhiman K. Kaw

Amita Das

______________________________ **Date : 24/08/2016**

Guide/Convener : Prof. Amita Das

Vinod Krishan

______________________________ **Date : 24/08/2016**

Examiner : Prof. Vinod Krishan

ABhjit

______________________________ **Date : 24/08/2016**

Member : Prof. Abhijit Sen

S.V. Kulkarni

______________________________ **Date : 24/08/2016**

Member : Dr. Sanjay V. Kulkarni

Final approval and acceptance of this thesis is contingent upon the candidate's submission of the final copies of the thesis to HBNI.

I hereby certify that I have read this thesis prepared under my direction and recommend that it may be accepted as fulfilling the thesis requirement.

Date : 24/08/2016

Place : Gandhinagar

Amita Das

Guide : Prof. Amita Das

STATEMENT BY AUTHOR

This dissertation has been submitted in partial fulfillment of requirements for an advanced degree at Homi Bhabha National Institute (HBNI) and is deposited in the Library to be made available to borrowers under rules of the HBNI.

Brief quotations from this dissertation are allowable without special permission, provided that accurate acknowledgement of source is made. Requests for permission for extended quotation from or reproduction of this manuscript in whole or in part may be granted by the Competent Authority of HBNI when in his or her judgment the proposed use of the material is in the interests of scholarship. In all other instances, however, permission must be obtained from the author.

Vikram Singh Dharodi

DECLARATION

I, hereby declare that the investigation presented in the thesis has been carried out by me. The work is original and the work has not been submitted earlier as a whole or in part for a degree/diploma at this or any other Institution or University.

Dharodi

Vikram Singh Dharodi

List of Publications arising from the thesis

Journal:

- **Sub- and super-luminar propagation of structures satisfying Poynting-like theorem for incompressible generalized hydrodynamic fluid model depicting strongly coupled dusty plasma medium**
  Vikram Singh Dharodi, Amita Das, Bhavesh G. Patel and Predhiman Kaw.
  Phys. Plasmas 23, 013707 (2016).

- **Visco-elastic fluid simulations of coherent structures in strongly coupled dusty plasma medium**
  Vikram Singh Dharodi, Sanat Kumar Tiwari and Amita Das.
  Phys. Plasmas 21, 073705 (2014).

- **Collective Dynamics in strongly coupled dusty plasma medium**
  Amita Das, Vikram Singh Dharodi and Sanat Kumar Tiwari.
  J. Plasma Physics 80(06), 855- 861(2014).

- **Kelvin-Helmholtz Instability in dusty plasma medium: Fluid and particle approach**
  Sanat Kumar Tiwari, Vikram Singh Dharodi, Amita Das, Predhiman Kaw and Abhijit Sen.
  J. Plasma Physics 80(06), 817- 823(2014).

- **Effect of strong coupling on the buoyancy-driven instability in strongly coupled dusty plasma medium**
  Vikram Singh Dharodi, Sandeep Kumar and, Amita Das.
  To be submitted.

- **Simulation of Rayleigh-Taylor instability in strongly coupled dusty plasma medium**
  Sandeep Kumar, Vikram Singh Dharodi, Amita Das, Predhiman Kaw, and Sanat Kumar Tiwari.
  To be submitted.

Conferences:

International Participation

- **A Poynting-like theorem for generalized hydrodynamic equations**
  10^{th} *Asia Plasma and Fusion Association Conference.*
  Institute for Plasma Research, Gandhinagar, India, 14 - 18 December 2015.

- **Rayleigh-Taylor instability in a visco-elastic medium using generalized hydrodynamic model**
  17^{th} *International Congress on Plasma Physics (ICPP - 2014).*
  Instituto Superior Técnico (IST), Lisbon, Portugal, 15 - 19 September 2014.

- **Evolution of coherent structures in visco-elastic medium using GHD model**
  40^{th} *COSPAR Scientific Assembly.*
  Lomonosov Moscow State University, Moscow, Russia, 2 - 10 August 2014.

- **Vortex studies in strongly coupled dusty plasma**
  7^{th} *International Conference on the Physics of Dusty Plasmas.*
  University of Delhi, New Delhi, India, 3 - 7 March 2014.

- **Elastic Turbulence: In context of dusty plasmas**
  International Conference on Complex Processes in Plasmas and Nonlinear Dynamical Systems.
  Institute for Plasma Research, Gandhinagar, India, 6 - 9 November 2012.

National Participation

- **Sub- and super-luminal dipoles in generalized hydrodynamic (GHD) model of strongly coupled visco-elastic fluid**
  30^{th} *National Symposium on Plasma Science and Technology (Plasma - 2015).*
  Saha Institute For Nuclear Physics (SINP), Kolkata, India, 1 - 4 December 2015.

- **A numerical study of Rayleigh-Taylor instability in Strongly Coupled Dusty Plasma Medium**
  29^{th} *National Symposium on Plasma Science and Technology (PLASMA-2014).*
  Mahatma Gandhi University, Kottayam, 8 - 11 December 2014.

- **Evolution of coherent structures in visco-elastic fluids**
  8^{th} *Conference on Nonlinear Systems and Dynamics.*
  Indian Institute of Technology, Indore, India, 11 - 14 December 2013.

- **A numerical study of rotating flows in strongly coupled dusty plasma**.
  28^{th} *National Symposium on Plasma Science and Technology-Plasma - 2013.*
  KIIT University, Bhubaneswar, India, 3 - 6 December 2013.

- **2-D Turbulence in Strongly Coupled Dusty Plasmas**,
  27^{th} *National Symposium on Plasma Science and Technology- Plasma-2012.*
  Pondicherry University, India, December 2012.

Schools:

- **DST SERC School on Tokamaks and Magnetized Plasma Fusion**
  Institute for Plasma Research, Gandhinagar, India, 25 February - 15 March 2013.

- **1st PSSI - Plasma Scholars Colloquium (PPSC - 2012)**
  Institute for Plasma Research, Gandhinagar, India, 3 - 4 July 2012.

- **THINK PARALLEL: Parallel Programming for Engineers and Scientists**
  C - DAC, Bangalore, India, 12 - 22 June 2012.

Dharodi

Vikram Singh Dharodi

Dedicated to.......

My family.......

ACKNOWLEDGEMENTS

Though this thesis belongs to me, there are many people who have helped me directly or indirectly during my Ph.D. tenure in different ways. It would not have been possible without their kind support and help. I am thankful to all.

First and foremost, I would like to acknowledge my thesis supervisor, Professor Amita Das. I am falling short of words in offering my deep sense of gratitude for her continued support, cooperation and guidance since the day one. I feel very fortunate to have an opportunity to work under her guidance. Her incisive supervision and kind support helped me a lot to overcome many tough situations and finally I could finish my thesis. She always has been available for listening to me and for discussions on my research work very patiently. Her vast knowledge and discerning insight have been inspiring. It would never have been possible for me to complete this thesis without her incredible support and encouragement.

I would like to pay my sincere regards to the members of my doctoral committee Professor Predhiman Kaw (Chairman), Professor Abhijit Sen and Dr. Sanjay Kulkarni for evaluating my work. Doctoral committee guided me through all these years. I would like to express my special gratitude and thanks to Professor Kaw and Professor Sen for their thoughtful suggestions and support during my research. I am deeply grateful to Professor Kaw for the long discussions that helped me to sort out some of the important physics issues of my research work.

I would like to acknowledge all the faculty members, Professor R. Jha, Professor S. Mukherjee, Professor R. Ganesh, Professor S. Sengupta, Dr. D. Raju, Dr. R. Goswami, Dr. A. K. Chattopadhyay, Dr. G. Ravi, Dr. C. Balasubramanian, and others, who have taught me during the course work. I also express my cordial thanks to Dr. Bhavesh Patel, for his continuous encouragement and valuable support to recover when my steps faltered. I wish to thank to Sanat Kumar Tiwari (senior and collaborator) for valuable conversation and suggestions in the conduct of my research work. I would like to extend my thanks to Gurudatt Gaur, Deepak Sangwan, Sharad Yadav, and Vikram Sagar for numerous discussions related to physics, thoughtful suggestions, elderly support, and to talk on social issues too.

I would like to thank my fellow labmates, Sharad, Sita, Gurudatt, Sanat, Deepa, Chandrasekhar, Ratan, Sandeep, Atul, and S. Sharma for valuable conversation on various topics that helped me to understand my research area better. My special thanks to Avadhesh Maurya for the technical support and help. It was his kind support that I never had to bother about viruses, losing files, creating backups or installing software. I would like to offer my special thanks to Daria Kuznetsova, alias Dasha, research scholar, Laboratoire d'Aérologie, Observatoire Midi-Pyrénées, University of Toulouse, France, for carefully reading and commenting on countless revisions of manuscripts, thesis chapters. I would like to acknowledge Neeraj, Mangilal, Avadhesh, D. P. Shinde, G. Veda, Rana, Aditya Gajjar separately for being a friend during my Ph.D. tenure, I find myself lucky to have friends like them in my life.

I would like to thank all my hostel friends who have always wished well and I have enjoyed the time that I spent with them. I record my courteous thanks to my seniors Kishor, Vikrant, Maya, Sharad, Satya, Shekar, Jugal, Sunita, Kshitish, Deepak, Ujjwal, Gurudatt, Vikram, Prabal, Ashwin, Sita, Rameswar, Sushil, Sanat, Pravesh, Sayak, Manjit, Aditya, Soumen. I would also like to convey my best wishes to my younger friends Rimza, Dushyant, Vara, Bibhu, Neeraj, Rupendra, Chandrasekhar, Mangilal, Meghraj, Akanksha, Vidhi, Deepa, Harish, Samir, Sonu, Debraj, Ratan, Narayan, Arghya, Umesh, Modhu, Amit, Bhumika, Surabhi, Sagar, Chetan, Atul, Deepak Verma, Alam, Prabhakar, Jervis, Sandeep, Pallavi, Minakshi, Harshita and other scholars and TTPs for creating a friendly ambiance around me. I warmly thanks all of you for being with me in ups and downs of life during my Ph.D. tenure.

My heartfelt thanks to my family for their patience and wishes for the successful completion of this research. They were always supporting me and encouraging me with their best wishes. Most importantly, I thank the Almighty for giving me the strength and patience to complete this thesis successfully.

I am also thankful to library, administration and computer center staff for their kind support during Ph.D. tenure. I am proud to be a research scholar at IPR. This institute has given to me so much love, respect and appreciation. I can never give back what I got from here. I will always remain indebted to IPR.

Contents

SYNOPSIS

Dusty plasma is often referred to as ‘Complex Plasma’ because the presence of dust in normal plasma gives rise to new types of dust-related modes and/or may also modify the existing modes which lead to complexity of plasma behavior [1–11]. Moreover, despite its complexity, the beauty of dusty plasma medium arises from the fact that it can be handled rather easily in experiments as well as in numerical simulations. This simplification comes from the fact that mass (typical mass of $10^{-15} - 10^{-10}$ Kg) as well as the size ($\sim$ micron) of the dust particles is quite large compared to that of normal electrons and typical ions in any electron-ion plasmas. Owing to heavy mass, the dust particle dynamics is quite slow in comparison to the background lighter species of electrons and ions in which it is interspersed. Thus one can assume inertia less response for the other species, while studying the dynamical response at dust time scales. The large size of the dust particles also ensures that the diagnostics involved in studying the system are simpler. The experimental observations can be carried out by naked eyes in the laboratory [12, 13] and can be recorded by simple cameras. Due to the large size of a dust, a huge number of charged particles (about a 10^3 to 10^5 [12, 14]) can stick over it. Thus, dust particles acquire high charge and the dusty plasma can readily go into the strongly coupled regime even at moderate temperature and a low density. Therefore, no sophisticated experimental efforts have to be carried out to cool the system and/or take it to the super-solid high density regimes for driving the system in the strongly coupled domain. The dusty plasma is thus a unique medium where one can directly observe simple interactions at micro-levels leading to complexity at macro-scales [15, 16].

Depending on value of the Coulomb coupling parameter Γ, the behaviour of dusty plasma can vary from that of a normal fluid to solid crystalline medium [17, 18]. It is found, experimentally/analytically and numerically, that crystallization is possible if $\Gamma \gg \Gamma_c$, here Γ_c is a critical parameter with the approximate value 172 [13, 19]. For the intermediate range $1 \leq \Gamma \leq \Gamma_c$, the dust species do not crystallize and neither do they behave like normal Newtonian fluids. In this regime, dusty plasma behave likes visco-elastic fluid having both traits, namely that of viscous (fluids) and elastic (solids) characteristics under strain. Viscous effects lead to the dissipation of energy, while elasticity of the medium is responsible for energy storage.

In this thesis we have employed 'Generalized Hydrodynamic (GHD) model' for the study of the dusty plasma medium. This phenomenological model takes into account both viscous and elastic effects [20, 21]. Lately, this model has been placed on firmer grounds by Diaw and Murillo using density functional approach [22]. In this model a parameter τ_m [20, 23–25] corresponding to memory relaxation time scales is introduced. The two features (viscosity and elasticity) are ascertained with respect to this characteristics relaxation time scale τ_m. For those phenomena which are faster compared to τ_m, the system retains the memory of the past configurations and the elasticity effects dominate. However, for times longer than τ_m the memory effects are insignificant and the usual viscous characteristics of the fluid phase dominate.

The thesis contains six chapters. We provide below the chapterwise summary of the work carried out in this thesis.

- **Chapter - I:** The first chapter provides a brief introduction of the dusty plasma medium. Here we have briefly listed commonly used fluid model descriptions and particle-based approaches used to explore the properties of the complex dusty plasma medium. Predictions based on model descriptions have often inspired experimental investigations of the dusty plasma medium in certain directions. Similarly, experimental observations have also led to significant progress in model development. We briefly list out some of the models that are being employed most often for the study of the complex medium of dusty plasma system.

  (i) The quasilocalized charge approximation was proposed by Rosenberg *et al.* [26] to derive the dispersion relation in strongly coupled plasma. This approach is based on the localization of dust particles in the strongly coupled liquid phase [27, 28]. It is assumed that the dust particles oscillate with small amplitude along their randomly quasi-localized positions.

(ii) Generalized Hydrodynamic fluid approach has already been successfully applied to study the visco-elastic nature of strongly coupled dusty plasma. The work in this thesis is based on this approach and has been described in details in present thesis.

(iii) Molecular dynamics is also often used to model this medium to understand relevance of various physical processes at microscopic level. In Molecular dynamic simulations one follows the trajectories of each individual particle in the combined force field that gets generated due to the presence of other particles and/or external agencies. This scheme was originally employed for the simulations of small molecules and/or molecular chains where the total particle number is significantly small. For fluid and plasma system the particle number being huge, such a scheme (particle based) is computationally not feasible. However, in the case of dusty plasmas the dust particle numbers are reasonably small to adopt this simulation procedure. The electrons and ions which constitute the background plasma are, however, huge in number and can not be treated by this approach. Thus, a scheme can be adopted wherein one does not follow the dynamics of individual electrons and ions but incorporates their effects in the formulation of force field for the evolution of dust particles, the MD approach can be applied to the individual dust particles.

The next four chapters, Chapters 2-5, are dedicated to our research work, the collective behavior of the dusty plasma medium under the formalism of Generalized Hydrodynamic (GHD) fluid model. In the last (sixth) chapter, the thesis work is summarized, and some future prospectives of the presented work are described.

- **Chapter - II:** The GHD model supports the existence of both incompressible transverse shear and compressible longitudinal modes [20]. To concentrate on the incompressible features of this system, we separate out the compressibility effects altogether. For this purpose, the incompressible limit of the GHD (i-GHD) coupled set of equations has been obtained in Chapter - II. The density perturbations in this limit are altogether ignored and the Poisson's equation is replaced by the quasi neutrality condition. The i-GHD set of equations then casts as a coupled set of convective equations which is numerically evolved with the help of the flux-corrected scheme of Boris *et al* [29].

The numerical code is validated by studying the emission of radially propagating transverse shear waves from a smooth circular rotating vortex. The radial transverse shear (TS) waves traveling with phase velocity $\sqrt{\eta/\tau_m}$ as predicted analytically by Kaw *et al.* [20] is confirmed by our simulations. Furthermore, the expected $1/r$ fall in the circular geometry of the system in the intensity of the waves is also confirmed by our studies.

Often the vorticity structure in a fluid may not have a circular shape. We consider, therefore, for our studies an initial distorted patch of vorticity. A simple elliptical form of distortion has been considered by us. We have also investigated the process of interaction between various vortex structures within the GHD formalism for a strongly coupled medium. It is well known that a sharp shear profile is susceptible to the well known Kelvin - Helmholtz (KH) instability. We avoided the KH destabilization by considering smooth vorticity patches and concentrated solely on understanding the evolution of vorticity patches in both strong and weak coupling limits. The prominent feature of i-GHD model is that it supports the transverse shear waves. To scrutinize the effect of these TS waves on the evolution and interaction between distinct vortex structures an extensive numerical simulation has been performed for i-GHD system. A comparison with Hydrodynamic (HD) system has also been provided. In particular, we consider two cases. First is the interaction and subsequent merging two like-signed vorticity patches. We observed that in i-GHD formalism the merging does not lead to a coherent final form like hydrodynamic fluids [30–32], the continuing emission of TS waves dominates over the merging process because each of the vortex patch also emits the TS waves, as expected. In second case we study a dipolar structure, which gets formed when two unlike-signed vorticity patches are brought in the vicinity of each other. This dipolar structure propagates along the direction of its axis as a single stable entity in hydrodynamic fluids. Moreover, keeping in view that TS waves travel with phase velocity $\sqrt{\eta/\tau_m}$. We have considered two types of dipoles, viz., moving slower/faster than the phase velocity of the emitted waves. In the former slower case, the dipole remains engulfed inside the continuous emission of waves which react and distorts the original structure ultimately. For the second case of faster dipoles, the TS waves are emitted from this dipolar structure, remain confined in the form of a wake. The dipole, therefore, continues to move as a stable entity with a conical wake of waves trailing behind it. The collisional interaction of oppositely propagating dipole structures has also been studied.

- **Chapter - III:** In the this chapter, a Poynting-like conservation theorem is constructed for the 2-D i-GHD model equations and obtained a enstrophy-like conserved quantity. The rate of change of this quantity (sum of square integrals of vorticity and the velocity strain) is controlled by radiative, convection and dissipative effects. The radiation term corresponds to the TS waves and shows a striking similarity with electromagnetic waves. The equation also indicates that convective and viscous dissipation are other important mechanism that could significantly change the conserved quantity.

  The Poynting-like theorem has been shown to be satisfied with great precision in our numerical simulations for all the cases of vortex evolution considered in Chapter - II. These observations are likely to be generic and applicable to all strongly coupled media.

- **Chapter - IV:** In this chapter, we study the evolution of sharp vorticity patches, which showed the KH destabilization. The interplay of transverse shear waves and the KH destabilization in the context of i-GHD fluid results in a good mixing of fluid material, unlike the HD case where the fluid seems to remain entrained in the confined domain for long. We also considered the evolution of a multi-circulation vortex profiles. We have found that at intermediate time range, it provides a complete picture of a turbulent flow which is a collection of small vortices and waves. When the system is left for a very long time, it ultimately relaxes to a single vortex faster than in hydrodynamic fluid. Additionally, we found that the relaxing rate of this turbulent medium increases with the increasing coupling strength.

To quantify the mixing and transport features in the presence of TS waves, we have also studied the dynamical evolution of test tracer particles. The diffusion and clustering of these test particles are directly linked to the mixing characteristic of a medium [33]. The displacement of these particles provides a quantitative estimate of the diffusion coefficient of the medium. We also showed that often these test particles organize themselves in a spatially inhomogeneous distribution. Phenomenon of clustering amongst these particles is clearly evident from the simulations results.

- **Chapter - V:** In the previous chapters we had restricted our studies to homogeneous dusty plasma medium. In this chapter we focus on the dusty plasma medium which is stratified against gravity. This configuration is unstable to the usual Rayleigh Taylor (RT) instability. We have shown that the RT instability gets suppressed in the presence of strong coupling. Such a suppression had been predicted earlier in the context of strongly coupled dense matter of the inertial fusion by Das. *et. al.* [34]. Simulations of localized rising low density bubbles and falling high density droplets are also considered. We found that the falling/rising rate of droplet/bubble gets decrease with increasing coupling strength.

- **Chapter - VI:** In the sixth and final chapter, we summarize our results and also provide the future scope of our work.

The thesis, thus carries out a series of detailed investigation of collective behaviour of the strongly coupled dusty plasma system using the GHD model representing a visco-elastic medium.

---

[1] N. N. Rao, P. K. Shukla, and M. Y. Yu. Dust-acoustic waves in dusty plasmas. *Planetary and Space Science*, 38(4), 543-546 (1990).

[2] F. Verheest. Nonlinear dust-acoustic waves in multispecies dusty plasmas. *Planetary and Space Science*, 40(1), 1-6 (1992).

[3] N. D'Angelo. Coulomb solids and low-frequency fluctuations in rf dusty plasmas. *Journal of Physics D: Applied Physics*, 28(5), 1009 (1995).

[4] A. Barkan, R. L. Merlino, and N. D'angelo. Laboratory observation of the dust-acoustic wave mode. *Physics of Plasmas*, 2(10), 3563-3565 (1995).

[5] C. Thompson, A. Barkan, R. L. Merlino, and N. D'Angelo. Video imaging of dust acoustic waves. *IEEE transactions on plasma science*, 27(1), 146-147 (1999).

[6] B. S. Xie and M. Y. Yu. Dust acoustic waves in strongly coupled dissipative plasmas. *Phys. Rev. E*, 62, 8501-8507 (2000).

[7] B. Eliasson and P. K. Shukla. Dust acoustic shock waves. *Phys. Rev. E*, 69, 067401 (2004).

[8] J. Heinrich, S. H. Kim, and R. L. Merlino. Laboratory observations of self-excited dust acoustic shocks. *Phys. Rev. Lett.*, 103, 115002 (2009).

[9] D. Samsonov, G. Morfill, H. Thomas, T. Hagl, H. Rothermel, V. Fortov, A. Lipaev, V. Molotkov, A. Nefedov, O. Petrov, A. Ivanov, and S. Krikalev. Kinetic measurements of shock wave propagation in a three-dimensional complex (dusty) plasma. *Phys. Rev. E*, 67, 036404 (2003).

[10] D. Samsonov, S. K. Zhdanov, R. A. Quinn, S. I. Popel, and G. E. Morfill. Shock melting of a two-dimensional complex (dusty) plasma. *Phys. Rev. Lett.*, 92, 255004 (2004).

[11] P. Bandyopadhyay, G. Prasad, A. Sen, and P. K. Kaw. Experimental study of nonlinear dust acoustic solitary waves in a dusty plasma. *Physical review letters*, 101(6), 065006 (2008).

[12] J. H. Chu and Lin I. Direct observation of coulomb crystals and liquids in strongly coupled rf dusty plasmas. *Phys. Rev. Lett.*, 72, 4009-4012 (1994).

[13] H. Thomas, G. E. Morfill, V. Demmel, J. Goree, B. Feuerbacher, and D. Möhlmann. Plasma crystal: Coulomb crystallization in a dusty plasma. *Phys. Rev. Lett.*, 73, 652-655 (1994).

[14] M. H. Thoma, M Kretschmer, H Rothermel, HM Thomas, and GE Morfill. The plasma crystal. *American journal of physics*, 73(5):420–424, 2005.

[15] R. L. Merlino and J. A. Goree. Dusty plasmas in the laboratory, industry, and space. *Physics Today*, 57(7), 32-39, (2004).

[16] H. M. Thomas, Morfill, and E. Gregor. Melting dynamics of a plasma crystal. *Nature Publishing Group*, 379, 806-809 (1996).

[17] W. L. Slattery, G. D. Doolen, and H. E. DeWitt. Improved equation of state for the classical one-component plasma. *Phys. Rev. A*, 21, 2087-2095 (1980).

[18] S. Ichimaru. Strongly coupled plasmas: high-density classical plasmas and degenerate electron liquids. *Rev. Mod. Phys.*, 54, 1017-1059 (1982).

[19] H. Ikezi. Coulomb solid of small particles in plasmas. *Physics of Fluids*, 29(6), (1986).

[20] P. K. Kaw and A. Sen. Low frequency modes in strongly coupled dusty plasmas. *Physics of Plasmas*, 5(10), 3552-3559 (1998).

[21] P. K. Kaw. Collective modes in a strongly coupled dusty plasma. *Physics of Plasmas*, 8(5), (2001).

[22] A. Diaw and M. S. Murillo. Generalized hydrodynamics model for strongly coupled plasmas. *Phys. Rev. E*, 92, 013107 (2015).

[23] J. Frenkel. *Kinetic Theory Of Liquids.* Dover Publications, 1955.

[24] M. A. Berkovsky. Spectrum of low frequency modes in strongly coupled plasmas. *Physics Letters A*, 166(5), 365-368 (1992).

[25] S. Ichimaru, H. Iyetomi, and S. Tanaka. Statistical physics of dense plasmas: Thermodynamics, transport coefficients and dynamic correlations. *Physics Reports*, 149(2-3), 91-205 (1987).

[26] G. Kalman and K. I. Golden. Response function and plasmon dispersion for strongly coupled coulomb liquids. *Phys. Rev. A*, 41, 5516-5527 (1990).

[27] K. I. Golden and G. J. Kalman. Erratum: quasilocalized charge approximation in strongly coupled plasma physics [phys. plasmas 7, 14 (2000)]. *Physics of Plasmas*,

List of Figures

1

Introduction

The understanding of strongly coupled state of matter is of prime importance in several contexts and frontier areas of research. The dusty plasma offers a unique opportunity of understanding such state of matter as it can easily be prepared in a strong coupling regime at low densities and room temperature. Thus, the study of dusty plasma medium may reveal interesting details of the strongly coupled state of matter. Since the collective response mirrors the dynamical traits of any medium, we have chosen to study certain collective properties (namely coherent structures, instabilities, transport and mixing) of the dusty plasma medium in the strong coupling limit.

Although many approaches are employed to study the dusty plasma medium in strong coupling limit, we have restricted our studies to the fluid description of Generalized Hydrodynamic (GHD) model which treats the medium as a visco-elastic system. This model introduces strong coupling effects in terms of relaxation parameter τ_m and the viscosity η.

In this chapter we provide a brief introduction of the dusty plasma medium, highlighting its unique characteristics. The various descriptions and models adopted so far for the depiction of this medium have been presented. A review of earlier work keeping in view the content of this thesis has been presented. Finally, the outline of the dissertation is also presented.

1.1 Background

The three well-known states of matter are solid, liquid and gas. By raising the temperature, solid gets converted to liquid and then at higher temperature it goes to a gaseous state. Plasma is known as the fourth state of matter, which forms when a gaseous medium is heated further so that individual atoms get ionized. The ionized medium with the constituent charged particles, however, interacts via long range electromagnetic forces and exhibits a host of interesting phenomena. This ionized state of plasma matter being the most abundant (e.g. 99 %) observed form in universe, is not only attractive from the fundamental research point of view but has many applications in different areas of science.

In many physical situations* the usual electron-ion plasma is interspersed with some heavier mass species (typical mass of $10^{-15} - 10^{-10}$ Kg). These particles are often termed as the dust particles. These dust particles can come in various shapes and sizes and often acquire charge when present in a plasma due to the electron and ion fluxes falling on their surface. In general, the lighter electron flux on the dust grain surface is comparatively higher than that of the ion flux, causing the dust species to acquire a net negative charge. In such a system, the dust component acts as a third species with a very high negative charge. It is found that a micron-sized dust particle may get negatively charged with about 10^3 to 10^5 [3, 4] of elementary electron charges. However, in some special circumstances, like secondary electron emission, dust grains may get positively charged [5]. When these dust particles participate in collective interaction, then the plasma is termed as "dusty plasmas" [5].

The dusty plasmas provide immense opportunities for applications ranging from industrial study to space physics. Sometimes the presence of dust particles can have desirable consequences and at times their presence can be unsolicited. For example in fusion plasma devices (tokamaks, sellarators, etc.), in industrial processes like plasma vapor deposition, chip production and etching [6,7] etc., dust species behave as contaminants in the plasma. On the other hand, the collection of dust leads to the formation of astronomical bodies e.g. asteroids, moons, stars and planets, thus

*Like the Earth's lower magnetosphere [1, 2], planetary atmospheres, cometary tails and comae, planetary and solar nebulae, asteroids, volcanoes, lighting discharge, interstellar clouds etc.

by studying the dynamics of dust species in a plasma one can hope to understand much of the behaviour of universe around us.

1.1.1 Comparison with electron-ion plasmas

The aggregation of charged species form a medium whose Coulomb coupling parameter $\Gamma_{coulomb}$[†] between these species is given as

$$\Gamma_{coulomb} = \frac{Q^2}{a_d k_B T} \propto \frac{Q^2 n^{1/3}}{T}. \tag{1.1}$$

Here, T and k_B are the average particle temperature and Boltzmann constant, respectively. Total charge $Q = Ze$, Z is the number of charges residing on a particle and e is elementary charge. Here, a_d is the average interparticle separation between two particles which is related to the number density n by ${a_d}^3 = 3/4\pi n$, for a three-dimensional system. Depending on the value of $\Gamma_{coulomb}$, a medium may be weakly coupled if $\Gamma_{coulomb} < 1$ and may be strongly coupled if $\Gamma_{coulomb} \geq 1$. For electron-ion plasmas, the value of $\Gamma_{coulomb} \ll 1$, since the species (electrons and ions) typically have low electronic charges (corresponding to their ionization state) at high temperature. For dusty plasma, on the other hand, the value of the Coulomb coupling parameter can be easily $\Gamma_{coulomb} \geq 1$. This is because significantly large numbers of electrons can reside on the surface of each dust particle, thereby making very high charged species. Thus, even at low dust density and at normal temperatures, the dust particles can be in the strongly coupled regime.

The presence of dust grains influences the dynamical traits of the medium at very slow time scales. It introduces new types of low frequency dust related modes [see Section 1.2].

1.1.2 Objective and motivation

Our objective is to study the slow time scale phenomena that results from the collective dynamics of massive dust particles. The response of electrons and ions

[†] $\Gamma_{coulomb}$ is defined as the ratio of electrostatic potential energy to average thermal energy between two particles of given medium.

being fast, their inertia can be ignored for the study of these phenomena. The balance between pressure and electric field then results in the Boltzmann distribution of electron and ion densities. The dust continuity and momentum along with the Poisson's equation constitute the governing set of equations for dust dynamics.

The movement of heavy dust particles is quite slow. In typical laboratory experiments one can observe the dust particles dynamics by ordinary cameras or even with naked eyes. Thus, one can directly view any of the dynamical phenomena as they occur. Thus, simple diagnostics are sufficient to follow the dynamics. Furthermore, as mentioned earlier, the medium can easily be prepared at room temperature and normal densities in strong coupling regime.

The entire physics community is currently grappling with questions and appropriate simplified descriptions of strongly coupled state of matter. The dusty plasma medium can play an important role in this regard due to its uniqueness, as its dynamical response typically falls within the perceptible grasp of human senses. It is thus a unique medium in which one can directly view simple interactions at micro levels leading to complexity at macro scales. So, the dusty plasma medium has attracted a significant research interest.

The dynamical response of any medium is best understood in terms of its collective behaviour. We, therefore, focus in this thesis on the influence of strong coupling on certain collective properties, namely coherent structures, instabilities and turbulent transport and mixing.

1.2 Description of complex dusty plasma medium

We provide here a brief overview of the dusty plasma medium along with various methods that have been adopted to explore the system in different physical regimes. Dusty plasma is also called "complex plasma" because the presence of dust in normal plasma enhance the complexity of such system by introducing new types of dust related modes and/or may also modify the existing modes such as dust-acoustic (DA) waves [‡] [8–13]; DA shocks [14–17]; DA solitons [18] etc, dust ion-acoustic (DIA) waves [19–21]; DIA shocks [22,23]; DIA solitons [24] etc, dust lattice (DL) waves [25–27] etc.

[‡] In the DA waves the massive dust particles act as a source of inertia and the restoring force comes from the pressure of background species (electrons and ions)

Dust particles present in plasma acquire negative charge because of high mobility of electrons in comparison to ions. The ions perform the Debye shielding of the negative potential on the dust surface. Thus the inter-dust interaction potential is a screened Coulomb potential. This modified potential is known as Yukawa or Debye-Huckel potential [4, 28]

$$U(r) = \frac{Q_d^2}{r} e^{-r/\lambda_d}. \tag{1.2}$$

Here $Q_d = Z_d e$ is the total charge on dust particle, Z_d is the number of charges residing on a dust particle and e is electron charge. The Debye length§ is given as

$$\lambda_d = \sqrt{\frac{\lambda_{de}^2 \lambda_{di}^2}{\lambda_{de}^2 + \lambda_{di}^2}}. \tag{1.3}$$

$\lambda_{de} = \sqrt{k_B T_e / 4\pi n_{e0} e^2}$ and $\lambda_{di} = \sqrt{k_B T_i / 4\pi n_{ei} e^2}$ are the electron and ion Debye length, respectively. T_d, T_e and T_i are the dust, electron and ion temperatures, respectively; n_{e0} and n_{i0} are the electron and ion equilibrium densities, respectively. The coupling parameter Γ amidst the dust particles taking into account the screening effects in the potential in Eq. (1.1) can be written as

$$\Gamma = \frac{Q_d^2}{a_d k_B T_d} e^{-a_d/\lambda_d}. \tag{1.4}$$

Even with the screening factor (e^{-a_d/λ_d}) the value of coupling parameter Γ can easily exceed unity for the dusty plasma medium, due to the high value of charge that resides on the surface of dust particles. Depending on value of Γ the behaviour of dusty plasma can span from normal conducting fluid to solid crystalline medium. One can usually find in the literature that crystallization is possible if $\Gamma \gg \Gamma_c$, here Γ_c is a critical parameter with the approximate value 172 [28,29]¶. For intermediate range $1 \leq \Gamma \leq \Gamma_c$, the dust species do not crystallize and neither do they behave like normal Newtonian fluids‖. In this regime, dusty plasma behave like a visco-elastic fluid. Visco-elastic fluids exhibit both viscous (fluids) and elastic (solids)

§ λ_d is the shielding parameter which define the the characteristics length scale of the exponential decay of dust potential

¶For the screening parameter $\kappa = a_d/\lambda_d$=0

‖ Fluids which obey the Newton's law of viscosity are called Newtonian fluids characteristics when undergoing deformation (viscous effects correspond to energy dissipation, while elastic effects correspond to energy storage).

We have employed a Generalized Hydrodynamic visco-elastic model which takes account of the viscous and elastic effects, for our numerical and theoretical studies [a detailed description of the same has been provided in the Subsection 1.3.2]. In this phenomenological model, elasticity is represented by the memory relaxation parameter τ_m [30]. The evolution of coherent vorticity patches, involving their propagation and transverse emission of waves from them, their susceptibility to the shear flow driven Kelvin-Helmholtz (K-H) mode, the mixing and transport of the fluid etc., are some questions that have been investigated in detail. The gravitational and buoyancy driven instabilities in this medium including Rayleigh-Taylor instability for a dusty plasma medium have also been studied. For the GHD model the numerical code was developed on the basis of the flux-corrected scheme [31]. To understand the mixing and transport properties of the considered visco-elastic medium, passive tracing particle (inertial and non-inertial) simulations have also been performed. The dynamics of these particles is simulated using a one-way coupled Lagrangian point-particle approach where the feedback effect of particles on the flow of the medium has been neglected. The diffusion and clustering of these particles are directly related to the mixing characteristic of a medium.

There are other approaches which have been employed for the understanding of this complex medium. A summary of those have been presented in Section 1.3.

1.3 Fluid and kinetic approaches

There have been many fluid model descriptions and particle based approaches that have been employed to explore the properties of the complex dusty plasma medium. Predictions based on model descriptions have often inspired experimental investigations of the dusty plasma medium in certain directions. Similarly, experimental observations have also led to significant progress in model development. We list below some of models that are being employed most often for the study of the complex medium of dusty plasma system.

1.3.1 Quasi-Localized Charge Approximation (QLCA) approach

The quasi-localized charge approximation was proposed by Rosenberg *et al.* [32] to derive the dispersion relation in strongly coupled plasma. This approach is based on the localization of dust particles in the strongly coupled liquid phase [33, 34]. It is assumed that the dust particles oscillate with small amplitude along their randomly quasi-localized positions. The strong coupling effects on DA waves in dusty plasmas have been considered by Rosenberg *et al.* [35,36]. Kalman *et al.* [37] studied the wave propagation in a strongly coupled dusty plasma by using QLCA model based on MD simulation data [38] and found a very good agreement except for the transverse mode which vanishes for small wave numbers. A comparative study between QLCA model and MD simulations was done by Kalman *et al.* [39]. This approach along with MD simulations has been successfully applied to describe waves in various strongly coupled liquid phases [40, 41]. This approach has been modified by Golden *et al.* [42–44] who treat the dipole interaction between dust particles. Recently, Hartmann *et al.* [45] calculated the wave dispersion relation where the dust particles interact via both Yukawa and magnetic dipole-dipole interaction i.e. modified QLCA approach.

1.3.2 Generalized Hydrodynamic (GHD) approach

Generalized Hydrodynamic fluid approach has already been successfully applied to study the visco-elastic nature of strongly coupled dusty plasma. This approach is physically understandable and models the dust system in both weak (simple charged fluids) and strong coupling limits (visco-elastic fluids). These two aspects (viscosity and elasticity) are ascertained with respect to a characteristic time scale τ_m which signifies the memory relaxation time. For those phenomena which are faster compared to τ_m the system retains the memory of past configurations and the elasticity effects dominate. However, at times longer than τ_m the memory fades and the usual viscous characteristics of the fluid phase dominates.

The visco-elastic description of the electrostatic response of strongly coupled dusty plasma medium is provided by the following coupled set of continuity equation, the evolution of velocity through a Generalized Hydrodynamic description and the Poisson's equation, respectively

$$\frac{\partial n_d}{\partial t} + \nabla \cdot (n_d \vec{v}_d) = 0, \tag{1.5}$$

$$\left[1 + \tau_m \frac{d}{dt}\right] \left[m_d n_d \frac{d\vec{v}_d}{dt} + \nabla P - n_d Z_d e \nabla \phi\right] = \eta \nabla^2 \vec{v}_d + \left(\zeta + \frac{\eta}{3}\right) \nabla(\nabla \cdot \vec{v}_d), \tag{1.6}$$

$$\nabla^2 \phi = -4\pi e \left(n_i - n_e - Z_d n_d\right). \tag{1.7}$$

Here η, ζ and τ_m are the shear, bulk viscosity coefficients and relaxation time parameter, respectively. The total time derivative is $\frac{d}{dt} = \left(\frac{\partial}{\partial t} + \vec{v}_d \cdot \nabla\right)$. The variables $\vec{v}_d$, ϕ and n_s $(s = e, i, d)$ are the dust fluid velocity, potential and number density of the charged species (electrons, ions and dust, respectively). To achieve dimensionless forms of Eqs. (1.5)-(1.7), we have normalised the time, length, velocity and potential by the dust plasma frequency $\omega_{pd} = \left(4\pi (Z_d e)^2 n_{d0}/m_{d0}\right)^{1/2}$, plasma Debye length $\lambda_d = \left(k_B T_i / 4\pi Z_d n_{d0} e^2\right)^{1/2}$, $\lambda_d \omega_{pd}$ and $Z_d e / k_B T_i$, respectively. Z_d is the charge on each dust grain, this charge is considered to be fixed. However, the charging equation can also be added to account for the fluctuating electron charge of the dust particles. The parameters m_d, T_i and k_B are the dust grain mass, ion temperature and Boltzmann constant, respectively. The densities n_s $(s = e, i, d)$ are normalised by their respective equilibrium values n_{s0}.

The pressure can be determined using the equation of state $P = \mu_d \gamma_d n_d k_B T_d$ with compressibility parameter $\mu_d = \frac{1}{T_d} \frac{\partial P}{\partial n_d}|_{T_d}$ and adiabatic index γ_d. The parameters μ_d, τ_m and η are empirically related to each other and their relationship is obtained by molecular dynamic simulations [46, 47]. The normalised continuity, momentum and the Poisson's equations for the dust fluid can be written as:

$$\frac{\partial n_d}{\partial t} + \nabla \cdot (n_d \vec{v}_d) = 0, \tag{1.8}$$

$$\begin{aligned} \left[1 + \tau_m \left(\frac{\partial}{\partial t} + \vec{v}_d \cdot \nabla\right)\right] \left[n_d \left(\frac{\partial \vec{v}_d}{\partial t} + \vec{v}_d \cdot \nabla \vec{v}_d\right) + \nabla P - n_d \nabla \phi\right] = \\ \eta \nabla^2 \vec{v}_d + \left(\zeta + \frac{\eta}{3}\right) \nabla(\nabla \cdot \vec{v}_d), \end{aligned} \tag{1.9}$$

$$\nabla^2 \phi = n_d + \mu_e exp(\sigma_e \phi) - \mu_i exp(-\phi), \tag{1.10}$$

with parameters $\sigma_e = T_i/T_e$, $\mu_e = n_{e0}/Z_d n_{d0}$ and $\mu_i = n_{i0}/Z_d n_{d0}$. The memory effect related to elasticity is incorporated through a relaxation time parameter τ_m [48–50] **. For $\tau_m \frac{\partial}{\partial t} < 1$, there are no memory effects and the equation of motion is that for a standard viscous fluid driven by self-consistent electric and pressure fields. For $\tau_m \frac{\partial}{\partial t} \geq 1$, the memory effects are strong (for the time scales of interest, each fluid element remembers where it came from) and the viscosity coefficient η becomes more like a non-dissipative elastic coefficient because of strong particle correlation. The inertia of electrons and ions is negligible at slow dust time scales and hence these species can be assumed to follow a Boltzmann distribution.

1.3.3 Viscoelastic-Density Functional (VEDF) approach

Recently, Diaw and Murillo derived a hydrodynamic model referred as the viscoelastic-density functional (VEDF) model for strongly coupled plasmas using density functional approach [51]. The authors validated this model by comparing its results with molecular dynamics simulations of Yukawa plasmas, and found an excellent agreement for three quite different types of systems: ultracold plasmas, dusty plasmas, and dense plasmas.

1.3.4 Molecular Dynamic (MD) simulation approach

In molecular dynamic simulations one follows the trajectories of each individual particle in the combined force field that gets generated due to the presence of other particles and/or external agencies. This scheme was originally employed for the simulations of small molecules and/or molecular chains where the total particle number is significantly small. For fluid and plasma system the particle number is huge, so such a scheme is computationally not feasible. However, in the case of dusty plasmas the dust particle numbers are reasonably small to adopt this simulation procedure. The electrons and ions which constitute the background plasma are, however, huge in number and cannot be treated by this approach. Thus, a scheme can be adopted wherein one does not follow the dynamics of individual electrons and ions but incorporates their effects in the formulation of force field for the evolution of dust particles, the MD approach can be applied to the individual dust particles. This is indeed what is done in the inertia less

**The relation between coupling constant Γ and τ_m is given in [48] approximation employed for ions and electrons, which is valid at the slow dust time scales. Such an approximation results in the Boltzmann distribution for electron and ion densities and retaining the linear terms of the Boltzmann form in the Poisson's equation for electron and ion density, yields a screened Yukawa potential for the dust-dust interaction. Using such an interaction potential the dust particles can be evolved with the help of molecular dynamics simulations.

Molecular dynamic simulations thus helps to observe the behavior of individual particles at the microscopic level. In dusty plasma experiments, illuminating the dust with laser light allows to capture the individual particles' positions with time, by means of ordinary videography. The MD simulations thus mimics this scenario directly.

This approach has been widely used for the understanding of the transport processes in strongly coupled dusty plasma medium, like diffusion [52–55], thermal conductivity [56] and viscosity [57–62], phase transitions [63,64] etc. The nonlinear behaviour of dusty medium has also been studied via coherent structures evolution [65], fluid instabilities like Rayleigh-Taylor [66] and Kelvin-Helmholtz [67, 68]. In the understanding of other phenomena like TS waves, DA waves, shock waves and thermodynamic properties i.e. excess free energy, internal energy and pressure etc., this approach plays a very important role. This technique is the easiest and the most realistic.

1.3.4.1 Hybrid approach: Particle-in-cell (PIC) and fluid simulations

The advantage of Particle-in-cell (PIC) approach is that one can simulate a high dense system with less computational effort by using the concept of super particle (aggregation of many particles of same species). The concept of super particle is very relevant for the description of charged particle system because it just rescales the number of particles while the ratio of charge to mass remains the same. Under the Lorentz force the trajectory of super particles will be same as the trajectory for a real particle. The standard PIC method is used to model the dynamics of the dust particles by integrating the Lorentz force equation.

The fluid approach is simplest but does not include the particle and wave interaction; PIC (where all three species i.e. dust, electrons and ions are governed by PIC with different time scales) and MD simulations would be prohibitively computationally expensive and often impossible as stated earlier. Hybrid approach may be most useful as one has freedom to work without loss of any physical concept and with a reasonable computational cost. Hybrid models use the particle-in-cell method for charged dust species, while other species like electrons and ions are treated as Boltzmann fluid at a constant temperature by D. Winske *et al.* [69, 70]. Hence, dust dynamics is governed by PIC methods and electric field is calculated by using the Poisson's equation.

1.4 Summary of the earlier studies

The initial research interest in dusty plasmas was motivated by astrophysical phenomena. The involvement of dust particles in many self-occurring natural phenomena make it a very intensively studied and interesting topic of research.

The first predictions for plasma crystal formation was made by W. L. Slattery [71] and H. Ichimaru [46]. They suggested that if the value of the coupling parameter $\Gamma \geq 172$[††], the particles should organize in a Coulomb lattice form. H. Ikezi [28] showed that $\Gamma \simeq 172$ can be achieved for highly charged dust grain easily. The expected dust crystal structure was achieved in laboratory experiments by two different groups Chu *et al.* [3] and Thomas *et al.* [29], this worked as stimulation in enhancing the interest of researchers in its basic studies. After that, the study of various phenomena like dust crystallization, phase transitions etc. have been made by numerous researchers [4, 72–76]. With this, the importance of dusty plasma in capturing the complex fluid and solid-like features was realised soon.

However, a complete theoretical description of this complex state of matter is quite challenging and in the past several different approaches have been adopted to understand the behaviour of this medium [a detailed description is given in section 1.3]. Among the most well-known descriptions are the Generalized Hydrodynamic visco-elastic approach used by Kaw *et al.* [48, 77], where they showed that in addition to longitudinal DA waves, strongly coupled media may also sustain transverse shear waves. The prediction based on GHD description was verified experimentally by Pramanik *et al.* [78] and Pintu *et al.* [18]. A plenty of research work has been carried out by using this approach, Sanat and coauthor/s

[††]For the screening parameter $\kappa = a_d/\lambda_d$=0

have observed nonlinear phenomena like nonlinear wave propagation, shear flow structures [79], the cusp formation [80], solitons in 1D [81] and Kelvin-Helmholtz instability [68, 82, 83] as well as turbulent characteristics [84] for this medium in 2D. The other phenomena like Jeans instability [85], viscoelastic modes [86], nonlinear wave propagation [87], viscosity gradient-driven instability [88] and shear wave vortex solution [89] in a strongly coupled dusty plasma have also been studied. Shukla *et al.* [90] stated the formation of shocks in strongly coupled dusty plasmas.

Apart from GHD model, theoretically, the existence of transverse modes in dusty plasma medium has also been predicted by several authors [91–93]. Schmidt *et al.* [94] showed such transverse modes in molecular dynamic simulations. Nunomura *et al.* [95] has also observed transverse modes in dusty plasma experiment. Recently, the strong coupling effects on DA waves in dusty plasmas have been considered by Rosenberg *et al.* [35, 36], based on the quasi-localized charge approximation, by Murillo [47], based on the multicomponent kinetic approach and by Winske *et al.* [69] and Ohta *et al.* [38], based on molecular dynamics simulations.

The vortex study plays a crucial role in the understanding of the behaviour of dusty plasma. There have been many studies on rotating vortices of dusty plasma, these vortices have been seen to form both in the presence as well as in the absence of magnetic field [96–101]. Recently Yoshifumi *et al.* [102] have presented interesting experimental results on dust rotation. Konopka *et al.* [103] and Sato *et al.* [103] have shown the rotation of dust particles experimentally in the magnetized dusty plasma. Schwabe *et al.* [104], reported in their dusty plasma experiment that the formation of variety of rotating dust structures depends on the varying magnetic field strength. The coherent solutions in the form of tripolar vortex have also been studied theoretically in the context of dusty plasma [105]. By particle simulation the coherent structures evolution has been observed [65].

The instabilities like Kelvin-Helmholtz and Rayleigh-Taylor are considered to be responsible for mixing and transport in any medium. Rayleigh-Taylor instability is observed in diverse situations such as supernova explosion [106, 107], planetary rings, geophysics, astrophysics, liquid atomization [108, 109], supersonic combustion, industrial plasmas, fusion physics [66, 110–112], oceans, turbulent mixing [113–115] etc. In normal electron-ion plasmas the effect of gravity is pretty weak due to the lightness of the electron and ion species. But in the dusty plasma where one of the main constituent is the micron-sized dust particle has the typical mass of $10^{-15} - 10^{-10}$ Kg, the role of gravitational force becomes important. A lot of research papers are dedicated to the dynamics of dusty plasma medium under the effect of gravitational force. To study the dynamics of dusty plasma in laboratory experiments, charged dust grains are sustained to levitate by applying the sufficient external electrical field against the gravitational force [29, 74, 116]. Recently, some dusty plasma experiments have been carried out in space under micro-gravity conditions to avoid the gravitational effect on dust [97, 117–119]. D'Angelo showed the Rayleigh-Taylor instability in dusty plasmas [120] for wave frequencies much smaller (or much larger) than the charging frequency of the dust grains. Veeresha *et al.* [121] showed that this instability has driven nonlinear vortices in dusty plasmas. Recently, the Taylor instability has been observed in dusty plasma experiments by Pacha *et al.* [122]. Das *et al.* [123] (in the context of inertial fusion) using GHD description have shown the stabilization of transverse modes due to the strong coupling effects. Avinash *et al.* [124] showed that the elasticity of the strongly coupled dust is shown to set a threshold for the RT instability. The shear in a flow of any medium leads to the instability i.e. Kelvin-Helmholtz. In dusty plasma shear driven i.e. Kelvin-Helmholtz instability has been observed analytically [125–127], experimentally [128] and by simulation [67].

An inhomogeneous medium under gravity may experience to the buoyancy evolution i.e. falling droplets and rising bubbles. The falling droplet [129,130] and rising bubble [131] has been studied extensively in hydrodynamic fluids. Schwabe *et al.* [132, 133] also investigated the formation of microparticle bubbles and droplets in complex plasmas. Chu *et al.* [134] report a direct experimental observation of traveling microbubbles in complex plasmas induced by intense laser.

One of our goals is to study the nonlinear behaviour of dusty plasma by adding passive inertial particles in the considered visco-elastic medium. The mixing and diffusion of these particles with flow is a topic of a great relevance in many natural and industrial applications. In fluid mechanics it has been studied extensively for flow visualization [135, 136] by means of theoretical [137–143] and computational [144–155] as well experimental [156–160] approaches. This technique is also used in complex fluids (polymers, colloids and biological materials) [161, 162]. Schwabe *et al.* [163] numerically studied the vortex movements by adding some micro particles around the void in complex plasma simulation.

1.5 Outline of the thesis

This doctoral thesis reports the collective behavior demonstrated by the GHD model for the dusty plasma medium. Emphasis is given to the understanding of the evolution of coherent structures, certain instabilities (e.g. Kelvin-Helmholtz, gravitational and buoyancy-driven instabilities) and their associated transport and mixing properties. Detailed numerical simulation studies have been carried out to understand the nonlinear regime of these phenomena. We provide below a chapterwise summary of the work carried out in this thesis.

In Chapter 2, the GHD model supports the existence of both incompressible transverse shear and compressible longitudinal modes [48]. To concentrate on the incompressible features of this system, we separate out the compressibility effects altogether. For this purpose, the incompressible limit of the GHD (i-GHD) coupled set of equations has been obtained. The density perturbations in this limit are altogether ignored and the Poisson's equation is replaced by the quasi-neutrality condition. The i-GHD set of equations then casts as a coupled set of convective equations which is numerically evolved with the help of the flux-corrected scheme of Boris *et al.* [31].

The numerical code is validated by studying the emission of radially propagating transverse shear waves from a smooth circular rotating vortex. The radial transverse shear waves traveling with phase velocity $\sqrt{\eta/\tau_m}$ as predicted analytically by Kaw *et al.* [48] are confirmed by our simulations. Furthermore, the expected $1/r$ fall of the intensity of the waves in the circular geometry of the system in is also confirmed by our studies.

Often the vorticity structure in a fluid may not have a circular shape. We consider, therefore, for our studies an initial distorted patch of vorticity. A simple elliptical form of distortion has been considered. We have also investigated the process of interaction between various vortex structures within the GHD formalism for a strongly coupled medium. It is well known that a sharp shear profile is susceptible to the well-known Kelvin-Helmholtz instability. We avoided the K-H destabilization by considering smooth vorticity patches and concentrated solely on understanding the evolution of vorticity patches in both strong and weak coupling limits. The prominent feature of i-GHD model is that it supports the transverse shear waves. To scrutinize the effect of these TS waves on the evolution and interaction between distinct vortex structures, an extensive numerical simulation has been performed for i-GHD system. A comparison with Hydrodynamic (HD) system has also been provided. In particular, we consider two cases. First is the interaction and subsequent merging of two like-signed vorticity patches. We observed that in i-GHD formalism the merging does not lead to a coherent final form like hydrodynamic fluids [164–166]. The continuing emission of TS waves dominates over the merging process because each of the vortex patches also emits the TS waves, as expected. In second case we study a dipolar structure, which gets formed when two unlike-signed vorticity patches are brought in the vicinity of each other. This dipolar structure propagates along the direction of its axis as a single stable entity in hydrodynamic fluids. Moreover, we keep in view that TS waves travel with the phase velocity $\sqrt{\eta/\tau_m}$. We have considered two types of dipoles, viz. moving slower/faster than the phase velocity of the emitted waves. In the former slower case, the dipole remains engulfed inside the continuous emission of waves which reacts and ultimately distorts the original structure. For the second case of faster dipoles, the TS waves which are emitted from this dipolar structure remain confined in the form of a wake. The dipole, therefore, continues to move as a stable entity with a conical wake of waves trailing behind it. The collisional interaction of oppositely propagating dipole structures has also been studied.

In Chapter 3, a Poynting-like conservation theorem is constructed for the 2-D i-GHD model equations and obtained an enstrophy-like conserved quantity. The rate of change of this quantity (sum of square integrals of the vorticity and the velocity strain) is controlled by radiative, convective and dissipative effects. The radiation term corresponds to the TS waves and shows a striking similarity with electromagnetic waves. The equation also indicates that convective and viscous dissipation is another important mechanism that could significantly change the conserved quantity.

The Poynting-like theorem has been shown to be satisfied with the great precision in our numerical simulations for all the cases of vortex evolution considered in Chapter 2. These observations are likely to be generic and applicable to all strongly coupled media.

In Chapter 4, we study the evolution of sharp vorticity patches, which showed the K-H destabilization. The interplay of transverse shear waves and the K-H destabilization in the context of i-GHD fluid results in a good mixing of fluid material, unlike the HD case where the fluid seems to remain inside a confined domain for a long time. We also considered the evolution of a multi-circulation vortex profiles. We have found that at intermediate time range, it provides a complete picture of a turbulent flow which is a collection of small vortices and waves. When the system is left for a very long time, it ultimately relaxes to a single vortex faster than in hydrodynamic fluid. Additionally, we found that the relaxing rate of this turbulent medium increases with the increasing coupling strength.

To quantify the mixing and transport features in the presence of TS waves, we have also studied the dynamical evolution of test tracer particles. The diffusion and clustering of these test particles are directly linked to the mixing characteristic of a medium [167]. The displacement of these particles provides a quantitative estimate of the diffusion coefficient of the medium. We also showed that often these test particles organize themselves in a spatially inhomogeneous distribution. Phenomenon of clustering amongst these particles is clearly evident from the simulation results.

In Chapter 5, we consider an inhomogeneous dusty plasma medium which is stratified against gravity. We observe that the visco-elasticity of the strongly coupled medium leads to a suppression of these instabilities. This has been illustrated by a local linear analysis as well as by numerical simulations of density inhomogeneity stratified against gravity. The dynamical evolution and propagation of light density bubbles in heavier fluid as well as higher density droplets in a lighter density media were also considered. We found that the falling/rising rate of droplet/bubble gets decreases with the increasing coupling strength.

In Chapter 6, we summarize our findings and also provide the future scope for the thesis work.

2

Visco-elastic fluid simulations of coherent structures in strongly coupled dusty plasma medium

In this chapter the incompressible limit of the Generalized Hydrodynamic equations for the dusty plasma medium has been obtained. The numerical implementation of the incompressible set of GHD (i-GHD) equations in 2-D has been illustrated. The validation of the code is carried out by considering a circular rotating vorticity profile using this set of equations and observing the emission of transverse shear (TS) waves.

Furthermore, the chapter focuses on the study of nonlinear dynamical characteristic features of this model. Specifically, the evolution of coherent vorticity patches is being investigated.

2.1 Introduction

The strongly coupled dusty plasma system has been analysed with the help of coupled set of continuity, generalized momentum and Poisson equations, both analytically as well as numerically to a great extent in the past studies [48, 68, 77, 83, 84, 87–90]. The set of these equations permits both the existence of incompressible transverse shear and compressible longitudinal modes. In this chapter, we concentrate on the incompressible features of this system by separating out the compressibility effects. For this purpose, the incompressible limit of the GHD (i-

GHD) set of equations has been obtained. In the incompressible limit the Poisson's equation is replaced by the quasi-neutrality condition and charge density fluctuations are ignored. The reduced set of equation not only caters to the strongly coupled incompressible dusty plasma medium but also is relevant for any other incompressible visco-elastic system. The derivation of this reduced equation is discussed in detail in subsequent sections along with the procedure of its numerical implementation and validation.

For the validation of the numerical code, we have shown that a circular rotating vortex in strongly coupled limit (where elastic effects do feature in the GHD formalism) emits TS waves for different coupling parameters. The phase velocity of the TS wave agrees with the analytical prediction made by Kaw *et al.* [48]. In addition the radially emitted waves show a $1/\sqrt{r}$ fall in the amplitude as expected in this 2-D geometry. The hydrodynamic fluid, on the other hand, shows no emission. The vortex structure in this case remains intact, provided the Kelvin-Helmholtz (K-H) destabilization condition is either not satisfied anywhere by the sheared rotational velocity in the vorticity patch or the time scale under consideration is too short compared to the growth rate of such a destabilization process.

The radiative emission from monopoles have the same circular symmetry of the structure. In this regard, it is interesting to study the emission of waves from non-symmetric structures. A simple elliptical form of distortion has been considered by us. It would also be interesting to see evolution and interaction between distinct vortex structures in presence of TS waves. We consider, therefore, the merging phenomenon between two like-signed vorticity patches and the propagation of two unlike-signed vortices as single entity (namely dipole structure) in the context of i-GHD model. This dipole structure propagates along the direction of its axis as a single stable entity in hydrodynamic fluids. The evolution of dipole structures are studied in detail and has been presented in subsection 2.5.1. In i-GHD formalism, it shows that the dipoles also emit transverse shear waves as expected. However, there are two different cases considered in the simulation. When the dipole moves slower than the phase velocity of the emitted waves (sub-luminar), it gets totally engulfed within the propagating waves which react and distort the original dipole structure pretty soon. In the other limit (super-luminar), when the dipoles move faster than phase velocity of the transverse shear waves in the medium, the TS waves are emitted from the tail of the structure in the form of a wake. The dipole, however, continues to move as a stable entity with a conical wake of waves trailing behind it. We also carry out studies to understand the collisional interaction of oppositely propagating dipole structures discussed in subsection 2.5.2. Here too they behave like hydrodynamic fluid, they exchange partners and move in the orthogonal direction in the super-luminar cases.

The chapter has been organized as follows. Section 2.2 contains the details of the governing equations. In Section 2.3, a brief description of the numerical approach has been discussed. In Section 2.4, we present the simulation studies of a circular rotating vortex in the context of i-GHD model which emits transverse shear waves. This confirm the validity of our code. In Section 2.5, the merging phenomenon and various cases of dipole evolution and interaction have been presented showing the influence of the emitted transverse shear waves on the integrity of these structures. Finally a summary of the whole chapter is provided in the Section 2.6.

The subsequent chapters of this thesis utilize the i-GHD model set of equations to study various phenomena related to normal modes and instabilities.

2.2 Governing Equations

Incompressibility is always a good approximation while considering disturbances in the medium whose propagation is much slower than the sound speed. In the limit of incompressible flow dynamics, the density/potential perturbations can be ignored. Hence the momentum and continuity equations for i-GHD of strongly coupled homogeneous dusty plasma can be written as:

$$\left[1+\tau_m\left(\frac{\partial}{\partial t}+\vec{v}_d\cdot\nabla\right)\right]\left[\frac{\partial\vec{v}_d}{\partial t}+\vec{v}_d\cdot\nabla\vec{v}_d+\frac{\nabla P}{n_d}-\nabla\phi\right]=\eta\nabla^2\vec{v}_d, \tag{2.1}$$

and

$$\nabla\cdot\vec{v}_d=0, \tag{2.2}$$

respectively. Here η and τ_m are the kinematic viscosity and relaxation time parameter, respectively. The variables $\vec{v}_d$, ϕ and n_d are the dust fluid velocity, potential and number density, respectively. The normalisaton scheme of these equations is already discussed in details in Chapter 1. The standard Navier-Stokes equation can be achieved from Eq. (2.1) by taking $\tau_m = 0$. For our convenience, we can split the Eq. (2.1) in following two coupled equations:

$$\frac{\partial \vec{v}_d}{\partial t} + \vec{v}_d \cdot \nabla \vec{v}_d + \frac{\nabla P}{n_d} - \nabla \phi = \vec{\psi}, \tag{2.3}$$

$$\frac{\partial \vec{\psi}}{\partial t} + \vec{v}_d \cdot \nabla \vec{\psi} = \frac{\eta}{\tau_m} \nabla^2 \vec{v}_d - \frac{\vec{\psi}}{\tau_m}. \tag{2.4}$$

Thus the Eq. (2.1) has now been expressed as a set of two coupled convective equations. The gradient terms are eliminated by taking the curl of Eq. (2.3) which yields an equation for the evolution of the vorticity field. So the coupled set of Eqs. (2.3)-(2.4) has been recast in the following form:

$$\frac{\partial \vec{\xi}}{\partial t} + \vec{v}_d \cdot \nabla \vec{\xi} = \nabla \times \vec{\psi}, \tag{2.5}$$

$$\frac{\partial \vec{\psi}}{\partial t} + \vec{v}_d \cdot \nabla \vec{\psi} = \frac{\eta}{\tau_m} \nabla^2 \vec{v}_d - \frac{\vec{\psi}}{\tau_m}. \tag{2.6}$$

Equations (2.5) and (2.6) are a coupled set of closed equations for a visco-elastic fluid in the incompressible limit. These equations would be referred as i-GHD model equations henceforth in the thesis. Here, $\vec{\xi} = \nabla \times \vec{v}_d$ (here $\vec{\xi}$ is normalised with dust plasma frequency) is the vorticity. It should be noted that in this particular limit there is nothing specific which is suggestive of the fact that the system corresponds to a strongly coupled dusty plasma medium.

2.3 Numerical implementation and validation

For the validation of the numerical procedure several things were tested out. These include the dispersion relation of transverse shear wave. The dispersion relation (Fourier transform in space and time) of the transverse shear wave [48], obtained by linearizing the above set of equations is

$$\omega = \frac{-i\eta k^2}{1 - i\omega\tau_m}. \tag{2.7}$$

In the strong coupling limit of ($\omega\tau_m >> 1$) this yields

$$\frac{\omega}{k} = \sqrt{\frac{\eta}{\tau_m}}, \tag{2.8}$$

which implies wave propagation and in the other limit of ($\omega\tau_m << 1$)

$$\omega = -i\eta k^2,$$

we have the usual damping due to viscosity in hydrodynamic fluids. We have used the flux corrected scheme (Boris *et al.* [31]) to evolve the coupled set of Eqs. (2.5)-(2.6). The velocity field at every time step is obtained using the equation $\nabla^2\vec{v}_d = -\vec{\nabla}\times\vec{\xi}$, which uses the incompressibility condition of $\nabla\cdot\vec{v}_d = 0$. The equations were evolved for a slab sinusoidal perturbation and the dispersion relation for the transverse shear wave was verified numerically as a part of code validation [79]. In the next section we would show that a rotating vortex structure also emits transverse shear waves. The dispersion relation again agrees with Eq. (2.8). Moreover, the radial fall of the wave amplitude is $1/\sqrt{r}$ as expected in the 2-D circular geometry is also clearly shown to be verified.

2.4 Evolution of vorticity patches

A typical fluid flow contains a wide variety of coherent patterns in the form of localized vorticity patches. Their interaction and evolution are important for the understanding of the system which in turn is responsible for the transport properties of the system. The objective of the present work is to understand the dynamical characteristics of these entities for a strongly coupled system within the framework of the visco-elastic i-GHD model. The vorticity patches are chosen to be quite smooth so as to avoid sharp shear flows which may lead to the K-H destabilization. The case of sharp shear structures are considered in Chapter 4 wherein the added process of K-H destabilization is added. We consider the following specific cases, in particular: (i) evolution of circular and elliptical vorticity patches and (ii) interaction between vorticity patches of like and unlike signs. The vorticity patch representing a sheared rotation emits the transverse shear wave for a visco-elastic fluid, making the evolution significant in terms of rapid mixing and transport behaviour of the GHD fluid system.

2.4.1 Evolution of monopoles

We consider a radially smooth vorticity profile (clockwise rotation of the fluid) initially having the following spatial profile :

$$\xi_0(x, y, t_0) = \Omega_0 exp\left(-\frac{\left((x - x_c)^2 + (y - y_c)^2\right)}{a_c^2}\right). \tag{2.9}$$

Here $\Omega_0 = \Gamma_0/\pi a_c^2$, Γ_0 is the total circulation, a_c is the vortex core radius. x_c and y_c are the x and y coordinates of the center of the vorticity profile. This vorticity profile has circular symmetry. The numerical simulation has been carried out for a_c=1.5, $\Omega_0 = 8$ and $x_c = y_c = 0$. The simulation region is a square box of length 12π units with periodic boundary (PB) conditions.

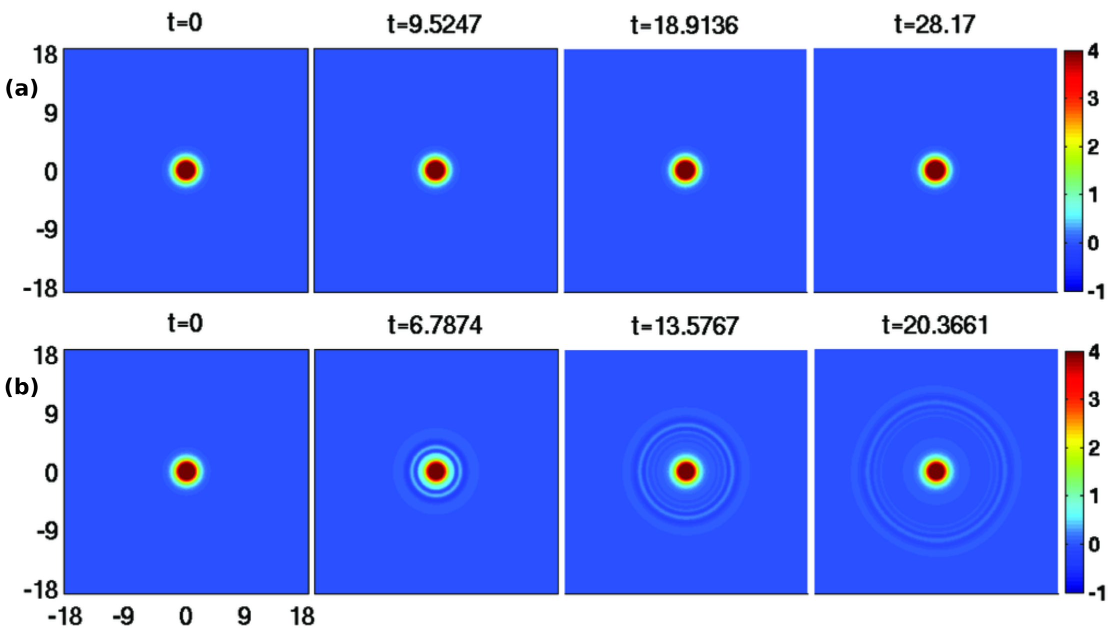

Figure 2.1: Evolution of smooth circular vorticity profile in time for (a) hydrodynamic fluid and (b) visco-elastic fluid with the parameters $\eta = 5$, $\tau_m = 20$.

In Fig. 2.1, we compare the evolution of such circular vorticity patch in the weakly coupled hydrodynamic fluid limit and the i-GHD model by plotting the color contours of vorticity. It can be observed that while the structure remains stable in the former case as shown in Fig. 2.1(a), in the latter strongly coupled limit the radial wave emission can be clearly observed in Fig. 2.1(b). This emerging waves have the same circular symmetry as that of the initially considered vorticity profile structure, until there is no boundary effect or no interaction with other waves or obstacle like vortex. The prime objective of the present section is to evaluate the speed of outgoing shear wave. Hence we limit our study to the time till the shear wave remains confined within the boundary. The boundary effects shall be discussed later.

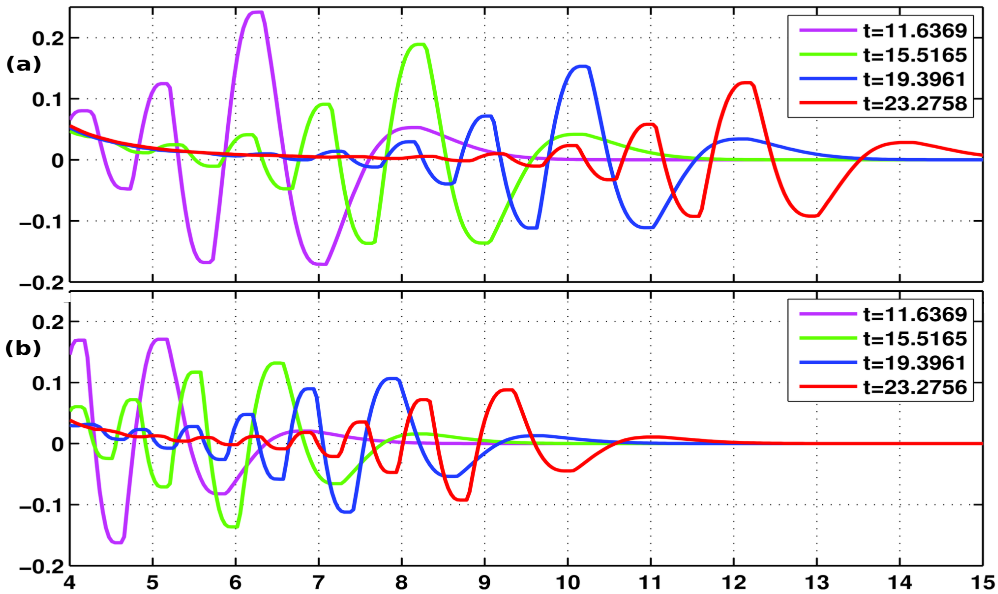

Figure 2.2: Radial emission (emerging wavefront) of TS waves along one of the axes at different times during vortex evolution in visco-elastic medium for the parameters (a) $\eta = 5, \tau_m = 20$ and (b) $\eta = 2.5$, $\tau_m = 20$ with different line styles.

A better depiction has been provided in Fig. 2.2, where the vorticity profile as a function of r has been plotted for various times. A perturbation clearly proceeds along radially outward direction. The radial speed of this perturbation has been evaluated and found to match with $\sqrt{\eta/\tau_m}$ as has been shown in Fig. 2.3(a). The circular nature of the emitted wave also suggests that the amplitude of these characteristic perturbations should display a $1/\sqrt{r}$ radial fall off. This has also been demonstrated numerically as shown in Fig. 2.3(b).

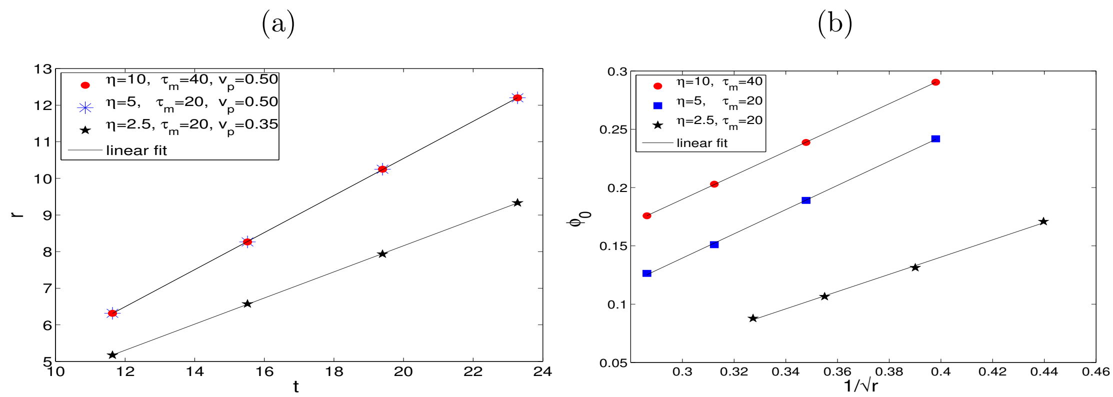

Figure 2.3: (a) Wavefront position of TS waves at different time steps with parameter values $\eta = 10, \tau_m = 40$ (●), $\eta = 5, \tau_m = 20$ ($*$) and $\eta = 2.5, \tau_m = 20$ (★), where v_p is the phase velocity related to corresponding parameters (of corresponding color) and black line is linear fitted curve and (b) Wavefront amplitude of TS waves with $1/\sqrt{r}$ with parameter values $\eta = 10, \tau_m = 40$ (●) , $\eta = 5, \tau_m = 20$ (■) and $\eta = 2.5, \tau_m = 20$ (★) with black line as linear fitted curve.

The emission of such TS waves is due to the possible local instability which has been found to exist in GHD description of strongly coupled dusty plasma medium as earlier discussed by Sanat *et al.* [79].

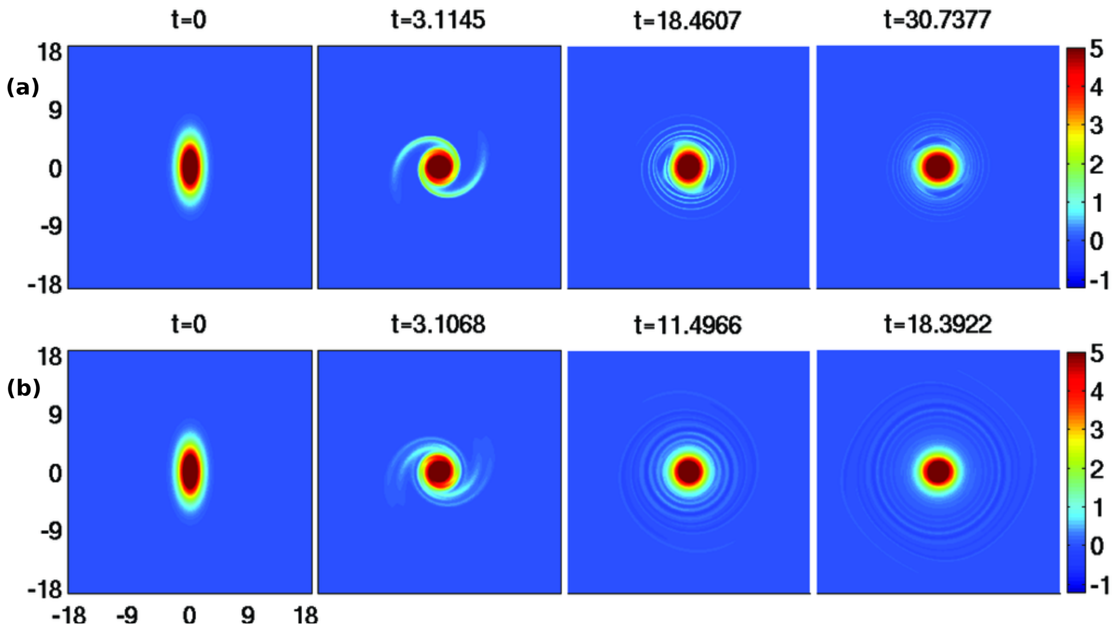

Figure 2.4: Evolution of elliptical vorticity profile in time for (a) hydrodynamic fluid and (b) visco-elastic fluid with parameters $\eta = 5, \tau_m = 20$.

Often the vorticity structure in a fluid may not have a circular shape. We consider, therefore, for our studies an initial distorted smooth elliptical vorticity patch. Various time frames of the evolution of such a vortex pattern in both HD and GHD case has been shown in Fig. 2.4 for smooth elliptical vorticity patch.

For the elliptical perturbation even the HD case is not stable and adjusts its vorticity to ultimately acquire a circular shape. The GHD seems to acquire this shape considerably faster by emitting the transverse shear waves.

2.5 Interaction between vorticity patches

We have also investigated the process of interaction between various vortex structures within the GHD formalism for a strongly coupled medium. A comparison with HD system has also been provided.

2.5.1 Evolution of dipole structures

When two monopoles rotating in opposite directions (i.e. unlike-sign vortices) are brought close, they take shape of a dipole which propagates along the direction of its axis as a single stable entity in the context of Newtonian fluids as shown in Fig 2.5.

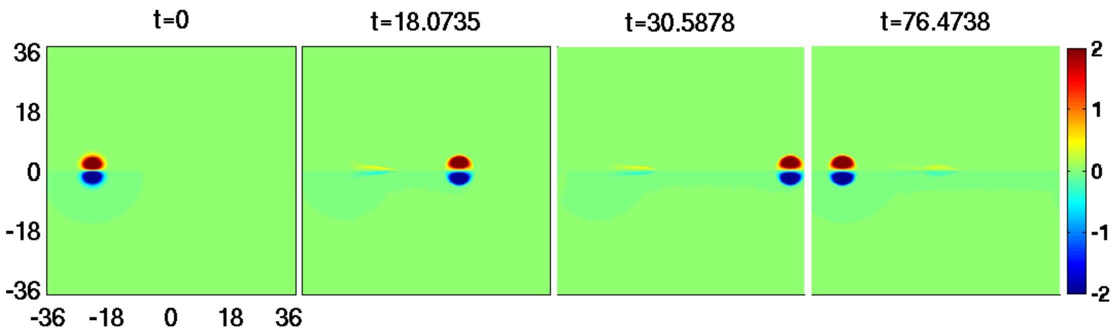

Figure 2.5: Evolution of dipole in time for hydrodynamic fluid

For present case the dipole vorticity profile is given by

$$\xi_0(x, y, t=0) = \Omega_0(y - y_c) exp\left(-\frac{((x-x_c)^2 + (y-y_c)^2)}{a_c^2}\right). \tag{2.10}$$

Here a_c is the vortex core radius and numerical simulation has been carried out for a_c=2.5, $x_c = -24$ and y_c=0. The simulation region is a square box of length 24π units with periodic boundary (PB) conditions.

Figures 2.6 to 2.8 show three different cases of simulations in the context of i-GHD model for the same system of dipole, shown in Fig 2.5. The values of the coupling parameters $\eta = 5$ and $\tau_m = 20$ have been chosen to be same for all these three cases. The transverse shear waves emerge with the phase velocity $v_p = \sqrt{\eta/\tau_m} = 0.5$ for the parameters chosen for these simulations. The three cases (a, b and c) have different amplitude of vorticity (Ω_0 of 3.5, 5 and 7.5 respectively) which makes them move with the increasing axial speeds. The axial speed of the dipoles v$_{dip}$ turns out to be 0.4$<v_p$, 1.14$>v_p$, and 2.29$>v_p$, for cases (a), (b) and (c) respectively. This is evident from the plot of traversed distance vs. time for the peak of the structure shown in Fig. 2.9 for the three cases, where the respective slope corresponds to v$_{dip}$. Clearly, while case (a) corresponds to the sub-luminar speed of the dipole, (b) and (c) are super-luminar.

For all these three cases the dipole emits transverse shear wave. However, in case (a) the sub-luminar dipole of Ω_0=3.5 gets completely engulfed into the emissions. These emissions then react on the original structure and the distortions increase with time. It should also be noted that the emission from each of the lobes gets significantly impeded by that of the other as a result of which the emission profile is no longer symmetrically centered around each of the lobe. The wave emission from each lobe pushes the other lobe as a result of which the tail end of the two lobes can be seen to get pushed away significantly apart. This increased separation between the two lobes, as well as the continuous sapping of the strength of the dipole due to wave emission, appears to impact the dipole propagation speed which can be observed to slow down as shown in Fig. 2.6 and there is also a considerable distortion in the structure. At later times the lobes have been observed to rotate and newer structures emerge, resulting in a reformed weak dipole with reversed polarity propagating backwards to its original direction. In the process of such a reformation the merging of like-sign vorticity patches and emission patterns play an important role. Ultimately, the identity of the original dipole structure gets completely lost.

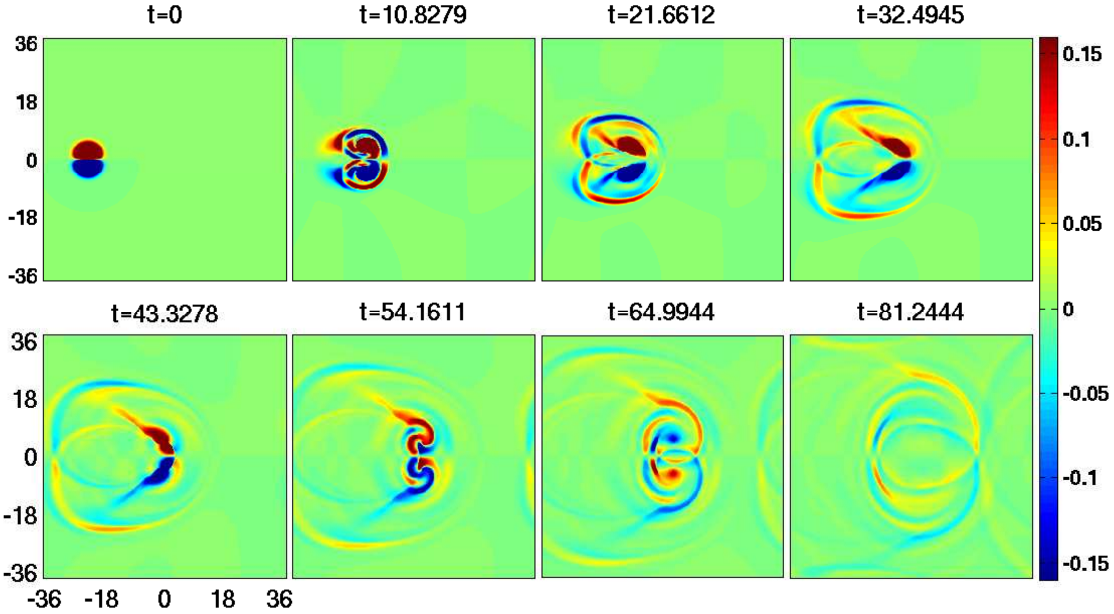

Figure 2.6: Evolution of sub-luminar dipole in time for visco-elastic fluid of Ω_0=3.5 with the coupling parameters $\eta = 5, \tau_m = 20$.

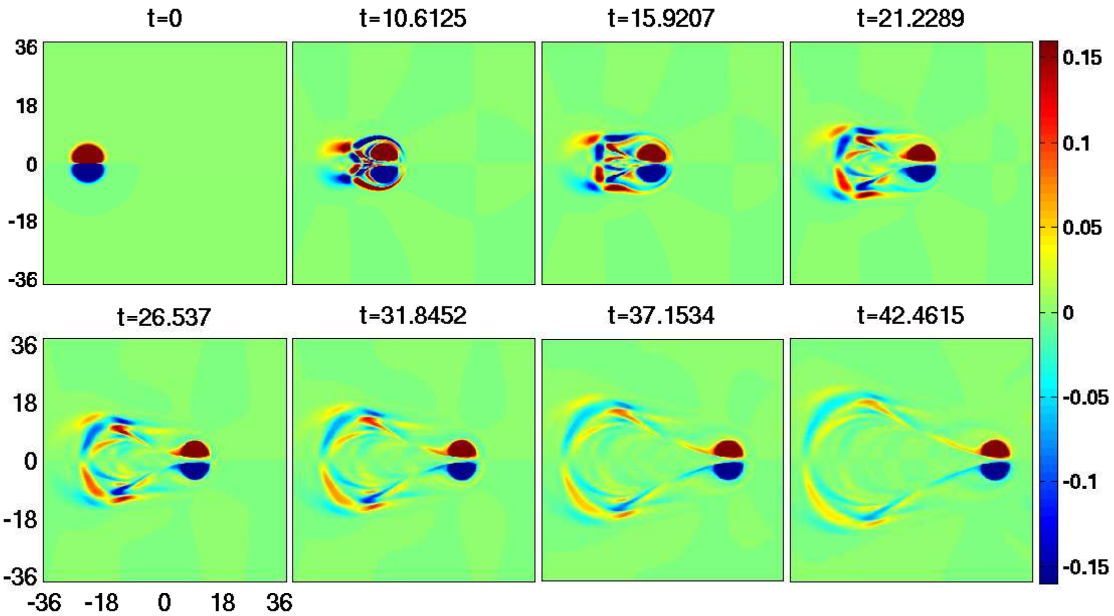

Figure 2.7: Evolution of super-luminar dipole in time for visco-elastic fluid of Ω_0=5 with the coupling parameters $\eta = 5, \tau_m = 20$.

In the other two cases (b) and (c) of Ω_0=5 and 7.5 respectively, however, the dipole structure continues to maintain its identity. The wave emission in these cases (because of the super-luminar velocity of dipole) remains confined to a conical spatial regime at the tail. The radiation merely separates the tail region of the dipole.

In case (b), we show the evolution of super-luminar dipole (i.e. larger velocity amplitude) with more strength of Ω_0=5 than the former case (a). In this case we restrict the speed of dipole to be not too large, so that it leaves behind wake structures. It can be observed that there is wake-type structure formation as it is evident from Fig. 2.7.

In Fig. 2.8, we consider the case (c) of another super-luminar dipole of Ω_0=7.5 moving with more strength than the both former cases (a) and (b). The dipole gets out of the cage of the wake structures.

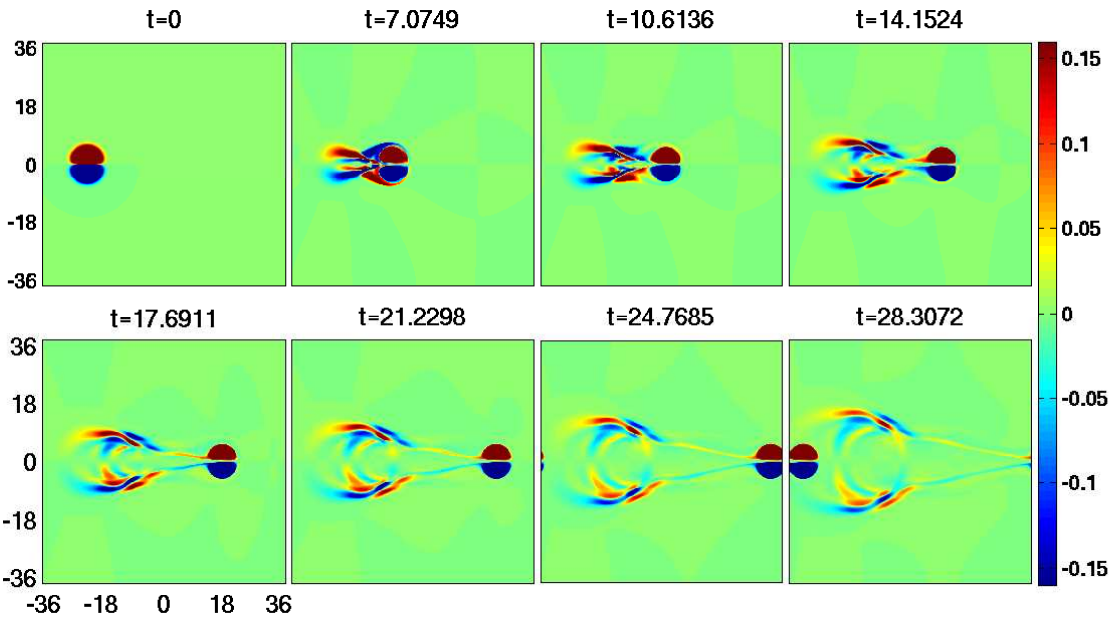

Figure 2.8: Evolution of super-luminar dipole in time for visco-elastic fluid of Ω_0=7.5 with the coupling parameters $\eta = 5, \tau_m = 20$.

We also observed that with the increase in the speed of the dipole, the angle of the cone that confines TS wave radiation gets reduced.

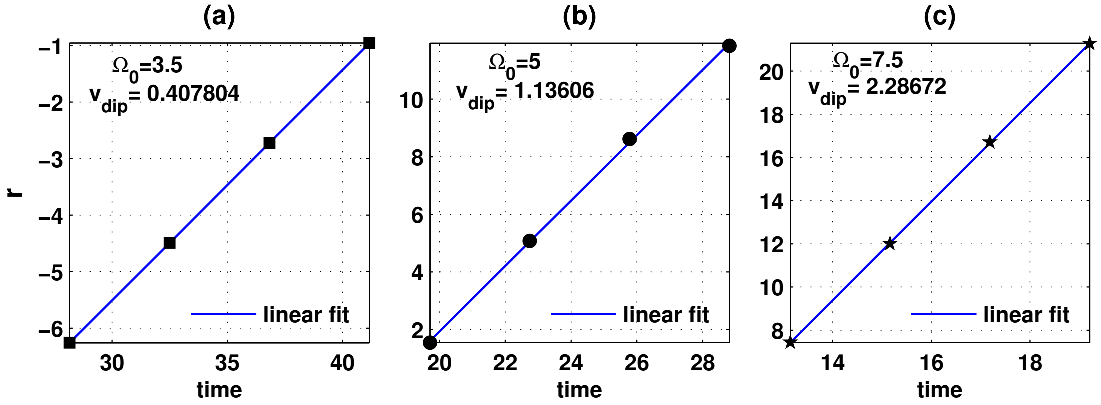

Figure 2.9: Position of the maximum of the dipole amplitude at different time steps along the axial direction with the parameter values (a) Ω_0=3.5 (■); v$_{dip}$ = 0.4<v_p corresponds to sub-luminar dipole, (b) Ω_0=5 (•); v$_{dip}$ = 1.14>v_p corresponds to super-luminar dipole, and (c) Ω_0=7.5 (★); v$_{dip}$ = 2.29>v_p is also corresponds to super-luminar dipole, where v$_{dip}$ is the corresponding axial velocity of dipole related to Ω_0 and the blue line is linear-fitted curve.

2.5.2 Head-on collision between dipoles

When two oppositely propagating dipoles collide with each other, it is well known in the context of hydrodynamics, that their lobes exchange partners and form a new dipolar structure which propagates orthogonally to the initial propagation direction. This can be observed from the Fig. 2.10. We consider two dipoles whose vorticity profile is given by $\xi_0(x, y, t_0) = \xi_{01}(x, y, t_0) + \xi_{02}(x, y, t_0)$. Here, the left side dipolar vorticity is:

$$\xi_{01}(x, y, t_0) = \Omega_{01}(y - y_{c1})exp\left(-\frac{\left((x - x_{c1})^2 + (y - y_{c1})^2\right)}{a_{c1}^2}\right), \tag{2.11}$$

and the right side dipolar vorticity is:

$$\xi_{02}(x, y, t_0) = \Omega_{02}(y - y_{c2})exp\left(-\frac{\left((x - x_{c2})^2 + (y - y_{c2})^2\right)}{a_{c2}^2}\right), \tag{2.12}$$

with the parameters a_{c1}=a_{c2}=2.5, $x_{c1} = -24$, y_{c1}=0, $x_{c2} = 24$, y_{c2}=0 and Ω_{01}=Ω_{02} for equal strength dipoles. In cases of disparate strength dipoles $\Omega_{01} \neq \Omega_{02}$.

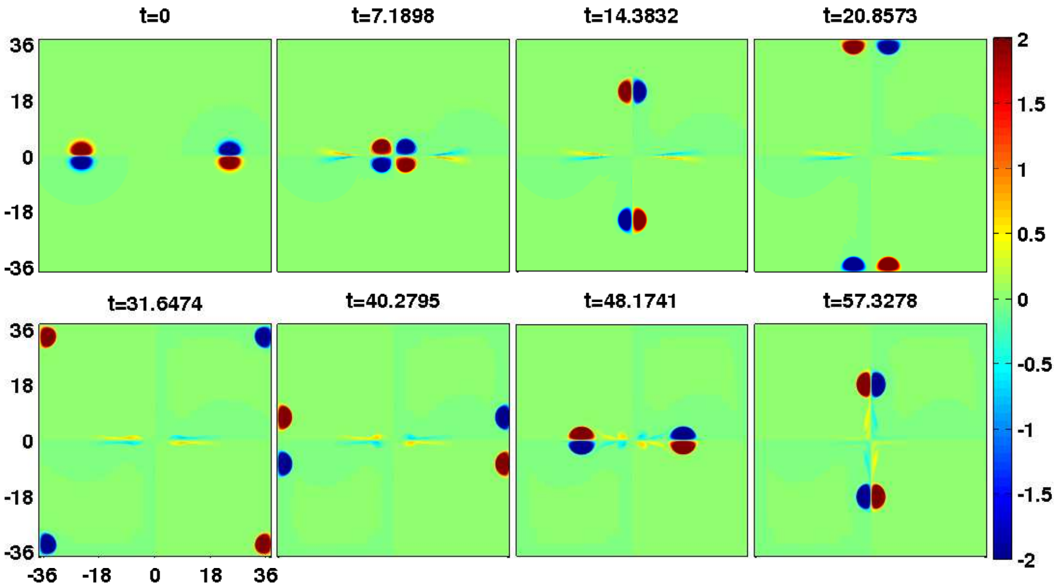

Figure 2.10: Head-on collision between two dipoles for hydrodynamic fluid with Ω_{01}=Ω_{02}=7.5.

Similar effect is observed in the context of collision in i-GHD system. We again consider the two cases of collision between two equal strength sub- and super-luminar pairs of dipoles in Fig. 2.11 and Figs. 2.12, 2.13 respectively. The coupling parameters ($\eta = 5, \tau_m = 20$) are same for all these cases.

In Fig. 2.11 the radiation engulfs the dipoles. The two equal strength sub-luminar dipoles of Ω_{01}=Ω_{02}=3.5 slow down considerably as they move towards each other. This happens due to the preceding waves from each structure that inhibits their propagation forward. They almost become standstill before exchanging partners and moving in the orthogonal direction. The identity of the dipolar lobes is ultimately completely lost due to the interaction with the emitted shear waves.

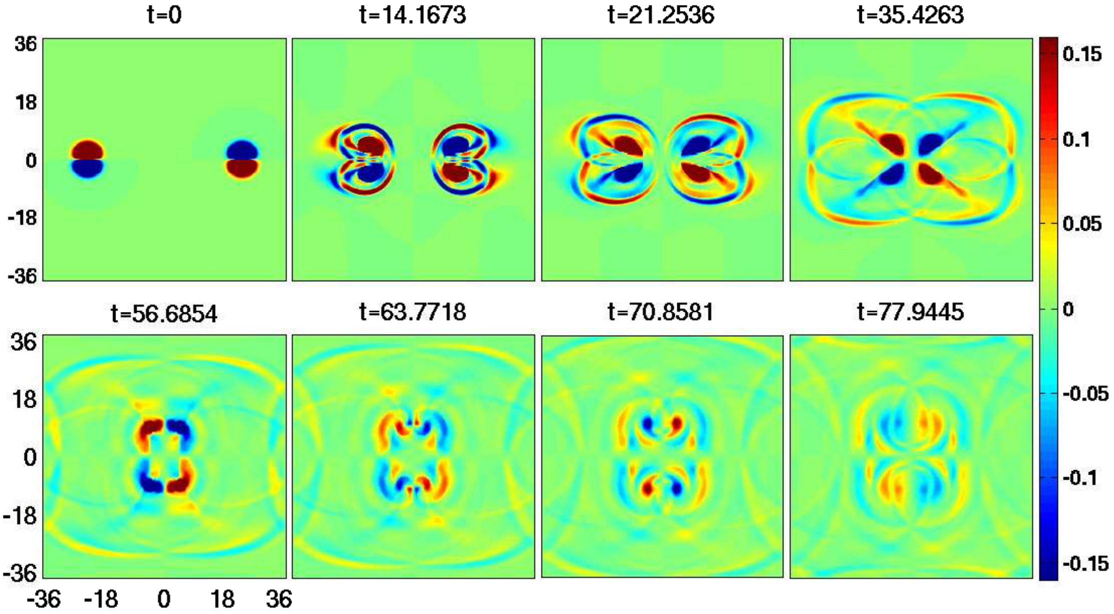

Figure 2.11: Head-on collision between two equal strength sub-luminar dipoles for visco-elastic fluid of Ω_{01}=Ω_{02}=3.5 with the coupling parameters $\eta = 5, \tau_m = 20$.

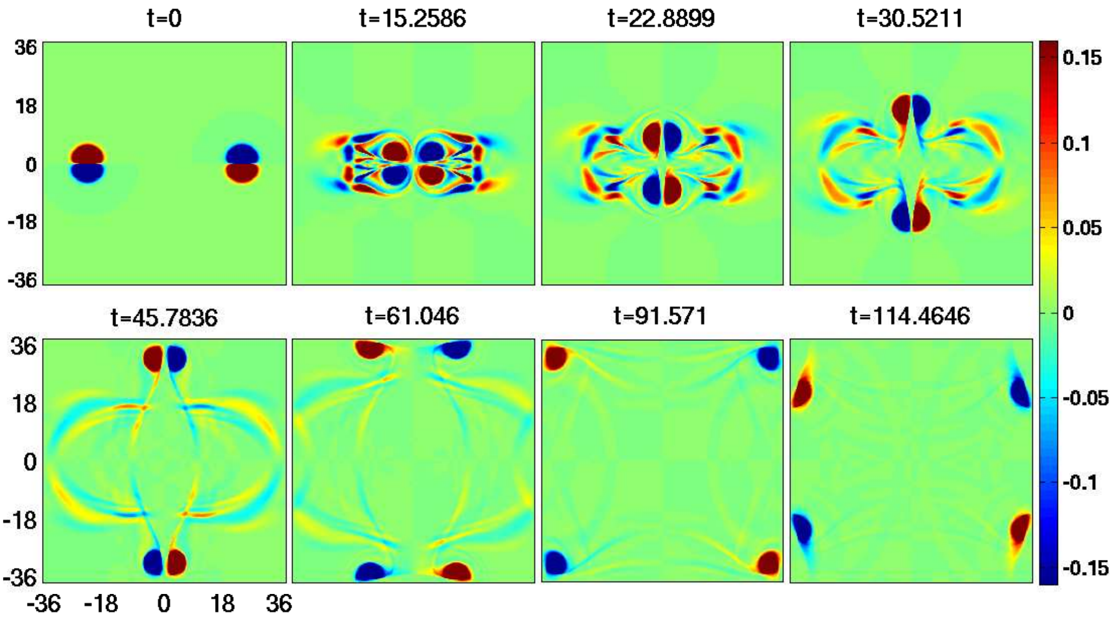

Figure 2.12: Head-on collision between two equal strength super-luminar dipoles for visco-elastic fluid of Ω_{01}=Ω_{02}=5 with the coupling parameters $\eta = 5, \tau_m = 20$.

In the second case the two equal strength super-luminar dipoles of Ω_{01}=Ω_{02}=5 exchange partners and move ahead in the orthogonal direction leaving the radiation behind. This can be observed from the Fig. 2.12.

In Fig. 2.13, we consider the case of an other two equal strength super-luminar dipoles of Ω_{01}=Ω_{02}=10 approaching toward each other with more strength than the former cases of Ω_{01}=Ω_{02}=3.5, 5. The damage in this case to the lobes is very weak and the dipoles retain their identity.

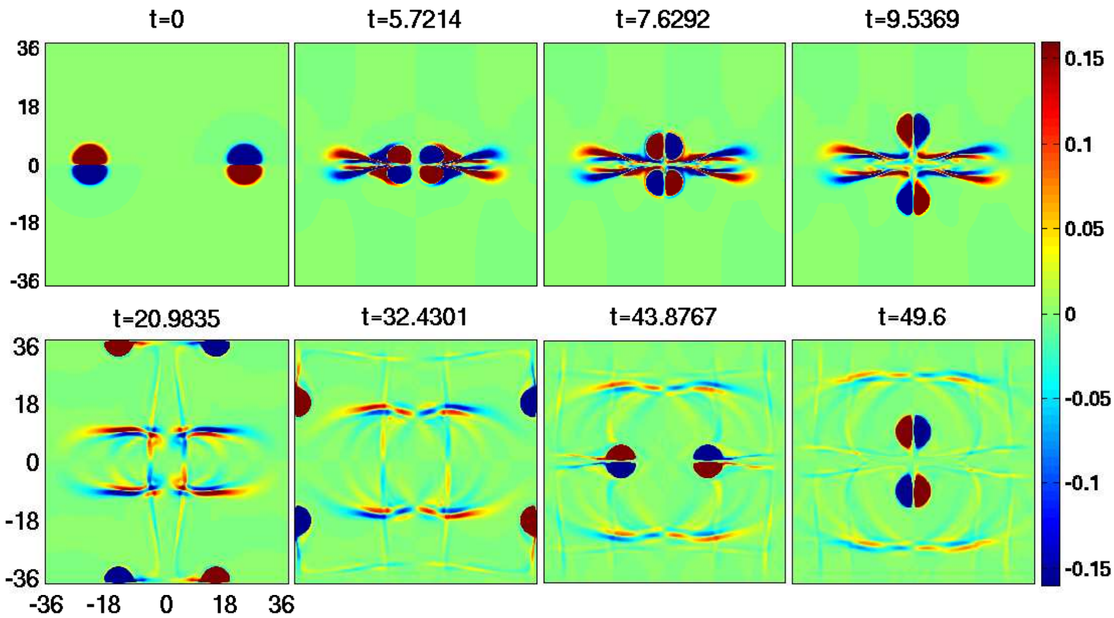

Figure 2.13: Head-on collision between two equal strength super-luminar dipoles for visco-elastic fluid each of Ω_{01}=Ω_{02}=10 with the coupling parameters $\eta = 5, \tau_m = 20$.

Collisional interactions of disparate strength dipoles have also been studied. In Fig. 2.14, we consider two disparate strength dipoles. The sub-luminar dipole on the left has Ω_{01}= 3.5 and the super-luminar dipole on the right has Ω_{02}=10. As opposed to the normal case where the dipoles of equal strength propagate in the direction normal to the direction of propagation before collision, for the present case as evident from Fig. 2.14, the super-luminar dipole pierces into the lobes of sub-luminar dipole. It can be clearly seen, after the accomplishment of this crossing process, the lobes of sub-luminar dipole again come close to each other and start propagating like an independent dipole. It is interesting to note that there is no exchange of lobes between dipoles. Both these dipoles (sub and super) propagate in the same direction as before collision. As time progresses, these dipoles interact with the wake-type structures (left behind by them) and sub-luminar dipole loses its identity earlier than super-luminar dipole.

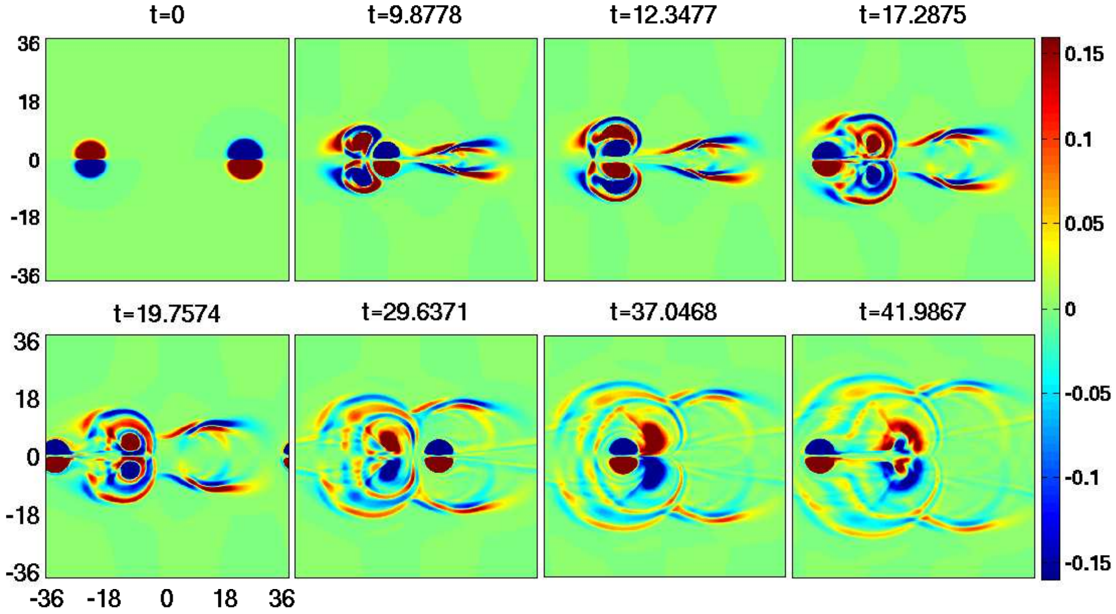

Figure 2.14: Head-on collision between two disparate strength dipoles, sub-luminar dipole (left) of Ω_{01}= 3.5 and super-luminar dipole (right) of Ω_{02}=10 with the coupling parameters $\eta = 5, \tau_m = 20$.

In Fig. 2.15, we consider two super-luminar disparate strength dipoles, of Ω_{01}=7.5 (left) and Ω_{02}=10 (right). It is observed after exchanging lobes, these new dipoles change their trajectory and along with the axial motion, the weaker lobe rotates around the stronger lobe. With this rotation, new dipoles of unequal lobe strength approach each other and collide again. The exchange of lobes takes place once again and the newly formed dipoles (with same lobes as before collision process) starts propagating in the same direction just as before collision. This collisional process repeats again and again due to PB conditions and the dipoles also experience the interaction with the wake left behind by them.

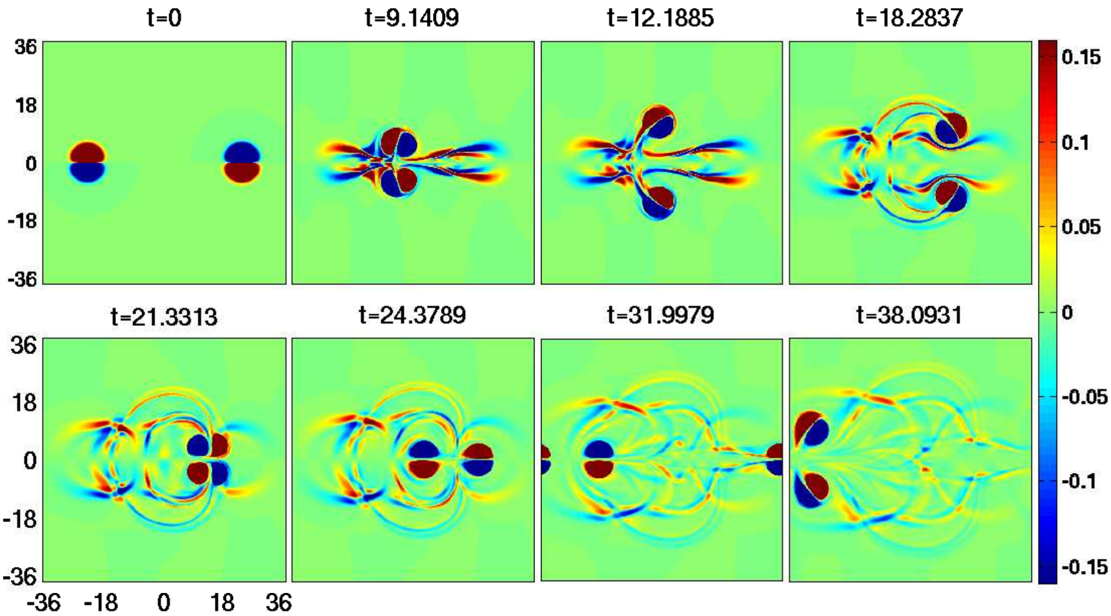

Figure 2.15: Head-on collision between two disparate strength super-luminar dipoles of Ω_{01}= 7.5 (left) and Ω_{02}= 10 (right) with the coupling parameters $\eta = 5, \tau_m = 20$.

2.5.3 Merging

The interaction and subsequent merging of two like signed vorticity patches have been well known in the context of a hydrodynamic system [164–166] as shown in Fig. 2.16(a). The same, in the case of i-GHD, has been illustrated in the subplots of Fig. 2.16(b).

In contrast to HD, the merging does not lead to a coherent final form, instead as expected the TS waves continue to dominate the system.

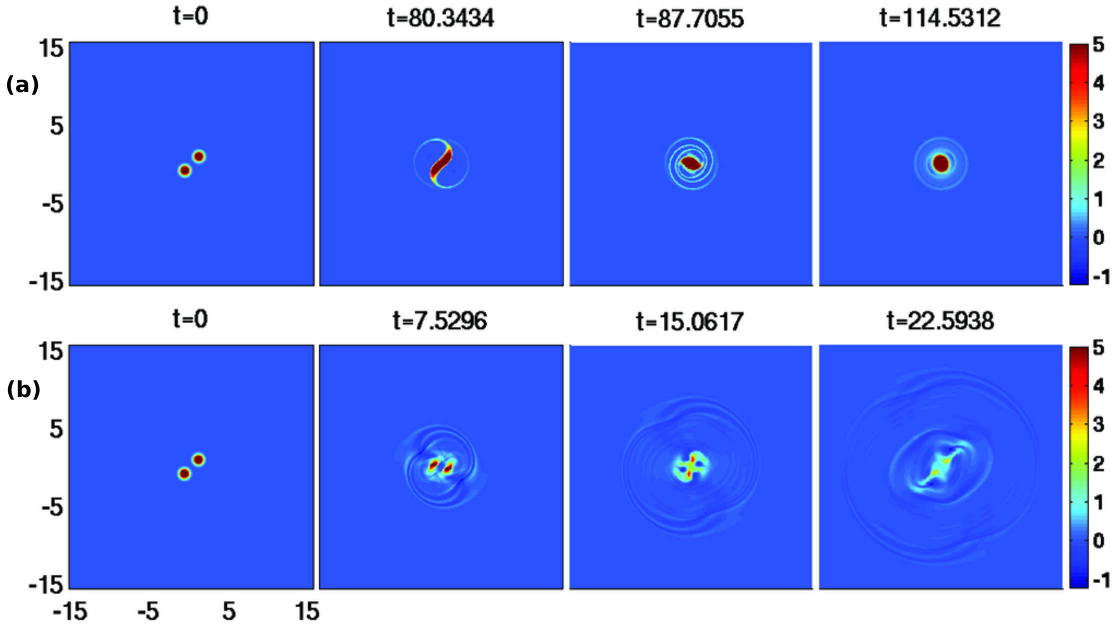

Figure 2.16: Evolution of two like sign vortices in time for (a) hydrodynamic fluid and (b) visco-elastic fluid with parameters $\eta = 5, \tau_m = 20$.

The emission of transverse shear waves appears to have a predominant role in the mixing and transport of the fluid elements in the context of the visco-elastic GHD system. The strong mixing can be suppressed provided that the TS waves have damped characteristics in the medium.

2.6 Summary

The evolution and interaction of localized vortex patterns for a strongly coupled medium depicted by the visco-elastic i-GHD description have been studied. The incompressible limit of the model which supports transverse shear wave mode is studied in detail. We have shown numerically, in particular, for the smooth rotating vorticity profile the emission of transverse shear waves traveling with phase velocity $\sqrt{\eta/\tau_m}$ as expected analytically from GHD model.

The interactions between TS waves and coherent structures have shown the generation of various complicated radiation and convection pattens during their evolution. To provide the insights on the evolutionary behavior of this complicated system, in the Chapter 3, a Poynting-like conservation law is constructed analytically for the i-GHD set of equations and numerically verified for the non-linear structures discussed in present Chapter i.e. monopole and dipole (sub- and super-luminar dipole) and their collision.

Our studies show that due to the existence of such transverse shear waves in the strongly coupled medium, the mixing and transport behaviour in these fluids are much better than in Newtonian hydrodynamic systems. The chances of fluid element and/or test particles to remain entrained for long duration within a localized region are insignificant in i-GHD when compared with the Newtonian fluid. In the Chapter 4, we have quantified this transport behaviour by carrying out test particle simulations in the system of i-GHD model.

3

A conservation theorem for incompressible Generalized Hydrodynamic fluid model

In the Chapter 2, the incompressible limit of GHD (i-GHD) model which supports transverse shear wave mode is studied in detail. In this chapter, a Poynting-like conservation law is obtained from the 2-D i-GHD equations, where radiative, convective and dissipative terms are shown to be responsible for the evolution of W, which is similar to "enstrophy" like quantity in normal hydrodynamic fluid systems. The conservation law is shown to be satisfied to a great accuracy for the evolution and interaction of nonlinear structures like monopole and dipole (sub-and super-luminar dipole) and their collision.

3.1 Introduction

In the Chapter 2, it was shown that in contrast to Newtonian fluids, visco-elastic fluid (described by i-GHD model) supports the emission of transverse shear waves from the rotating vorticity patches. The phase propagation speed was observed to match the theoretical prediction of $\sqrt{\eta/\tau_m}$ as predicted by Kaw *et al.* [48]. The other important structure which has been studied extensively in the context of i-GHD has dipolar symmetry.

The conservation laws satisfied by any evolution equation help to provide important insights on the evolutionary behavior of any system. Keeping this in view, the i-GHD set of equations was analyzed for a possible construction of such laws. We obtain a kind of Poynting theorem for an enstrophy-like integral associated with the i-GHD system. The mean square integral quantity is shown to decay due to dissipation and through convection and emission of waves. The validity of this theorem is then numerically verified over a considered local circular regime for nonlinear structures like monopole and dipole structures in both sub/super luminar limits (i.e. when the propagation speed of the dipole is slower/faster than the TS wave phase velocity) and their collision. It is shown that monopole structures which do not move at all but merely radiate shear waves, the radiative term and dissipative losses solely contribute to the evolution of W. The dipolar structures, on the other hand, propagate in the medium and hence convection also plays an important role in the evolution of W.

The present chapter has been organized as follows. In Section 3.2, we derive analytically a Poynting-like conservation equation for our i-GHD system. In Section 3.3, we present the simulation studies which confirm the validity of the Poynting-like theorem and help to identify the dominant mechanism of the decay for the enstrophy-like integral of the system. Section 3.4 contains the summary of the whole chapter.

3.2 A Poynting-like theorem for the coupled set of i-GHD

A Poynting-like theorem can be obtained for the i-GHD model. Such conservation equations are in general a powerful tool for any system. They provide new interesting physical insights for the system and can also be employed for validating as well as discerning the accuracy of any numerical program.

Taking the dot products with respect to $\vec{\xi}$ and $\vec{\psi}$ for Eqs. (2.5) and (2.6) respectively, we obtain:

$$\frac{1}{2}\frac{\partial \xi_z^2}{\partial t} + \vec{\xi}\cdot(\vec{v}_d \cdot \nabla)\,\vec{\xi} = \vec{\xi}\cdot\nabla\times\vec{\psi}, \tag{3.1}$$

$$\frac{1}{2}\frac{\partial \psi^2}{\partial t} + \vec{\psi}\cdot(\vec{v}_d \cdot \nabla)\,\vec{\psi} = \vec{\psi}\cdot\frac{\eta}{\tau_m}\nabla^2\vec{v}_d - \frac{\psi^2}{\tau_m}. \tag{3.2}$$

It should be noted that the vorticity vector $\vec{\xi}$ in the 2-D geometry has only $\hat{z}$

component. We have the following vector relations:

$$\vec{\xi}\cdot(\vec{v}_d\cdot\nabla)\,\vec{\xi} = \nabla\cdot(\vec{v}_d\frac{\xi_z^2}{2}),$$

$$\vec{\psi}\cdot(\vec{v}_d\cdot\nabla)\,\vec{\psi} = \nabla\cdot(\vec{v}_d\frac{\psi^2}{2}),$$

$$\vec{\psi}\cdot\nabla^2\vec{v}_d = -\xi_z\cdot(\nabla\times\vec{\psi}) - \nabla\cdot(\xi_z\times\vec{\psi}).$$

Using the first vector relation and multiplying Eq. (3.1) by η/τ_m we have

$$\frac{1}{2}\frac{\eta}{\tau_m}\frac{\partial\xi_z^2}{\partial t} + \frac{\eta}{\tau_m}\nabla\cdot(\vec{v}_d\frac{\xi_z^2}{2}) = \frac{\eta}{\tau_m}\xi_z\cdot\nabla\times\vec{\psi}. \tag{3.3}$$

The other two vector relations are used in Eq. (3.2) to obtain:

$$\frac{1}{2}\frac{\partial\psi^2}{\partial t} + \nabla\cdot(\vec{v}_d\frac{\psi^2}{2}) = -\frac{\eta}{\tau_m}\xi_z\cdot(\nabla\times\vec{\psi}) - \frac{\eta}{\tau_m}\nabla\cdot(\xi_z\times\vec{\psi}) - \frac{\psi^2}{\tau_m}. \tag{3.4}$$

Now summing Eqs. (3.3) and (3.4), we get

$$\frac{\partial}{\partial t}\left(\frac{\psi^2}{2} + \frac{\eta}{\tau_m}\frac{\xi_z^2}{2}\right) + \nabla\cdot\frac{\eta}{\tau_m}(\xi_z\times\vec{\psi}) + \nabla\cdot\vec{v}_d\left(\frac{\psi^2}{2} + \frac{\eta}{\tau_m}\frac{\xi_z^2}{2}\right) = -\frac{\psi^2}{\tau_m}. \tag{3.5}$$

Clearly, the form of Eq. (3.5) is that of the Poynting-like equation:

$$\frac{\partial W}{\partial t} + \nabla\cdot\vec{S} + \nabla\cdot(T_d\vec{v}_d) + P_d = 0, \tag{3.6}$$

with following identifications:

$$W \equiv \left(\frac{\psi^2}{2} + \frac{\eta}{\tau_m}\frac{\xi_z^2}{2}\right),\quad \vec{S} \equiv \frac{\eta}{\tau_m}(\xi_z\times\vec{\psi}),\quad P_d \equiv \frac{\psi^2}{\tau_m}\quad and\quad T_d\vec{v}_d \equiv \left(\frac{\psi^2}{2} + \frac{\eta}{\tau_m}\frac{\xi_z^2}{2}\right)\vec{v}_d.$$

This shows that the rate of change of W depends on dissipation through P_d in the medium, a convective and radiative flux of $T_d\vec{v}_d$ and $\vec{S}$, respectively. The radiative Poynting flux, as we will see later, is associated with the emission of transverse shear waves in the medium. Equation (3.5) can also be recast in the following integral form:

$$\frac{\partial}{\partial t}\int_V W dv + \oint_S \vec{S}\cdot d\vec{a} + \oint_S T_d\ \vec{v}_d\cdot d\vec{a} = -\int_V P_d dv, \tag{3.7}$$

which corresponds to

$$\frac{\partial}{\partial t}\int_V \left(\frac{\psi^2}{2} + \frac{\eta}{\tau_m}\frac{\xi_z^2}{2}\right) dv + \frac{\eta}{\tau_m}\oint_S (\xi_z \times \vec{\psi})\cdot d\mathbf{a} + \oint_S \left(\frac{\psi^2}{2} + \frac{\eta}{\tau_m}\frac{\xi_z^2}{2}\right)\vec{v}_d\cdot d\mathbf{a} = -\int_V \frac{\psi^2}{\tau_m} dv \tag{3.8}$$

or

$$\underbrace{\frac{\partial}{\partial t}\int_V \left(\frac{\psi^2}{2} + \frac{\eta}{\tau_m}\frac{\xi_z^2}{2}\right) dv}_{\mathbf{dWdt}} = - \underbrace{\frac{\eta}{\tau_m}\oint_S (\xi_z \times \vec{\psi})\cdot d\mathbf{a}}_{\mathbf{S}} - \underbrace{\oint_S \left(\frac{\psi^2}{2} + \frac{\eta}{\tau_m}\frac{\xi_z^2}{2}\right)\vec{v}_d\cdot d\mathbf{a}}_{\mathbf{T}} - \underbrace{\int_V \frac{\psi^2}{\tau_m} dv}_{\mathbf{P}}. \tag{3.9}$$

It is important to physically analyse each of the terms. The contributions to **dWdt** arise from two mean square integrals. While ξ_z can easily be identified with the z component of vorticity which is typically conserved in two-dimensional Newtonian fluids, the quantity $\vec{\psi}$ relates to the strain created in the elastic medium by the time-varying velocity fields. Thus, **dWdt** is the sum of square integrals of vorticity and velocity strain. The radiation term **S** contains the integral of the cross product of $\xi_z\hat{z}$ and $\vec{\psi}$. This term is like a Poynting flux for the radiation corresponding to the transverse shear waves. A comparison with electromagnetic light waves where $\vec{E}\times\vec{B}$ acts as a radiation flux, shows that the corresponding two fields here are $\xi_z\hat{z}$ and $\vec{\psi}$. The equation also indicates that convection **T** (which would vanish if the velocity normal to the boundary region is zero) and viscous dissipation **P** through η are other important mechanism that could significantly change W.

Later, in Section 3.3 simulation studies have been presented and it is showed that the theorem is remarkably accurate even for the most complicated simulation cases that have been considered by us. It also helps to identify the prominent mechanism of decay in W in various scenarios.

3.3 Numerical verification of Poynting-like equation for i-GHD

We now study the role of different transport processes in the integral equation Eq. (3.9) on the evolution of W in the context of monopole, dipole evolution and dipole-dipole collision.

3.3.1 Monopole evolution

In the Chapter 2, we have investigated the emission of transverse shear waves from the rotating smooth vorticity profile in strongly coupled dusty plasma medium [168]. In this case the smooth vorticity profile is given by

$$\xi_0(x, y, t_0) = \Omega_0 exp\left(-\frac{\left((x-x_c)^2+(y-y_c)^2\right)}{a_c^2}\right). \tag{3.10}$$

The numerical simulation has been carried out for a_c=0.5, $\Omega_0 = 8$ and $x_c = y_c$=0. We found that phase velocity v_p of such waves is proportional to the coupling strength of the medium.

In Fig. 3.1 the evolution of a circular vorticity patch in the strong coupling limit with parameters $\eta = 2.5$ and $\tau_m = 20$ for i-GHD system has been shown. A circle with a radius of 0.6π units has been drawn in the plots. Initially all the action is within this circular boundary. However, as time progresses, the waves are emitted which cross this boundary. We investigate the validity of the integral Eq. (3.9) within this boundary. Our simulation region is a square box of the length 2π units with periodic boundary (PB) conditions. The PB ensures that the waves would not only propagate out of the circular demarcated region but would also enter it subsequently from the other side due to the periodicity of the square box. In fact, the evidence is clear from the subplots in the second row of the Fig. 3.1*.

*Fig. 3.1 appeared on the cover page of the *Phys. Plasmas 23(1), 2016*

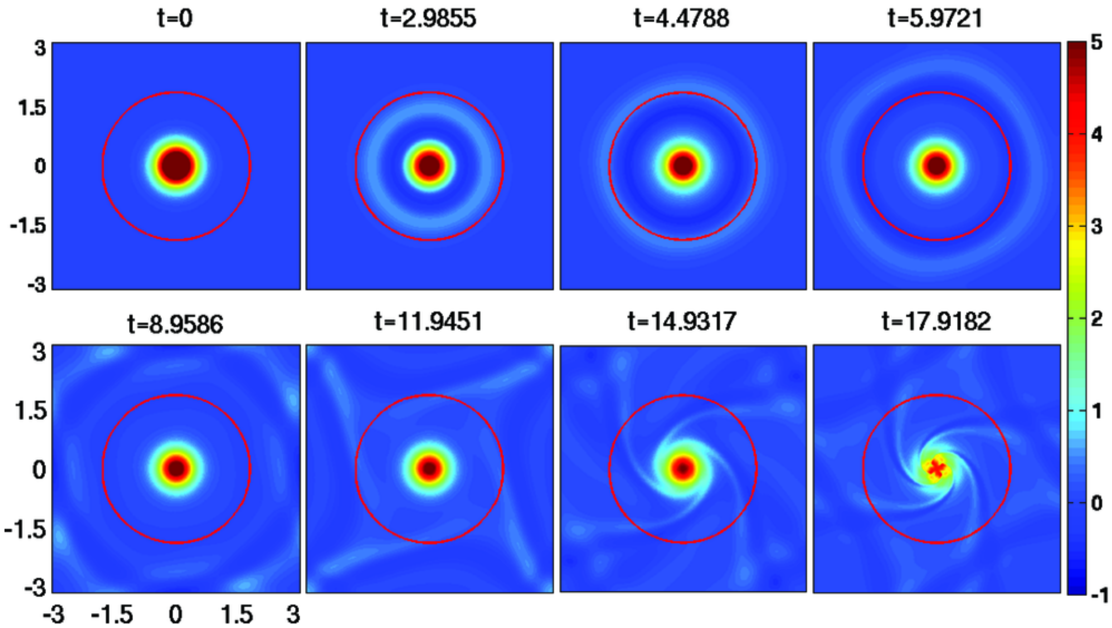

Figure 3.1: Evolution of smooth circular vorticity profile in time for visco-elastic fluid with the parameters $\eta = 2.5, \tau_m = 20$ and a circular local volume element (inside the circumference) over which the different transport quantities are calculated.

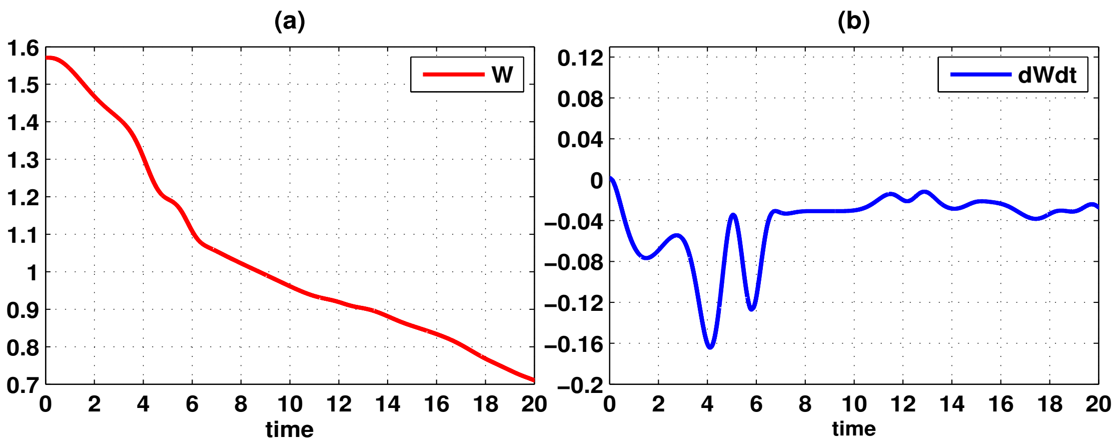

Figure 3.2: Subplot (a) shows the evolution of W and the subplot (b) shows $\mathbf{dWdt}$ for the rotating circular vorticity profile within our considered regime.

The change in the magnitude of W within the circular region with time is shown in the Fig. 3.2(a). We observe a steady decay in the magnitude of W. It is clear from the plot that the rate of decay of W is not constant. Thus, the sum of the contribution of various terms in Eq. (3.9), which defines the evolution of W, changes with time. The Fig. 3.2(b) shows the corresponding change in **dWdt** *i.e* the left hand side of integral Eq. (3.9) with time. The evolution of various terms has been shown in the subplots of Fig. 3.3.

Figure 3.3(a) represents the change in W by wave emission. It is positive when the waves leave the region and negative when they enter the region. The comparison of Fig. 3.3(a) with Fig. 3.1 clearly indicates that the positive peak in this subplot corresponds to the time when the transverse shear waves pulse leaves the circular boundary. Similarly, the negative peak here denotes the time when the waves enter the region after re-entering the simulation box from the other end due to the PB condition. As the monopolar vortex remains stationary and merely rotates about its axis, there is no convection of the fluid across the region. Thus, there is no contribution of convection in W for this particular case as it is evident from Fig. 3.3(b). The role of the dissipating term, which is shown in Fig. 3.3(c), is also observed to be finite.

It should be noted that while the contribution from the Poynting flux of wave and convective term can either decrease or increase W, the last dissipative term is always positive and would only cause W to decay.

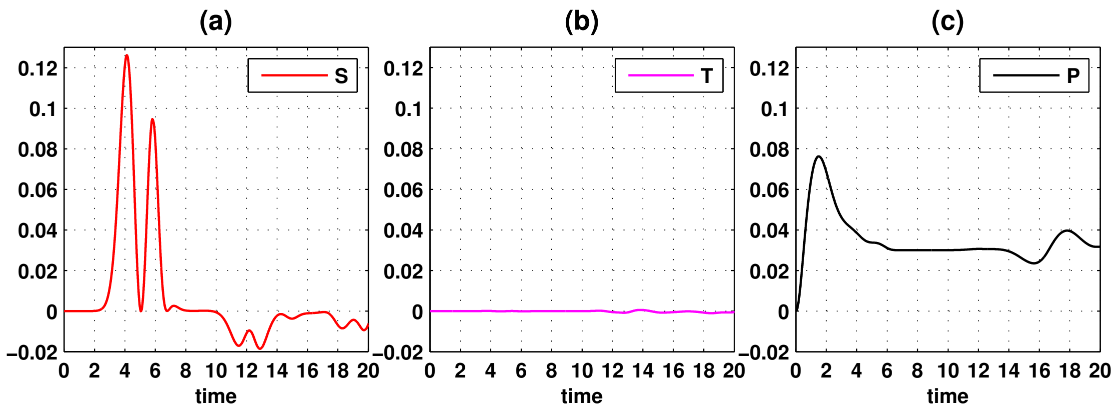

Figure 3.3: Subplot (a) represents the change in W by wave emission term **S**, the positive peak corresponds to the time when the TS wave pulse leaves the circular boundary. Similarly, the negative peak denotes the time when the waves enter the region after re-entering the simulation box from the other end due to the PB condition. The contribution of convection (shown in subplot (b)) is almost zero because the rotating monopole remains stationary. In subplot (c) the role of dissipating term is shown, which is observed to be finite.

In Fig. 3.4, we plot **dWdt** (solid line) and the sum of all the three terms **S+T+P** (dotted line) separately. It can be seen that the two curves are the accurate mirror image of each other proving that their sum is exactly zero as expected from Eq. (3.9).

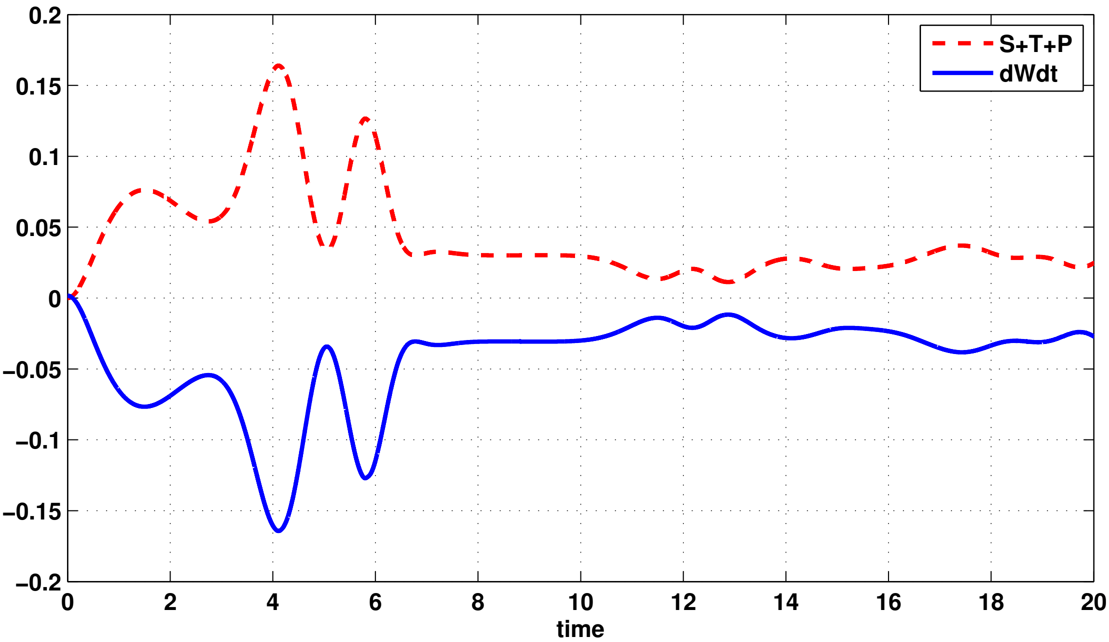

Figure 3.4: Time derivative of conserved quantity W (−) is the mirror image to the total sum (**S+T+P**) of all remaining quantities (−−) during the run time of the rotating circular vorticity profile.

3.3.2 Dipole evolution and dipole-dipole collision

Monopoles being static structures, the contribution due to the convective terms in the Eq. (3.9) was negligible as we saw in the previous subsection. We now choose some specific cases of dipoles evolution and their collision from the previous Chapter 2 and study the evolution of the various terms in the Eq. (3.9) in a circular region of radius 6π units. Again, the simulation region is a square box of length 24π units with PB conditions. The PB condition ensures that the dipole as well as the emitted waves can enter and leave the region multiple times. The system parameters (system length and circular local volume element) and coupling parameters ($\eta = 5$ and $\tau_m = 20$) are same for all the cases mentioned below.

3.3.2.1 Dipole evolution

We now show the validity of Eq. (3.9) for different dipoles with varying strength, Ω_0, in the subsequent discussion. Figure 3.5 shows the propagation of the dipolar structures along with the emitted waves.

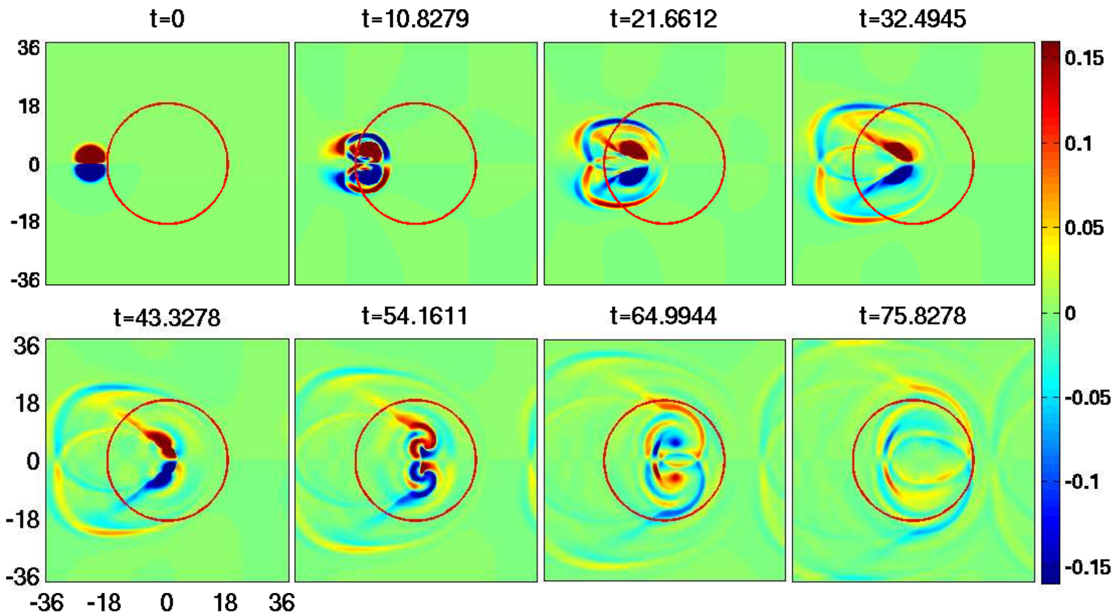

Figure 3.5: Evolution of dipole with time for visco-elastic fluid of Ω_0=3.5 with the coupling parameters $\eta = 5, \tau_m = 20$ and a circular local volume element (inside the circumference) over which the different transport quantities are calculated.

The region inside the circular region is considered for studying the evolution of W. The total change in magnitude of conserved quantity W within this region with time is shown in Fig. 3.6 (a). The Fig. 3.6(b) shows the corresponding change in **dWdt** with time.

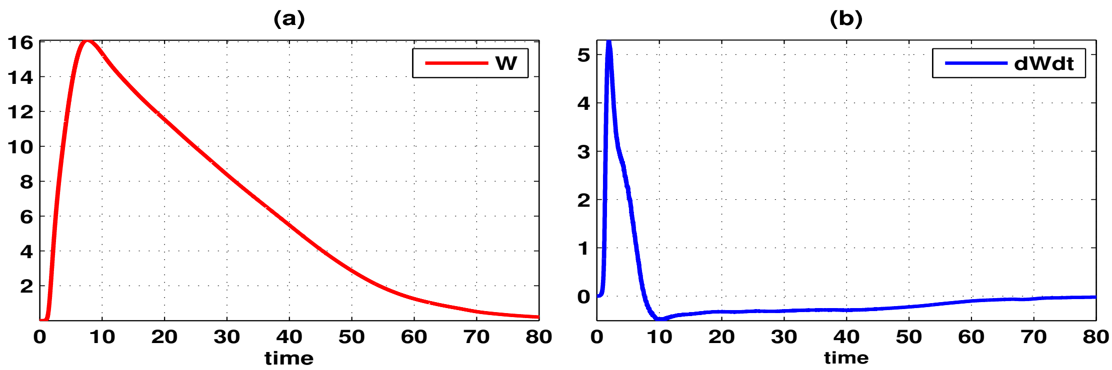

Figure 3.6: Subplot (a) shows the evolution of W within our considered regime and the subplot (b) shows **dWdt** for the dipole of strength Ω_0=3.5.

Since the dipole was placed outside this region initially, W was zero to begin with. When the dipole enters this boundary at around time 1.0, W shows a sharp increase. This entrance is also indicated by the occurrence of a negative peak in the Fig. 3.7(b). As time progresses, the value of W steadily falls owing to the dissipative term shown in Fig. 3.7(c) and the contribution of convection term becomes almost zero because the dipole gets completely engulfed into the emission inside this region and not able to cross this region. Due to the transverse wave emission, the contribution of transverse term $\mathbf{T}$ can be seen clearly in the Fig. 3.7(a).

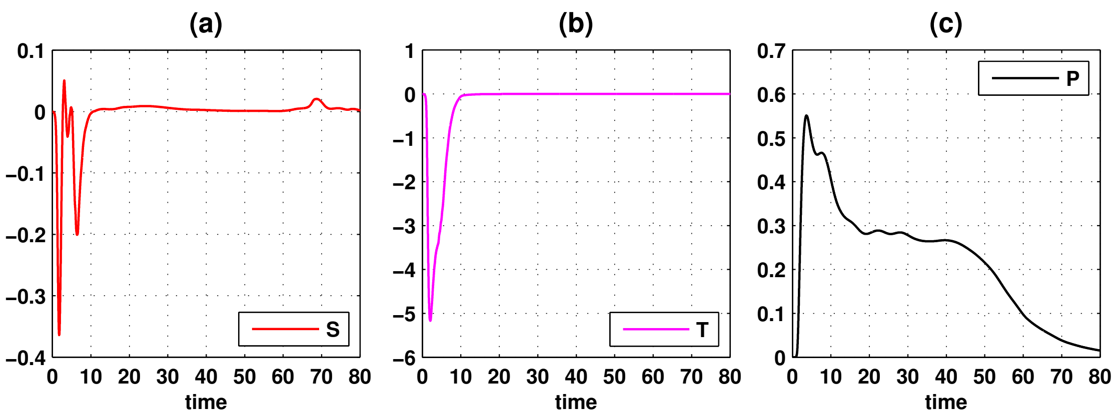

Figure 3.7: Subplot (a) represents the change in W by wave emission. The contribution of the convection term is shown in the subplot (b), here the negative peak denotes the time when the dipole enter the considered circular region. The role of dissipating term is shown in the subplot (c), this term is observed to be finite.

The conservation equation is pretty accurately satisfied as can be seen from Fig. 3.8 where **dWdt** (solid line) and the sum of the three terms (dotted line) are plotted. They are the identical mirror image curves, illustrating that the conservation equation $\mathbf{dWdt} + \mathbf{S} + \mathbf{P} + \mathbf{T} = \mathbf{0}$ is satisfied with very good precision.

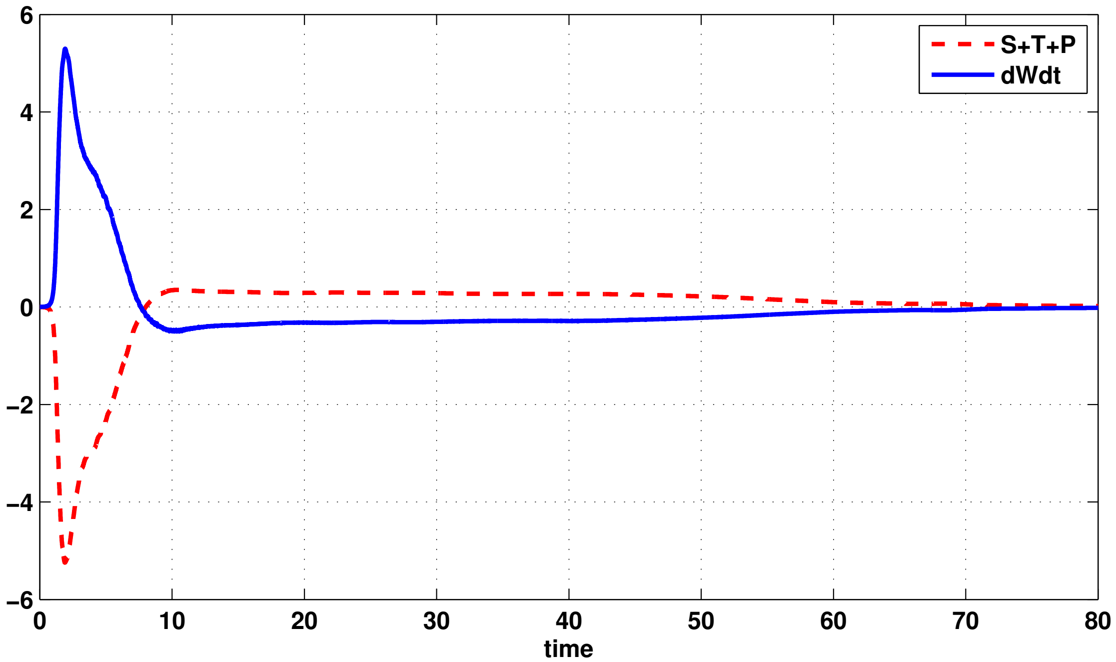

Figure 3.8: Time derivative of conserved quantity W (−) is the mirror image to the total sum ($\mathbf{S}$+$\mathbf{T}$+$\mathbf{P}$) of all remaining quantities (−−) during the run time for the evolution of dipole of Ω_0=3.5.

In the earlier case (Fig. 3.5), the dipole was of lesser strength and hence it dissipated inside the circular region considered by us. In Fig. 3.9, the strength of the dipole is chosen to be sufficiently high so that it can cross the region marked by the circle over which we are calculating different transport quantities.

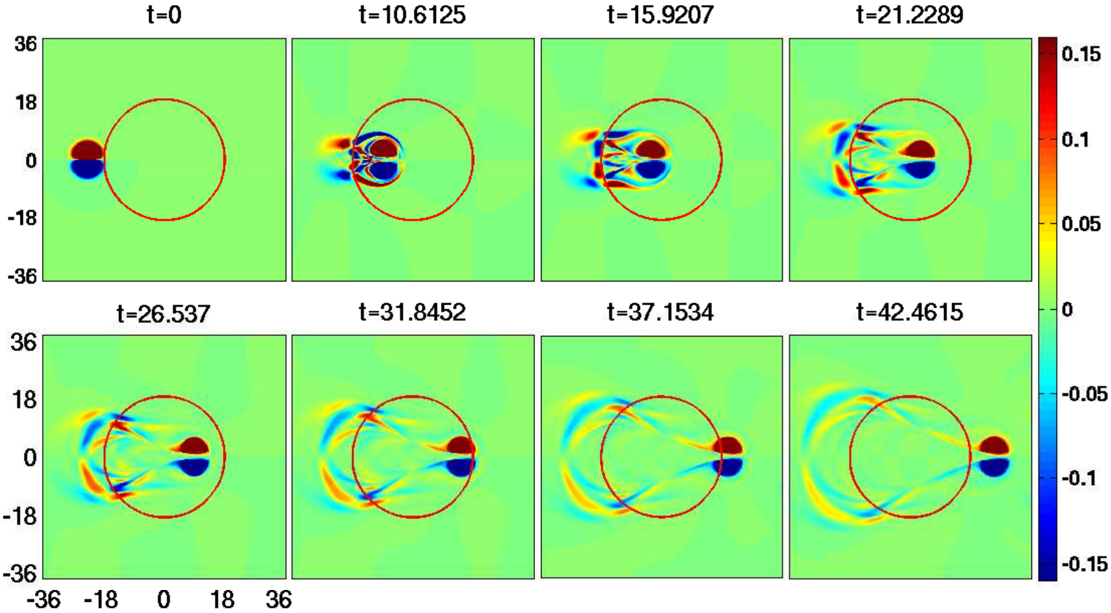

Figure 3.9: Evolution of the dipole with time for visco-elastic fluid of Ω_0=5.0 with the coupling parameters $\eta = 5, \tau_m = 20$ and the circular local volume element (inside the circumference) over which the different transport quantities are calculated.

From Fig. 3.9, it is clear that as the dipole enters and leaves the considered circular region at around time 1 and 35 respectively, there is a sharp rise and fall in W which are also observed in Fig. 3.10 (a).

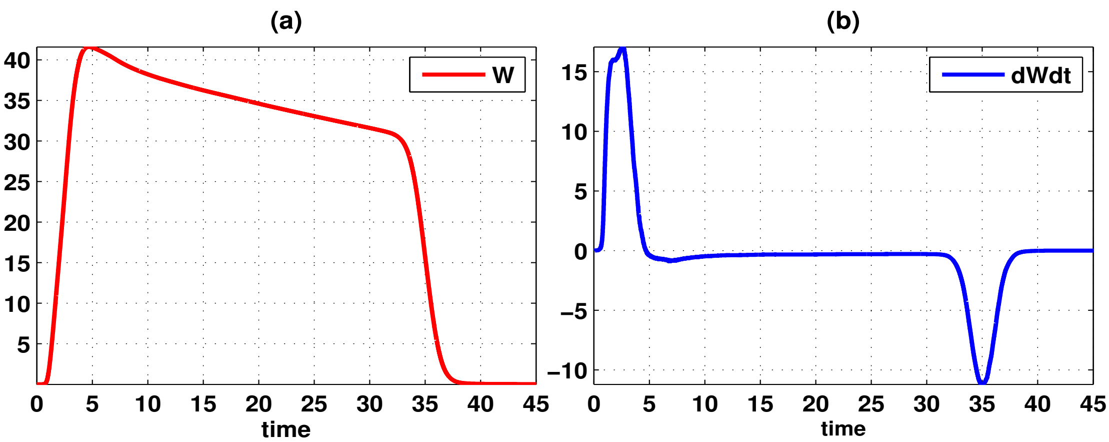

Figure 3.10: Subplot (a) shows the evolution of W within our considered regime and the subplot (b) shows **dWdt** for the dipole of strength Ω_0=5.0

In this time period the convection term contributes significantly. The entrance is indicated by a negative peak while a positive peak marks the exit of the dipole in Fig. 3.11(b). However, in the intervening time a steady decrease in W occurs mainly because of the dissipative term shown in Fig. 3.11(c). The contribution of radiation term (Fig. 3.11(a)) is smaller as compared to the convection term.

The Fig. 3.10(b) shows the corresponding change in the left hand side of integral Eq. (3.9) with time.

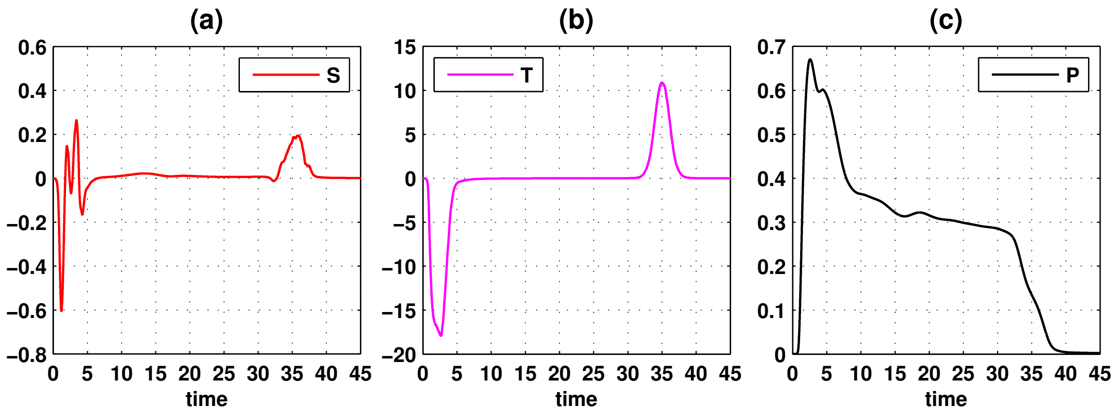

Figure 3.11: Subplot (a) represents the change in W by the wave emission. The contribution of the convection term is shown in subplot (b), here the negative peak denotes the time when the dipole enters the circular region and positive peak corresponds to the leaving time of dipole. The role of dissipating term is shown in subplot (c), which is observed to be finite.

From Fig. 3.12, one can see that **dWdt** is the mirror image to the total sum $(\mathbf{S}+\mathbf{T}+\mathbf{P})$ of all remaining quantities during the run time as observed for earlier cases.

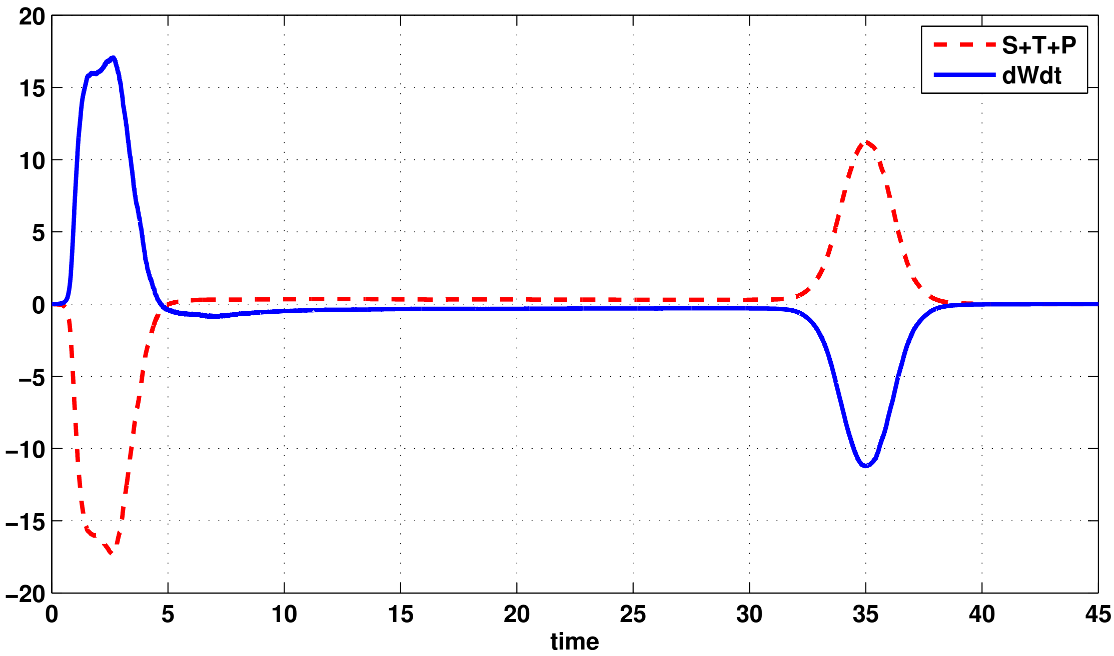

Figure 3.12: Time derivative of conserved quantity W (—) is the mirror image to the total sum ($\mathbf{S}+\mathbf{T}+\mathbf{P}$) of all remaining quantities (−−) during the run time for the evolution of dipole of Ω_0=5.0.

3.3.2.2 Dipole-dipole collision

In order to confirm the validity of the conservation relation for a more complex scenario, we consider the case of two colliding super-luminar disparate strength dipoles of Ω_{01}=7.5 (left) and Ω_{02}=10 (right) shown in Fig. 3.13. The complexity of the motion of dipole is evident in Fig. 3.13. Here the dipoles exhibit linear/circular motion and collide multiple times inside, outside and along the circumference. This complex evolution of dipoles can be closely related to the evolution of various terms in the conservation relation.

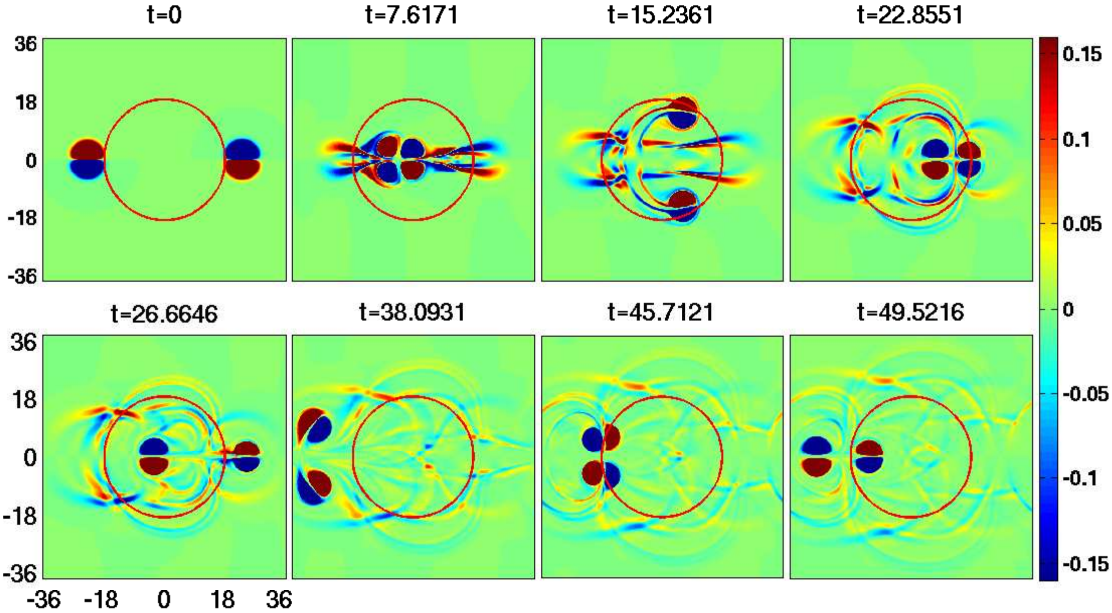

Figure 3.13: Head-on collision between two disparate strength super-luminar dipoles of Ω_{01}= 7.5 (left) and Ω_{02}= 10 (right) with the coupling parameters $\eta = 5, \tau_m = 20$ and a circular local volume element (inside the circumference) over which the different transport quantities are calculated.

The changing value of W with time also reflects this dynamics as shown in Fig. 3.14(a). During time period from 5 to 10, the dipoles collide axially inside the considered region so W remains almost constant during this period. The dipoles then move along a curved trajectory at time around 14. As the trajectory of dipoles does not coincide with the circumference of the region under consideration, the value of W changes when the structures enter or leave the region and finally the dipoles collide orthogonally in respect to the first collision. Further, in time duration ranging from 33 to 43 dipoles leave completely this region so W almost becomes zero. Again we observe a sharp increase in W at time around 44 because of the collision between the dipoles at the circumference.

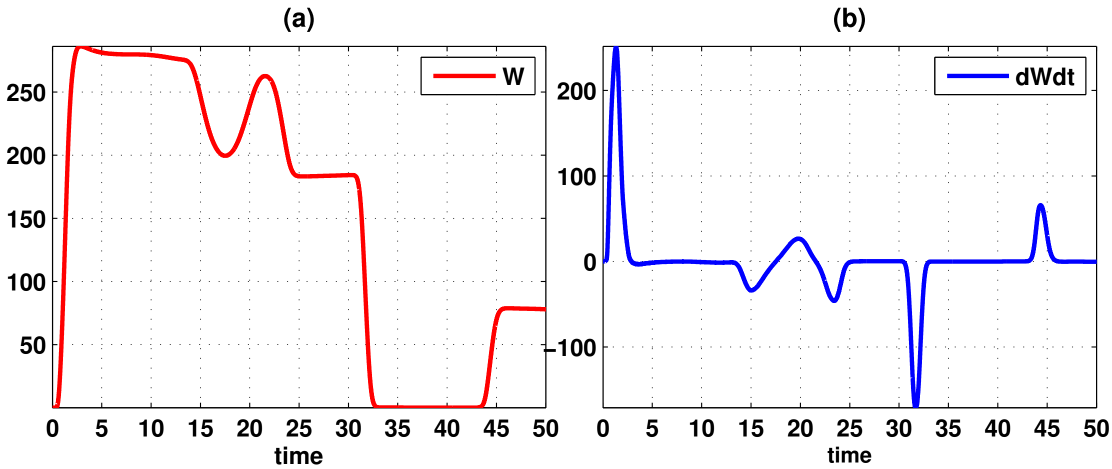

Figure 3.14: Subplot (a) shows the evolution of W within our considered regime and the subplot (b) shows **dWdt** for the head-on collision between two disparate strength super-luminar dipoles.

The Fig. 3.14(b) shows the corresponding change in **dWdt** *i.e* the left hand side of integral Eq. (3.9) with time. These events can be corroborated well by observing the contour plot of Fig. 3.13 and the evolution of the various terms namely, the Poynting, convective and dissipative terms shown in Fig. 3.15.

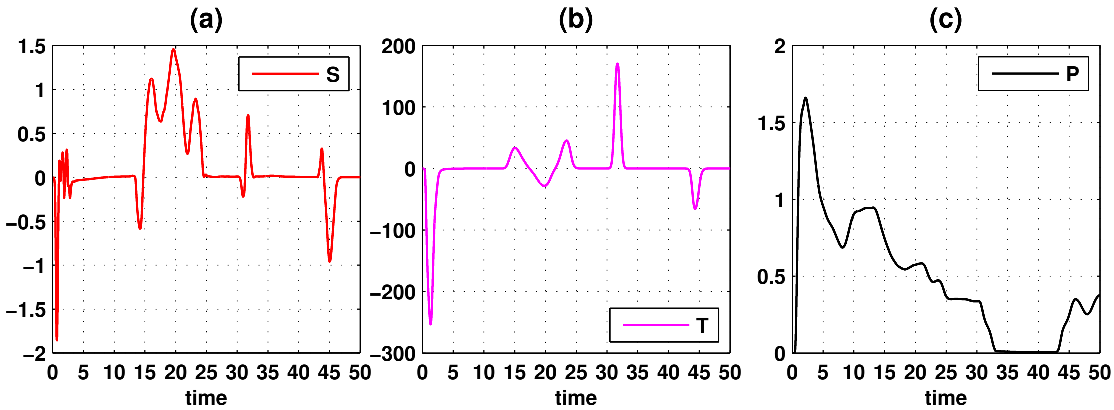

Figure 3.15: Subplot (a) represents the change in W by wave emission. The major transport process which is the convection phenomena can be seen in subplot (b). The role of the dissipating term is shown in subplot (c), this term is observed to be finite.

Here too the integral condition of Eq. (3.9) is satisfied identically at every time moment, this can be seen in Fig. 3.16.

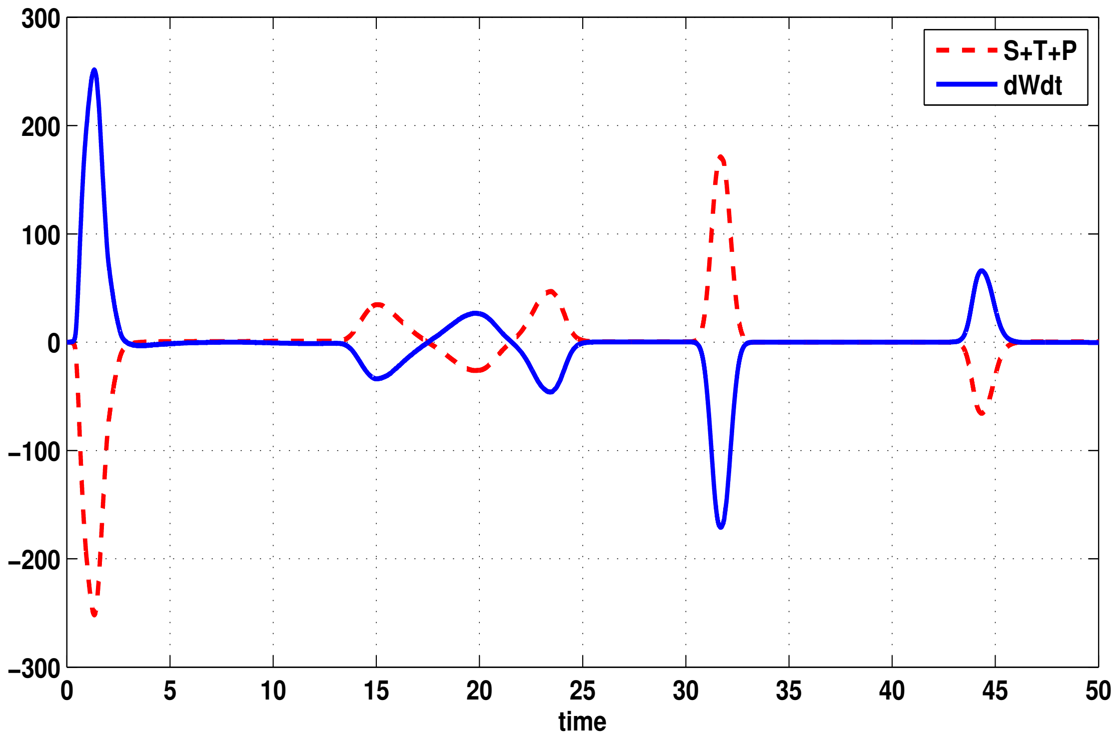

Figure 3.16: Time derivative of the conserved quantity W ($-$) is the mirror image to the total sum ($\mathbf{S}+\mathbf{T}+\mathbf{P}$) of all remaining quantities ($--$) during the run time for the head-on collision between two disparate strength super-luminar dipoles.

3.4 Summary

A Poynting-like conservation theorem has been constructed for the 2-D i-GHD model equations and an enstrophy-like conserved quantity was obtained. This conserved quantity is the sum of square integrals of vorticity and the velocity strain. The time rate of change of this quantity is controlled by radiative, convection and dissipative effects. The radiation term corresponds to the TS waves and shows a striking similarity with electromagnetic waves. The theorem has been shown to be satisfied for many complex evolution cases e.g. rotating monopole vortex, propagating and colliding dipole structures for the dusty plasma medium.

4

Transport and mixing in i-GHD model

In this chapter we focus on the studies related to the transport and mixing properties of the visco-elastic fluid governed by i-GHD model. In hydrodynamic fluids the Kelvin-Helmholtz (K-H) instability is considered to be one of the prominent instability responsible for mixing and transport in the fluid. The visco-elastic i-GHD model, in addition, also supports emission of transverse shear waves. Therefore, it is interesting to see how the interplay of K-H and Transverse Shear (TS) Waves in the context of this model govern the mixing and transport traits in the medium.

In earlier chapters we had specifically avoided the development of fluid K-H instability (which develops across the sharp interfaces of shear flows) by choosing smooth flow profiles. Here for the purpose of quantifying the role of mixing, we consider sharp profiles where K-H arises. We have also studied the dynamics of passive tracer particles.

4.1 Introduction

A typical turbulent flow contains a wide variety of coherent structures in the form of localized vorticity patches. The stability and evolution of these structures for visco-elastic fluids is quite different than that of Newtonian fluids owing to the existence of TS waves. In the Chapters 2 and 3, the interactions between TS waves and coherent structures were studied extensively and only smooth structures were considered to avoid K-H destabilization. In the present chapter, sharp shear flows which favor the K-H instability across their interfaces are considered for study. In such flows the interplay between the emitted transverse shear waves and the vortices of K-H instability occurs. The mixing and transport features associated with this interplay in GHD is compared with the evolution of Newtonian fluids. The results show that the GHD fluid shows a better mixing trait. The chances of a fluid element and/or test particles to remain entrained for a long duration within a localized region are smaller in GHD compared with the Newtonian fluid. To substantiate this point, we have studied the evolution and disbursal of passive tracer particles for HD as well GHD systems.

In test particle simulation, the diffusion and clustering of particles are directly related to the mixing characteristic of a medium. We have considered two kinds of point-like particles, (i) non-inertial tracers which are governed by the local flow velocity and have density same as that of fluid, (ii) inertial particles which have density different from that of fluid. The velocity of inertial tracers differs from the local flow velocity due to viscous drag (Stokes) force. The feedback effect of particles on the flow of the medium has been neglected in both cases. Essentially the particle dynamics is simulated using a one-way coupled Lagrangian point-particle approach.

This chapter has been organized as follows. Section 4.2 presents the evolution of sharp vorticity patches which emit transverse shear waves and are also K-H unstable. To understand transport we have immersed some passive particles in the fluid. The mean square displacement of these particles serves as a good measure of transport in the medium. This methodology and numerical observations are described in Section 4.3 and Section 4.4, respectively. Finally the whole chapter is summarized in Section 4.5.

4.2 Evolution of sharp vortex

We consider the following specific cases of sharp vorticity patches: (i) sharp circular and elliptical, and (ii) multi-circulation vorticity shell profile.

4.2.1 Evolution of sharp circular and elliptical vortices

The velocity profile for the sharp circular vortex considered for present case is as follows

$$\vec{v}_0(x,y,t_0) = \begin{cases} v_{x0} = -\theta_0\frac{(y-y_c)}{b};\ v_{y0} = \theta_0\frac{(x-x_c)}{a} & |r| \leq 6 \\ 0 & \text{otherwise.} \end{cases} \tag{4.1}$$

The vorticity corresponding to the above velocity profile is given below.

$$\xi_{z0}(x,y,t_0) = \begin{cases} \theta_0\left(\frac{1}{a}+\frac{1}{b}\right) & |r| \leq 6 \\ 0 & \text{otherwise.} \end{cases} \tag{4.2}$$

Here $|r| = \sqrt{((x-x_c)/a)^2 + ((y-y_c)/b)^2}$, a and b are the major and minor axes, respectively. x_c and y_c are the x and y coordinates of the center of the vorticity profile. The numerical simulation has been carried out for amplitude $\theta_0 = 1$ and $x_c = y_c = 0$. The simulation region is a square box of length 12π units with periodic boundary (PB) conditions.

We consider the circular vortex (a=b=1) with a sharp cutoff at distance $|r|$=6 units away from the centre of the circular vortex. This rotating vorticity profile has circular symmetry. The abruptness of the vorticity profile generates a strong rotational sheared flow, which in turn is drastically unstable to the K-H instability for both the HD fluid as well as the GHD system. Figures 4.1, 4.2 show the vorticity contours at various times for both HD and GHD system, respectively.

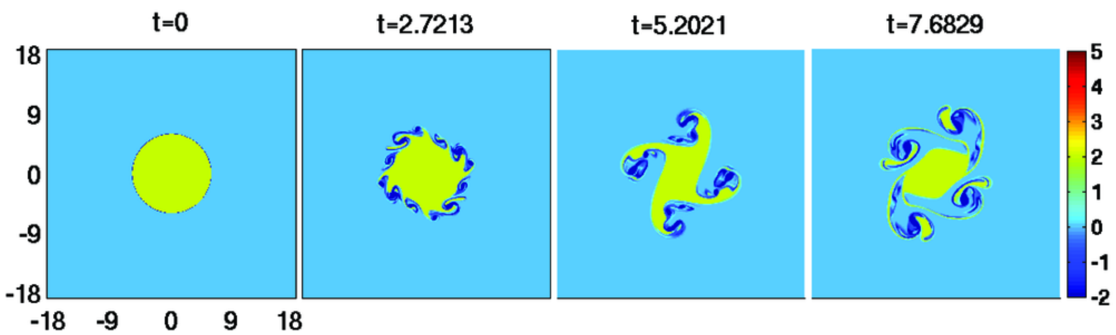

Figure 4.1: Evolution of circular sharp vorticity profile in time for hydrodynamic fluid.

It is evident from the Fig. 4.1 that for HD system the initial K-H perturbation evolves towards a very anisotropic isolated structure. For GHD system, besides K-H instability, transverse shear waves are also emitted at the sharp interface. For this single sharp interface we observe two transverse shear waves for the GHD system. The propagation of these two transverse wave fronts, one inward and the other outward and a concomitant K-H destabilization at each of these fronts is clearly visible in Fig. 4.2.

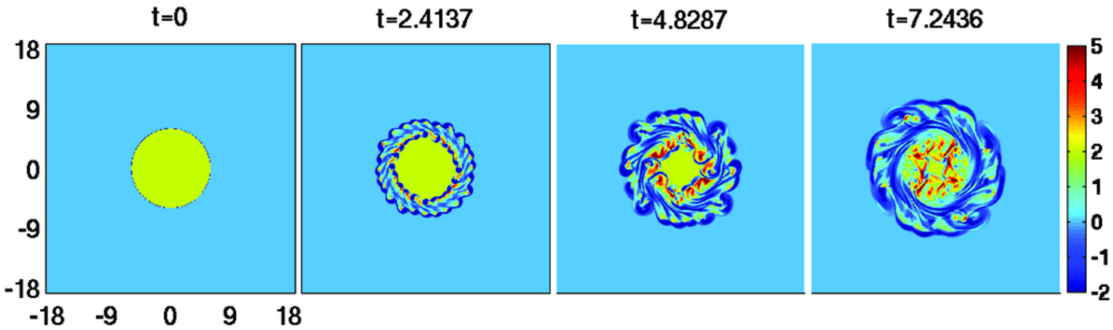

Figure 4.2: Evolution of circular sharp vorticity profile in time for visco-elastic fluid with parameters $\eta = 5, \tau_m = 20$.

It can be seen clearly that the TS waves are instrumental in efficient mixing of the fluids entrained inside the vortex structure with that which is outside the initial vortex pattern. In Figs. 4.3, 4.4, we have considered two different cases of GHD simulation, with different values of η and τ_m parameter ($\eta = 2.5, \tau_m = 20, v_p$=0.35 for Fig. 4.3 and $\eta = 10, \tau_m = 40, v_p$=0.5 for Fig. 4.4).

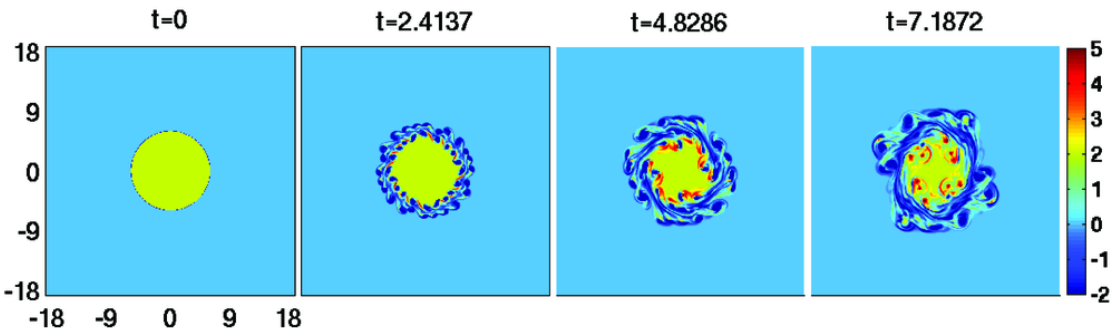

Figure 4.3: Evolution of sharp circular vorticity profile in time for strongly coupled dusty plasma medium for $\eta = 2.5, \tau_m = 20$.

We observe that the higher phase velocity of the TS wave helps in mixing the internal fluid with that external to the initial vortex more rapidly. Also, the

Figs. 4.2, 4.4 show that the vortex evolution is similar in time for the same value of TS wave phase velocity ($v_p = \sqrt{\eta/\tau_m}$=0.5).

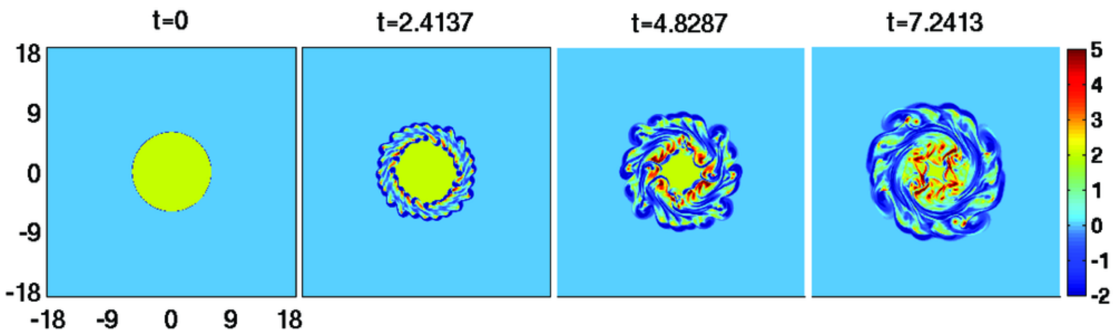

Figure 4.4: Evolution of sharp circular vorticity profile in time for strongly coupled dusty plasma medium for $\eta = 10, \tau_m = 40$

Often the vorticity structure in any physical flow may not have a circular shape. Therefore, we consider for our studies an initial distorted patch of vorticity. A simple elliptical form of distortion have been considered, with parameters θ_0=1, a=1.1, and b=1/a. Various time frames of the evolution of such a vortex pattern in both HD and GHD case have been shown in Figs. 4.5, 4.6 for sharp elliptical vorticity profile.

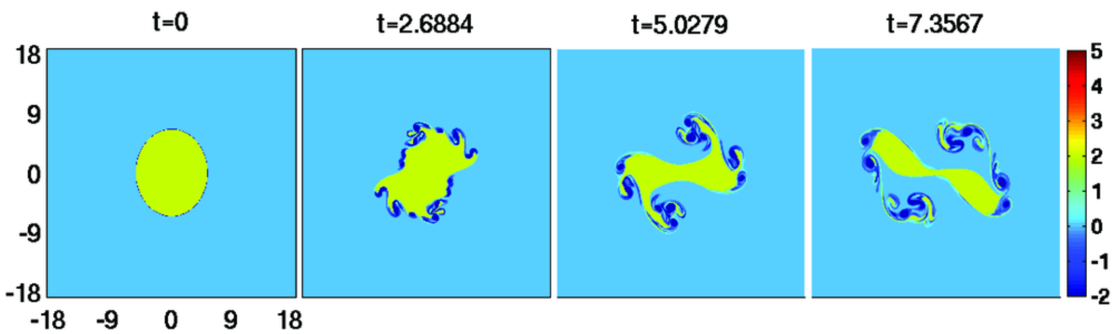

Figure 4.5: Vorticity evolution for sharp elliptical profile in time for hydrodynamic fluid.

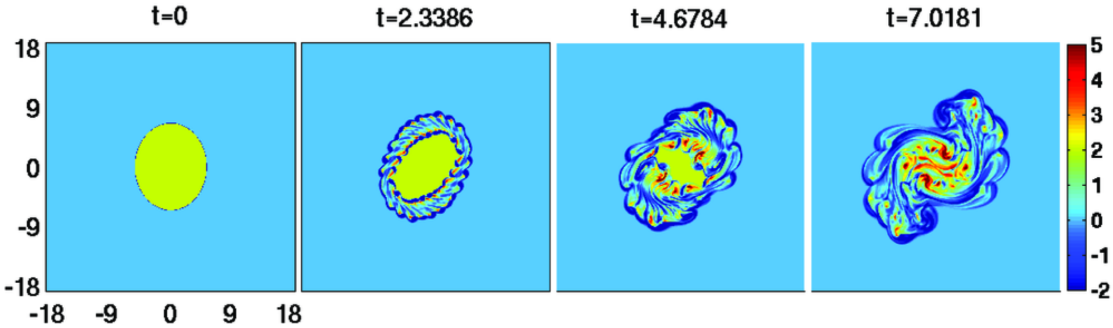

Figure 4.6: Vorticity evolution for sharp elliptical profile in time for visco-elastic fluid with parameters $\eta = 5, \tau_m = 20$.

It can be seen that while the distorted shape of the vorticity patch does help in making the transport better in the context of HD, the GHD case still proves to be more efficiently mixing the fluids.

4.2.2 Multi-circulation vorticity shell profile

As discussed in earlier subsection, the single circular interface of sharp shear vorticity profile acts as a source of two (inward and outward moving) wavefronts of TS waves along with K-H instability at each of the boundaries. And these wavefronts enhance the mixing rate of visco-elastic fluids. With these observations one can anticipate that presence of multiple sharp interfaces in the velocity profile for the GHD fluid should significantly enhance intermixing. A final relaxed form can, therefore, easily emerge.

Here, we first consider the simplest case of multiple shells of vorticities, with each consecutive one having a reversal in its circulation. The velocity profile for this configuration is given below.

$$\vec{v}_0(x, y, t_0) = \begin{cases} v_{x0} = -\theta_0(y - y_c);\ v_{y0} = \theta_0(x - x_c) & |r| \leq 5 \\ v_{x0} = \theta_0(y - y_c);\ v_{y0} = -\theta_0(x - x_c) & 5 < |r| \leq 10 \\ 0 & \text{otherwise.} \end{cases} \tag{4.3}$$

The vorticity corresponding to the above velocity profile is given below,

$$\xi_{z0}(x,y,t_0) = \begin{cases} 2\theta_0 & |r| \leq 5 \\ -2\theta_0 & 5 < |r| \leq 10 \\ 0 & \text{otherwise,} \end{cases} \tag{4.4}$$

with the parameter θ_0=1. Figures 4.7, 4.8 show the evolution of the vorticity profile considered above for HD and GHD mediums respectively. It is evident from the Fig. 4.7 that for HD system the initial K-H perturbation evolves towards a very anisotropic isolated structure at both interfaces.

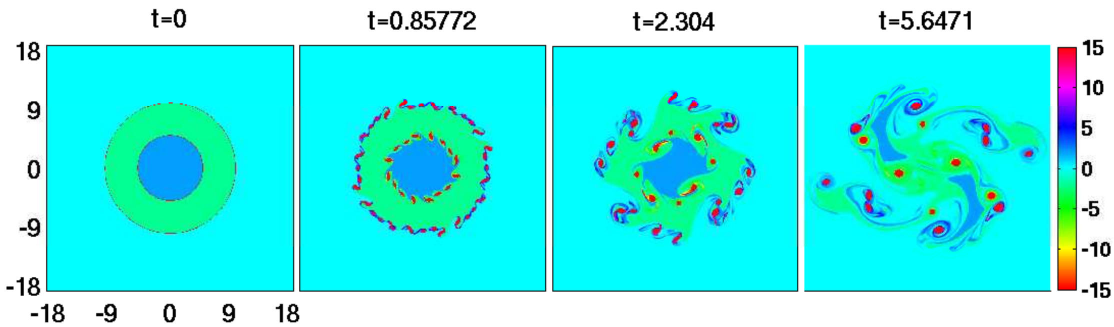

Figure 4.7: Evolution of sharp circular vorticity profile in time for HD.

In Fig. 4.8, we observe that a pair of inward and outward moving wavefronts emanates from each of the two sharp interfaces of the vortex structure.

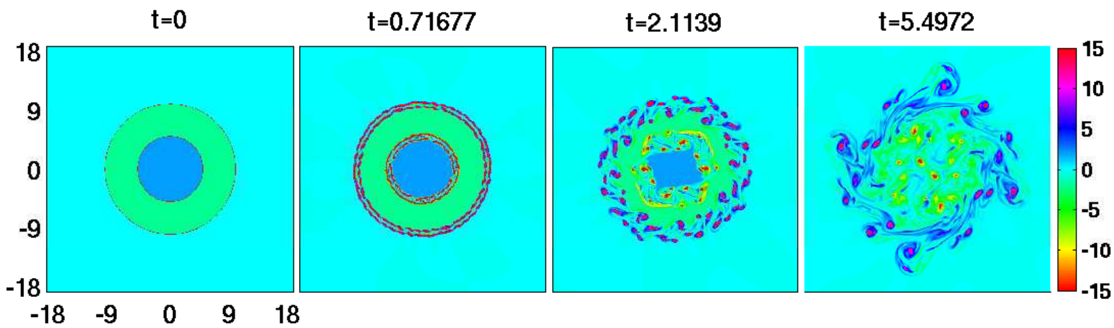

Figure 4.8: Evolution of sharp circular vorticity profile in time for strongly coupled dusty plasma medium for the $\eta = 5, \tau_m = 20$.

Further, the formation of K-H vortices too can be observed at each of these two interfaces. While the stagnant fluid in the outermost region ($|r| \geq 10$) undergoes mixing due to the outgoing wave from the outermost interface at 10, the innermost vortex region undergoes mixing due to the ingoing wave emanating from the sharp interface located at 5. Interestingly, the vortex region confined within the two sharp interfaces ($5 < |r| \leq 10$) undergoes mixing due to the ingoing wave from the outermost interface and the outgoing wave from the innermost interface. As the results of these wave-wave, wave-K-H instability and wave-medium interaction the mixing is fast and efficient.

Thus far our study shows that TS wavefronts are the two fronts (inward and outward) across the each interface where the circulation reversal occurs. In order to make a qualitative comparative numerical analysis about the mixing rate and to see how fast a system (between HD and GHD, and in GHD to see the role of coupling strength) achieves a final relaxed state, we have also considered a more complex scenario of multiple circulations having the following velocity flow profile:

$$\vec{v}_0(x,y,t_0) = \begin{cases} v_{x0} = -\theta_0(y-y_c);\ v_{y0} = \theta_0(x-x_c) & |r| \leq 2.5 \\ v_{x0} = \theta_0(y-y_c);\ v_{y0} = -\theta_0(x-x_c) & 2.5 < |r| \leq 5 \\ v_{x0} = -\theta_0(y-y_c);\ v_{y0} = \theta_0(x-x_c) & 5 < |r| \leq 7.5 \\ v_{x0} = \theta_0(y-y_c);\ v_{y0} = -\theta_0(x-x_c) & 7.5 < |r| \leq 10 \\ 0 & \text{otherwise.} \end{cases} \tag{4.5}$$

The vorticity corresponding to the above velocity profile is given below,

$$\xi_{z0}(x,y,t_0) = \begin{cases} 2\theta_0 & |r| \leq 2.5 \\ -2\theta_0 & 2.5 < |r| \leq 5 \\ 2\theta_0 & 5 < |r| \leq 7.5 \\ -2\theta_0 & 5 < |r| \leq 10 \\ 0 & \text{otherwise.} \end{cases} \tag{4.6}$$

The complexity of this motion of multi-circulation structure is evident from the subplots of Fig. 4.9 for inviscid hydrodynamic fluid. In initial time period, the vortices of K-H instability develop across the interface of each shell. At intermediate time range, this evolution provides a complete picture of a turbulent flow which is collection of several small symmetric and non-symmetric vortices. The transport phenomena like convection, merging, diffusion, and instabilities like elliptical and K-H can also be observed.

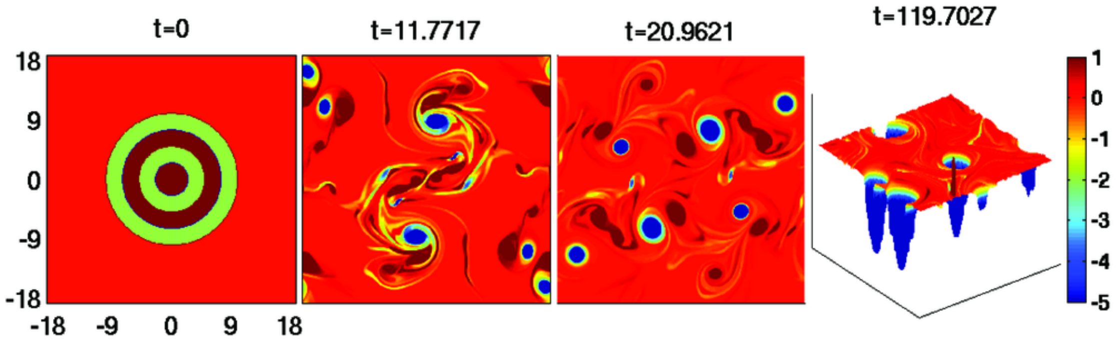

Figure 4.9: Evolution of different circular sharp vorticity profiles in time for hydrodynamic fluid

Figure 4.10, represents the evolution of same initial profile (Fig. 4.9) of vorticity for GHD with coupling parameters $\eta = 5$, τ_m=20. We reported in Chapters 2 and 3 that each of vortices in GHD system emits TS waves having phase velocity v_p=$\sqrt{\eta/\tau_m}$, so for this present case v_p=0.5. From the comparative observations between Fig. 4.9 and Fig. 4.10, it is interesting to notice that the presence of TS waves leads to the relaxing of this turbulent medium to a single vortex faster than in hydrodynamic fluid.

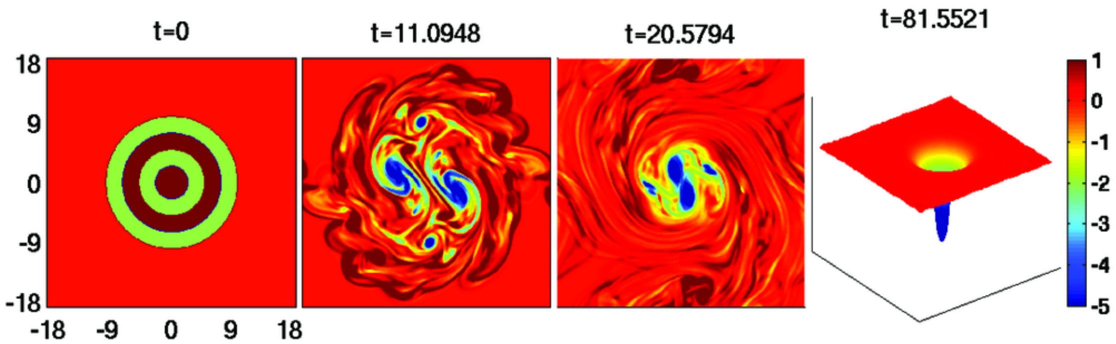

Figure 4.10: Evolution of different circular sharp vorticity profiles in time for visco-elastic fluid with the parameters $\eta = 5, \tau_m = 20$.

Next, we compare this GHD simulation (Fig. 4.10) with another GHD system having lower coupling strength i.e. $\eta = 2.5, \tau_m = 20, v_p$=0.35 (Fig. 4.11). We observe that the relaxing rate of this turbulent medium increases with increasing coupling strength. Consequently, we obtain a single vorticity patch in the final relaxed state earlier in stronger coupling medium with v_p=0.5 than with v_p=0.35.

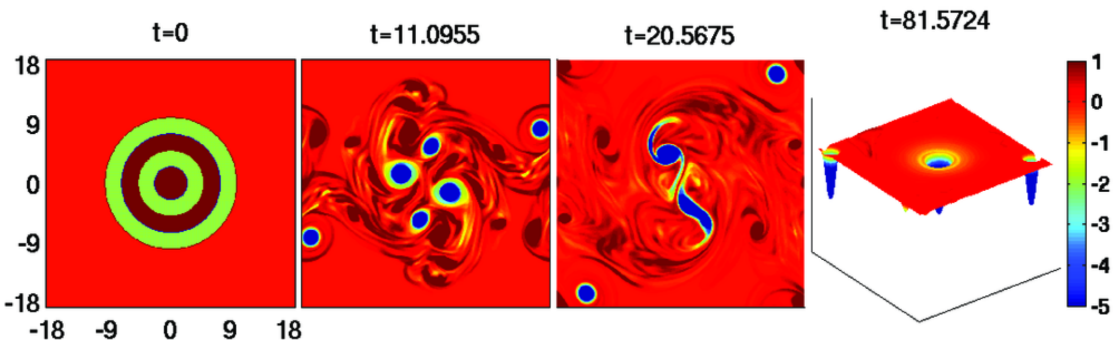

Figure 4.11: Evolution of different circular sharp vorticity profiles in time for visco-elastic fluid with the parameters $\eta = 2.5, \tau_m = 20$.

Heretofore we have presented a picturesque description of transport properties in terms of the mixing of fluids. In next section, we employ the displacement of passive tracers as a quantification of transport in these fluids.

4.3 Test Particle Simulation: Advection of passive tracer particles

We have assumed that the passive particles (inertial and non-inertial) have no size and that the motion of these particles is governed by the fluid flow alone. We calculate the mean square displacement of these particles to find out the diffusivity of the system. We also show that often these passive particles organize themselves in a spatially inhomogeneous distribution. Phenomenon of clustering amongst these particles is clearly evident from the simulations.

4.3.1 Simulation methodology

The feedback effect of particles on the flow of the medium has been neglected. Essentially the particles dynamics are simulated using a one-way coupled Lagrangian point-particle approach. We consider a point test particle with a density ρ_p greater than the density ρ_d of the background incompressible visco-elastic fluid which evolves according to the dynamics

$$\frac{d\vec{r}_p}{dt} = \vec{v}_p(t), \tag{4.7}$$

$$\frac{d\vec{v}_p}{dt} = \frac{1}{\tau_s}(\vec{v}_d(\vec{r},t) - \vec{v}_p(t)), \tag{4.8}$$

where $\vec{v}_d$ is the dust fluid velocity at the location $\mathbf{r}$ of the particle that moves with velocity $\vec{v}_p$, and τ_s=$2a_0^2\rho_p/(9\nu\rho_d)$ is the Stokes time (ν is the kinematic viscosity of the fluid).

Equations (4.7)-(4.8) hold true when the flow surrounding the particle is a Stokes flow. We have used the flux corrected scheme (Boris et al.) to evolve the coupled set of Eqs. (2.5) and (2.6), which gives velocities $\vec{v}_d$ at cell edges of the simulation grid. Then we integrate the equation of motion of a fluid particle to find its present position $\vec{r}_p$ for which governing velocity $\vec{v}_p$ is calculated by interpolating the velocity defined on nearby grid points. For comparison, we also study the motion of neutral particles that follow the dynamics $d\vec{r}_p/dt = \vec{v}_d(\vec{r},t)$ which corresponds to the limit $\tau_s \to 0$ in Eqs.(4.7)-(4.8).

4.3.2 Mixing: mean square displacement and diffusivity

Our interest is to calculate the mean square displacement (MSD) and diffusion coefficient (Dcoeff) for particles for i-GHD medium. MSD and Dcoeff characterize the diffusivity of a medium and show whether it is normal or anomalous (i.e. either subdiffusive or superdiffusive). We have

$$MSD = \langle |r_j(t) - r_j(0)|^2 \rangle \propto t^{\alpha},$$

where $r_j(t)$ represents the position of jth particle at time t. The corresponding values of $\alpha = 1, \alpha < 1, \alpha > 1$ represent normal diffusion, subdiffusion and superdiffusion, respectively. The Dcoeff of particle system may be evaluated from Einstein Relation (1995)

$$D = \lim_{t\to\infty} \frac{MSD}{2dt},$$

where d is number of space dimensions.

4.4 Diffusion and clustering of inertial and non-inertial test particles

The clustering/diffusion phenomenon depends on the particle type as well as the flow conditions. On the basis of inertia, mainly, test particles can be with very low, intermediate and very high inertia. Particles with very low inertia will typically follow the flow passively as tracers, while particles with very high inertia will remain almost unaffected by the medium fluctuations. It is between these two limits i.e. 'intermediate' particles that show the strongest response to the vorticity gradient. To validate our simulation with respect to this statement, we show a the evolution of a smooth circular vorticity patch

$$\xi_0(x,y,t_0) = \Omega_0 exp\left(-\frac{\left((x-x_c)^2+(y-y_c)^2\right)}{a_c^2}\right), \tag{4.9}$$

with different time scale τ_s for a hydrodynamic fluid, here a_c=1.0, $\Omega_0 = 2.5$ and $x_c = y_c$=0.

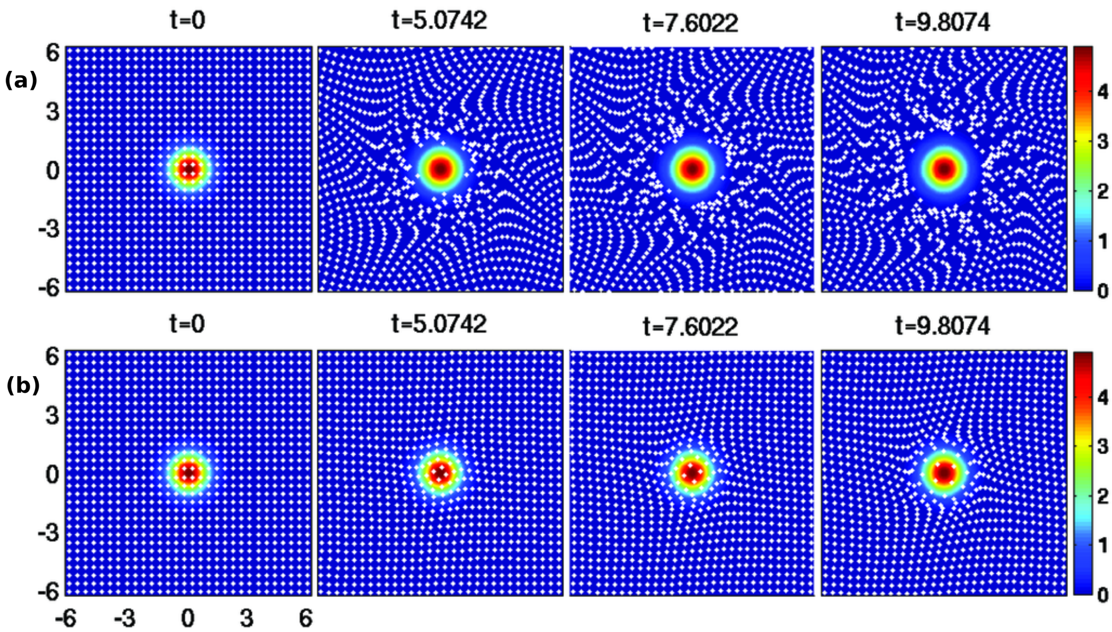

Figure 4.12: Vorticity contour of hydrodynamic fluid with tracers (white dots) having (a) low inertia i.e τ_s=0.1, (b) high inertia i.e τ_s= 50.

Initially (t=0), we distributed 900 inertial particles (shown by white dots) homogeneously throughout the domain. From Fig. 4.12, it is clear that low inertial particles i.e τ_s =0.1 (Fig. 4.12(a)) follow the dynamics along the rotating vortex and the particles with larger inertia τ_s= 50 (Fig. 4.12(b)) show negligible response to the vorticity gradient.

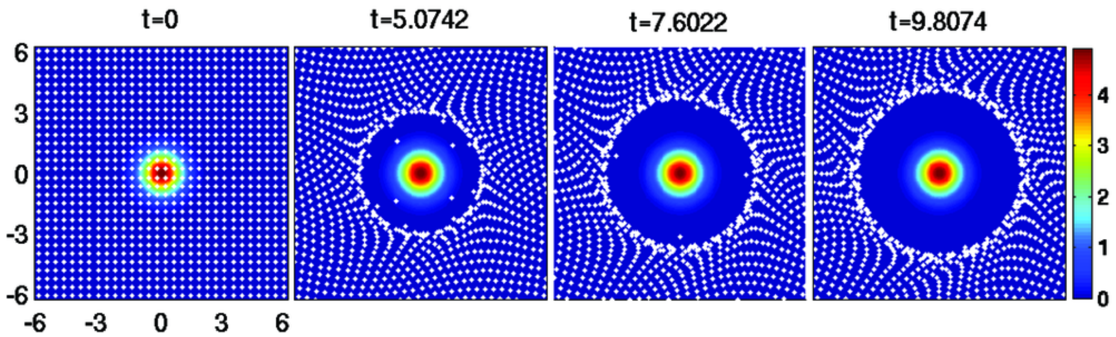

Figure 4.13: Vorticity contour of hydrodynamic fluid with tracers (white dots) having intermediate inertia i.e τ_s=2.

In comparison to previous cases (Fig. 4.12), Fig. 4.13 shows that the particles with intermediate/moderate value of τ_s=2 counter a significant outward push because of vorticity gradient experience centrifugal force.

In subsequent simulations, we are going to employ this knowledge to the sharp rotating vortex profile, which we considered earlier.

4.4.0.1 Sharp vortex: inertial and non-inertial particles

In Fig. 4.14 (second row), we considered the same vorticity profile (Fig. 4.1) as discussed in the earlier Section 4.2 for the case of hydrodynamic fluid. Initially (t=0), we distributed 3600 inertial particles (shown by red dots) homogeneously throughout the system. In Fig. 4.14, the first and the third row visualize the pattern of inhomogeneous distribution of non-inertial particles and inertial particles (τ_s=1), respectively, with time.

It is evident from first row of Fig. 4.14 that the cluster of non-inertial particles can be observed along the vortex. Therefore, these particles accumulate in rotation-dominated regions.

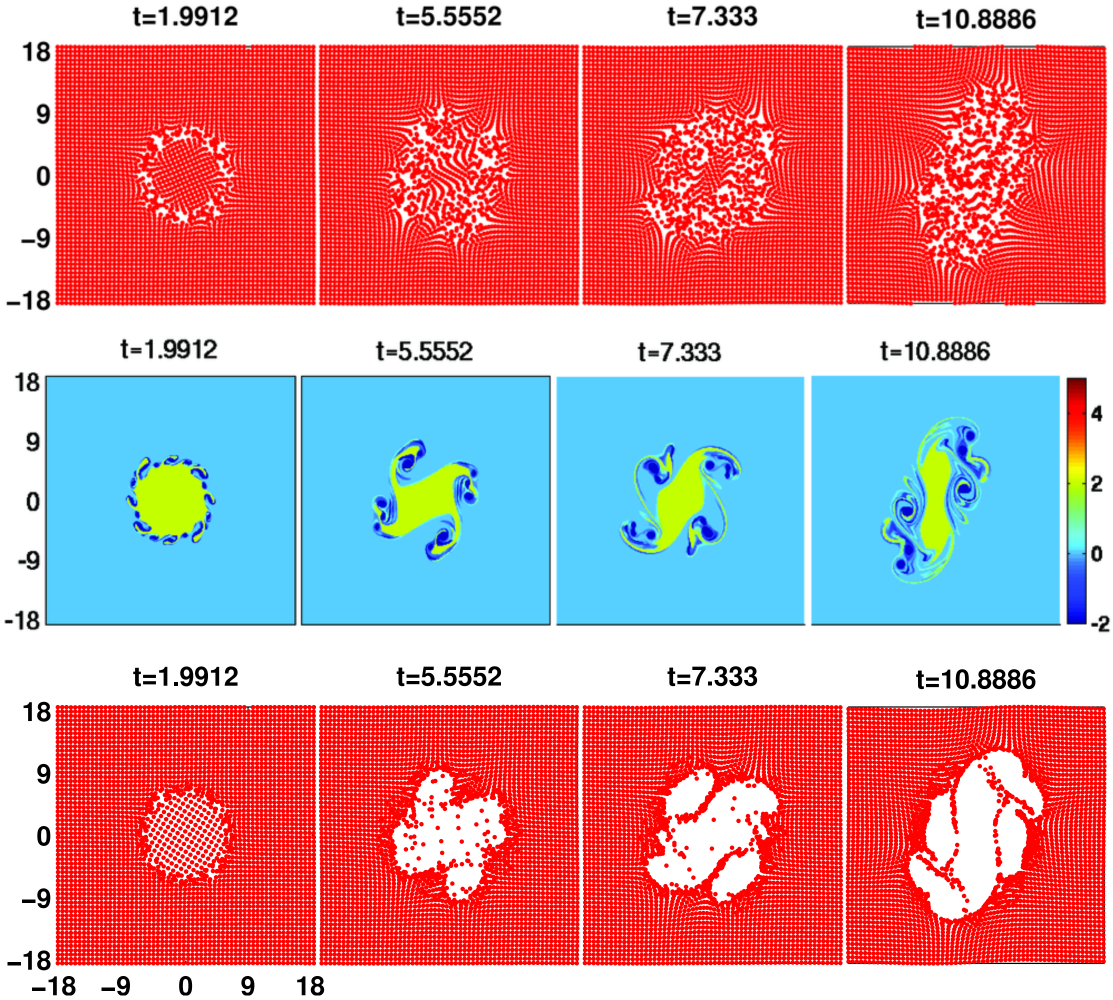

Figure 4.14: First and third row show the temporal and spatial distribution of non-inertial particles and inertial particles (τ_s=1), respectively, corresponding to the sharp vorticity profile evolution for hydrodynamic fluid (second row).

The third row of Fig. 4.14 shows that the inertial particles (τ_s=1) are pushed away from regions where the flow is strong enough. Consequently, the inertial particles accumulate in strain-dominated regions.

Figure 4.15 represents the distribution of test particles (first/third row corresponds to non-inertial/inertial particles) for visco-elastic fluid to the corresponding vorticity profile (second row) as considered in Section 4.2.

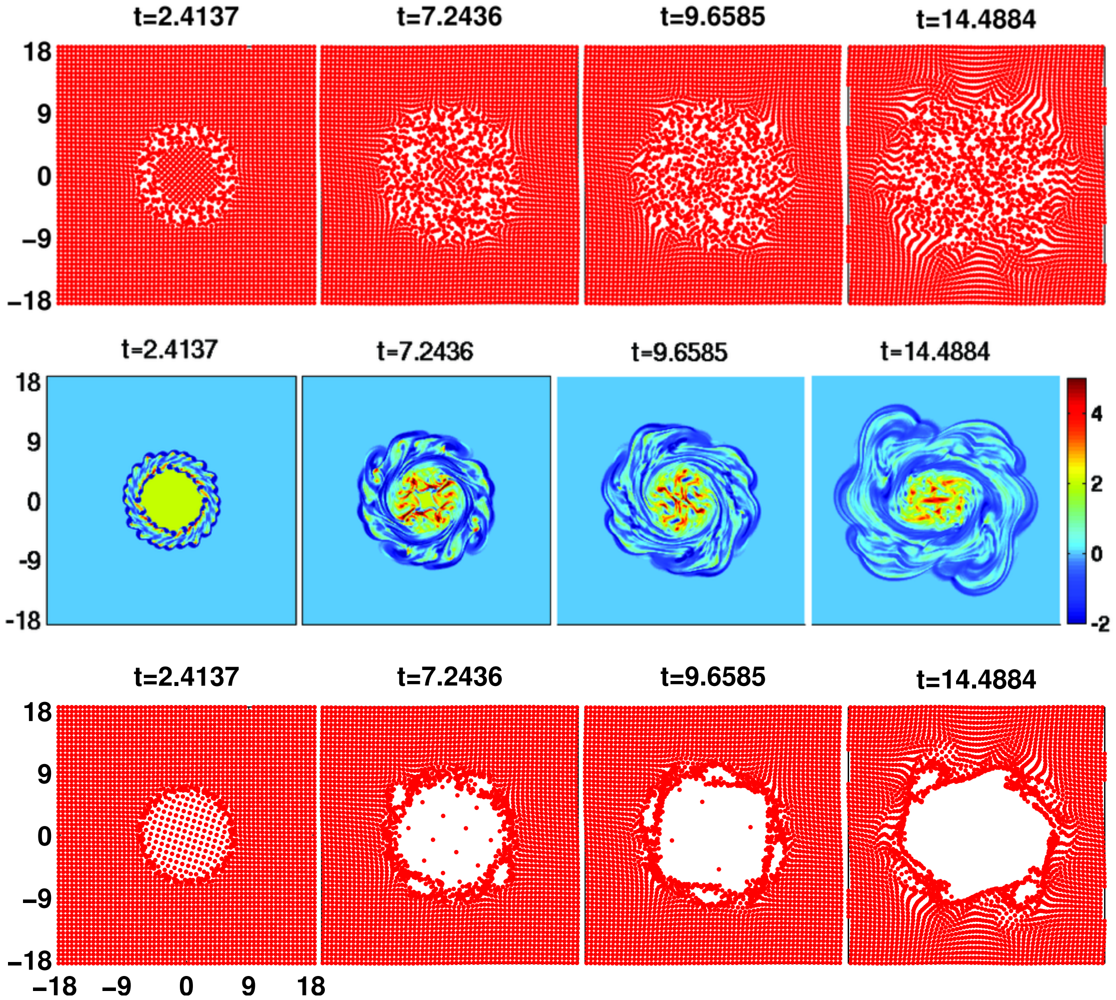

Figure 4.15: First and third row show the temporal and spatial distribution of non-inertial particles and inertial particles (τ_s=1), respectively, corresponding to the sharp vorticity profile evolution for visco-elastic fluid with coupling parameters $\eta = 5$ and $\tau_m = 20$ (second row).

From the comparative observations between Fig. 4.14 and Fig. 4.15, one can notice that the clustering phenomenon for visco-elastic fluids is different because of the continuous emission of TS waves from the vortices. Thus, the diffusion/mixing of these test particles in visco-elastic fluids should also be different from the hydrodynamic fluids and be vary with coupling strength of visco-elastic fluids. As we have already discussed, mean square displacement (MSD) and diffusion coefficient (Dcoeff) characterize the diffusivity of a medium. The diffusivity of a medium is responsible for mixing rate.

Figure 4.16 shows the diffusion of aforementioned test particles ($\tau_s = 1$). The comparative observation showed that the MSD/Dcoeff shows the diffusion of test particles is higher for viscoelastic fluids in comparison to hydrodynamic fluid. It also shows that the diffusion is proportional to the coupling strength.

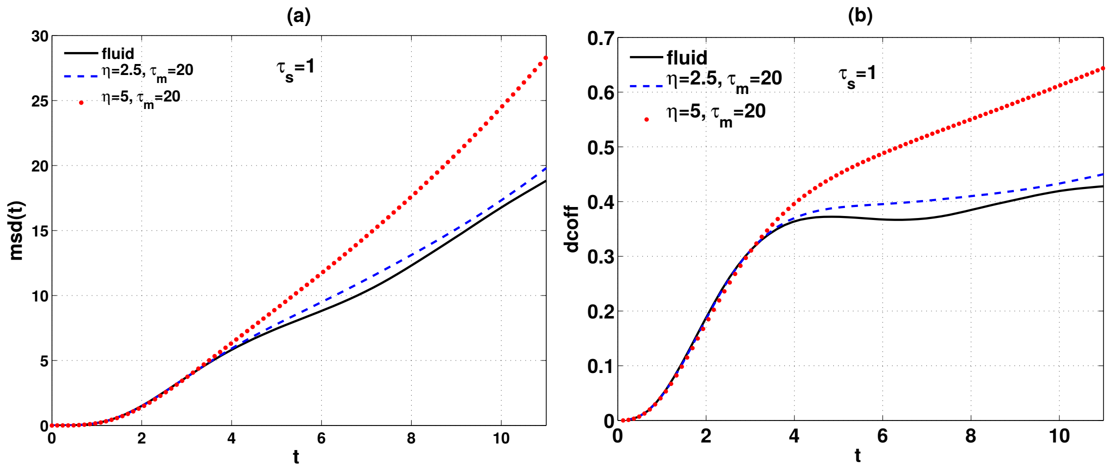

Figure 4.16: (a) Mean square displacement(MSD) and (b) diffusion coefficient (Dcoeff) for $\tau_s = 1$.

Figure 4.17 ($\tau_s = 0.5$) shows the same trend that the diffusion of particles increasing with coupling strength.

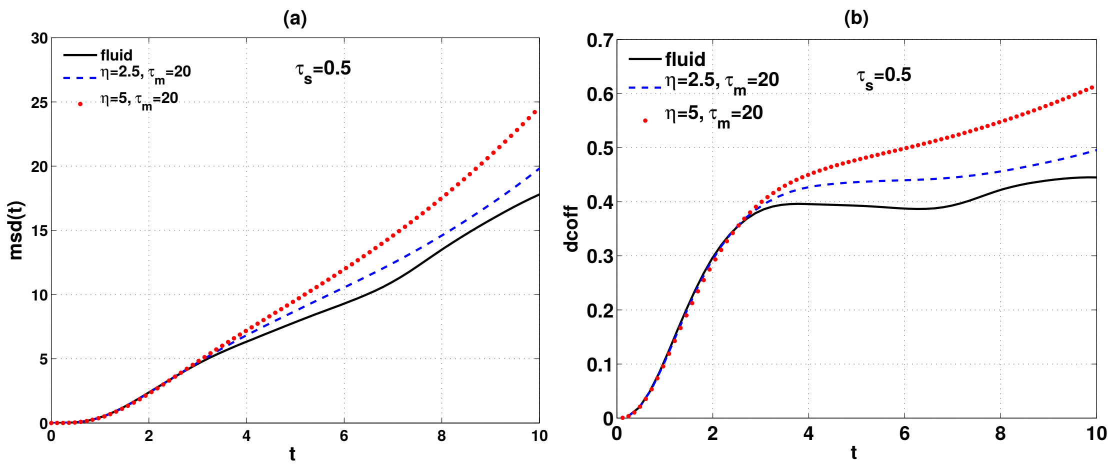

Figure 4.17: (a) Mean square displacement(MSD) and (b) diffusion coefficient (Dcoeff) for $\tau_s = 0.5$.

Thus, in case of visco-elastic fluid, we observed diffusion of particles higher from Newtonian fluids because of the interaction of transverse shear waves and the particles which results in a better mixing and is proportional to coupling strength of the medium.

4.5 Summary

The evolution and interaction of sharp localized vortex patterns for a strongly coupled medium depicted by the visco-elastic GHD description have been studied. We observe that the rotational shear flow in a localized vortex patterns is susceptible to the Kelvin-Helmholtz destabilization which is similar to the Newtonian fluids. It is, however, necessary that for K-H destabilization the shear in flow should be strong and have an inflection point. This is possible when we considered the sharp cutoff in the vorticity patches. In contrast to the Newtonian fluid the GHD visco-elastic medium, in addition to K-H also permits the emission of radially (inward as well as outward) propagating transverse shear waves.

Our studies show that due to the existence of such transverse shear waves in the strongly coupled medium, the mixing and transport behaviour in these fluids is much better than in Newtonian hydrodynamic systems. For this, we have carried out a study of the evolution of tracer particles. The comparison of the MSD for GHD and HD shows that the visco-elastic medium has efficient transport characteristics.

5

Effect of strong coupling in gravitational and buoyancy instability

So far in our previous chapters we have focused on homogeneous strongly coupled dusty Plasma (SCDP) medium. We had also ignored the role of gravity on the medium. However, unlike electrons and typical ions, since the dust particles are pretty massive, the gravitational attraction of earth has a significant role. In this chapter we take account of that and consider the role of strong coupling in the context of one of the most prominent instability arising when the density is stratified against the gravitational force. We demonstrate that the visco-elasticity of the strongly coupled medium leads to a suppression of this instability. Detailed numerical simulation studies have been carried out to elucidate this effect and study the nonlinear regime. We also consider the case of buoyancy driven instability, which would arise when spatially localized (in both dimensions) low/high density regions are placed in a background homogeneous medium in the presence of gravity.

5.1 Introduction

In the present chapter, we present a detailed discussion on the evolution of a strongly coupled medium in the presence of gravity. The case of density stratification against gravity leading to Rayleigh-Taylor (R-T) instability has been studied in detail both analytically and with the help of numerical simulation. We also consider the buoyancy-driven evolution of two dimensional spatially localized high/low density region placed in a background medium in the presence of gravity.

The R-T instability is one of the most prominent fluid instability. The equivalence of gravity and acceleration leads to several manifestations of the instability. Furthermore, in the context of plasma medium the charged species respond to electromagnetic forces and various scenarios arise where an inverse stratification against a force (and/or a pseudo force due to the choice of the frame) leads to this instability. It is for this reason that R-T instability is observed in diverse situations such as supernova explosion [106, 107], planetary rings, geophysics, astrophysics, liquid atomization [108, 109], supersonic combustion, industrial plasmas, fusion physics [66, 110–112], oceans, turbulent mixing [113–115] etc.

Buoyant force acts in the direction opposite to gravity for low density regions. The buoyancy-driven (B-D) instability decides whether an object will float (if the density of an object is less than background fluid) or sink (if density of object is greater than background fluid) in fluid. The floating of boats and ships while sinking of small objects like rocks in water, or the pouring cream (heavy fluid) into coffee (light fluid) and petroleum wells are some examples where buoyant force plays a major role.

Our objective here is to understand how the R-T instability and buoyancy-driven instability behave when the medium is in a strongly coupled state. For this purpose we consider the case of dusty plasma medium here specifically. It is well known the dusty plasmas can be prepared/found in the strong coupling regime rather easily. So the role of strong coupling in the behaviour of these instabilities can be readily investigated in the context of this medium. The role of gravitational force becomes important in dusty plasma because a micron-sized dust particle has enough mass (typical mass of $10^{-15} - 10^{-10}$ Kg) so it can feel the effects of gravity. To avoid the dust particles from falling under gravity, space experiments are carried out under microgravity conditions [97, 117–119]. In ground laboratories the way to keep the dust species levitated against gravity is by applying external electrical field [29, 74, 116].

In the generalized fluid model the elasticity of the medium is represented by a memory relaxation parameter τ_m [30]. This elastic behaviour of the system is known to produce transverse shear (TS) waves in the medium. Recently, the interplay of TS wave on the propagation of coherent structures has been extensively studied by us. In fact, a Poynting-like theorem was constructed which shows the losses by waves emission, convection and dissipation. In fact, the elastic shear waves take away the available free energy of the system, thereby weakening the growth rate of typical instabilities. This has been illustrated earlier in the context of the Kelvin-Helmholtz instability [83]. An analytical work for strongly coupled electron-ion plasma medium in the context of inertial confinement fusion [123] also demonstrates that the R-T instability would be weakened due to the presence of shear waves in the strongly coupled plasma medium. We demonstrate this suppression of the instability analytically and by carrying out a fully nonlinear simulation of the GHD model for the dusty plasma medium.

The chapter has been organized as follows. Section 5.2 contains the detailed description of GHD model and the governing equations for visco-elastic medium in the presence of gravity. In Section 5.2.1, we find the dispersion relation for visco-elastic fluid under gravitational force and a detailed linear local analytical study have been carried out for 2-D system with the assumptions of incompressible flow. Section 5.3 describe the model equations used for numerical simulation, where momentum equation is re-casted in terms of vorticity and then decoupled in the form of two different equations. Additionally, under Boussinesq approximation, we derive the model equations which we use in our simulation work. In Section 5.4, we describe the numerical evolution of density profiles with time for different values of coupling parameters (shear viscosity coefficient η and relaxation time parameter τ_m) under the same assumptions as for analytical calculations. The suppression of the both instabilities i.e. R-T and B-D has been clearly depicted by numerical simulation, as one moves from weakly coupled to strongly coupled regime. The last Section 5.5 contains the summary of the whole chapter.

5.2 Analytical Description

The continuity, momentum and the Poisson's equations for the dust fluid under gravity acceleration $\vec{g}$ can be written as:

$$\frac{\partial \rho_d}{\partial t} + \vec{v}_d \cdot \nabla \rho_d = 0, \tag{5.1}$$

$$\left[1 + \tau_m \left(\frac{\partial}{\partial t} + \vec{v}_d \cdot \nabla\right)\right] \left[\rho_d \left(\frac{\partial \vec{v}_d}{\partial t} + \vec{v}_d \cdot \nabla \vec{v}_d\right) + \rho_d \vec{g} + \rho_c \nabla \phi_d\right] = \eta \nabla^2 \vec{v}_d, \tag{5.2}$$

$$0 = [\rho_d + \mu_e exp(\sigma_e \phi_d) - \mu_i exp(-\phi_d)] \,, \tag{5.3}$$

respectively and the incompressible condition is given as

$$\nabla \cdot \vec{v}_d = 0. \tag{5.4}$$

Here, ρ_d and ρ_c are the mass density and charge density respectively. The entire numerical and analytical work will be carried out for a two-dimensional incompressible system of dusty plasma.

5.2.1 Gradual density gradient

Here, we consider two-dimensional (x-y coordinate) incompressible system where density/potential gradient chosen along y axis i.e. $\partial \rho_d / \partial y$, $\partial \phi_{d0} / \partial y$, respectively and acceleration $\vec{g}$ applied in opposite direction of fluid density gradient $-g\hat{y}$.

Initially, we consider no initial flow i.e. $\vec{v}_{d0} = 0$ at t=0, the equilibrium condition Eq. (5.2) becomes

$$\rho_{d0} g = -\rho_c \frac{\partial \phi_{d0}}{\partial y}. \tag{5.5}$$

A small perturbation in the various fields, e.g. density, scalar potential and dust velocity can be written as

$$\rho_d(x, y, t) = \rho_{d0}(y, t = 0) + \rho_{d1}(x, y, t), \tag{5.6}$$

$$\phi_d(x, y, t) = \phi_{d0}(y, t = 0) + \phi_{d1}(x, y, t), \tag{5.7}$$

$$\vec{v}_d(x, y, t) = 0 + \vec{v}_{d1}(x, y, t), \tag{5.8}$$

respectively. Retaining only linear terms in the perturbed fields we obtain the following equations for the linearized instability analysis.

$$\frac{\partial \rho_{d1}}{\partial t} + (\vec{v_{d1}} \cdot \nabla) \, \rho_{d0} = 0, \tag{5.9}$$

$$\left[1 + \tau_m \frac{\partial}{\partial t}\right] \left[\rho_{d0} \frac{\partial v_{d1y}}{\partial t} + \rho_{d1} g \hat{y} + \rho_c \frac{\partial \phi_{d1y}}{\partial y}\right] = \eta \nabla^2 v_{d1y}, \tag{5.10}$$

$$\left[1 + \tau_m \frac{\partial}{\partial t}\right] \left[\rho_{d0} \frac{\partial v_{d1x}}{\partial t} + \rho_c \frac{\partial \phi_{d1x}}{\partial x}\right] = \eta \nabla^2 v_{d1x}, \tag{5.11}$$

$$\nabla \cdot \vec{v}_{d1} = 0. \tag{5.12}$$

Since equilibrium fields vary along $\hat{y}$, the above set of equations can only be Fourier analysed in time and spatial coordinate x. However, assuming the perturbations to be of much smaller scale compared to the equilibrium variation along y we invoke the local approximation and proceed with the Fourier decomposition along y also. This leads to

$$\rho_{d1} = -\frac{i}{\omega}\frac{\partial \rho_{d0}}{\partial y} v_{1y}. \tag{5.13}$$

The $\hat{y}$ component

$$[1 - i\omega\tau_m][-i\omega\rho_{d0}v_{1y} + \rho_{d1}g + i\mathrm{k}_y\rho_c\phi_1] = -\eta \mathrm{k}^2 v_{1y}. \tag{5.14}$$

The $\hat{x}$ component

$$[1 - i\omega\tau_m][-i\omega\rho_{d0}v_{1x} + i\mathrm{k}_x\rho_c\phi_1] = -\eta \mathrm{k}^2 v_{1x}, \tag{5.15}$$

$$i\mathrm{k}_x v_{1x} = -i\mathrm{k}_y v_{1y} \Rightarrow v_{1y} = -\frac{\mathrm{k}_x}{\mathrm{k}_y} v_{1x}. \tag{5.16}$$

Obtain ϕ_{d1}, using above relation and Eqs. (5.13) (5.14) (5.15), and (5.16), we get

$$\phi_{d1} = -\frac{g\mathrm{k}_x v_{1x}}{\rho_c \omega \mathrm{k}^2}\frac{\partial \rho_{d0}}{\partial y}, \tag{5.17}$$

using the above relation Eq. (5.17) in Eq. (5.15), we get the dispersion relation as

$$(1 - i\omega\tau_m)\left[\omega^2\mathrm{k}^2 + \frac{g\mathrm{k}_x^2}{\rho_{d0}}\frac{\partial \rho_{d0}}{\partial y}\right] = -i\omega\eta^*\mathrm{k}^4, \tag{5.18}$$

where η^*=η/ρ_{d0}.

In strongly coupled regime i.e. $\omega\tau_m \gg 1$, the above dispersion Eq. (5.18) becomes

$$\omega^2 = \frac{\eta^*}{\tau_m}\mathrm{k}^2 - \frac{g}{\rho_{d0}}\frac{\partial \rho_{d0}}{\partial y}\frac{\mathrm{k}_\mathrm{x}^2}{\mathrm{k}^2}. \tag{5.19}$$

For hydrodynamic fluid case where (η^*/τ_m=0), the above dispersion relation reduces to the usual expression of the R-T growth rate

$$\omega^2 = -\frac{g}{\rho_{d0}}\frac{\partial \rho_{d0}}{\partial y}\frac{\mathrm{k}_\mathrm{x}^2}{\mathrm{k}^2}. \tag{5.20}$$

5.2.2 Sharp interface

When the interface is sharp we can show that the dispersion relation becomes

$$\omega^2 = \frac{\eta^*}{\tau_m}\mathrm{k}^2 - g\mathrm{k}A_T, \tag{5.21}$$

where $A_T = (\rho_{d02} - \rho_{d01})/(\rho_{d01} + \rho_{d02})$ is the Atwood's number. ρ_{d02} is heavier fluid density is supported by lighter fluid density ρ_{d01}. Here, too the hydrodynamic limit is recovered when the transverse shear wave velocity $\eta^*/\tau_m = 0$ is chosen.

$$\omega^2 = -g\mathrm{k}A_T. \tag{5.22}$$

Eqs. (5.19) and (5.21) imply the existence of transverse shear wave moving with phase velocity $\sqrt{\eta^*/\tau_m}$ for g=0. Also these equations imply that as one increases the value of η^*/τ_m, first term starts to dominate over second which implies the suppression of the Rayleigh-Taylor instability with the increasing phase velocity. This analytical result similar to the strongly coupled electron ion plasma predicted by A. Das *et al.* [123] in context of inertial fusion.

5.3 Numerical simulation

We next carry out the numerical simulation of the system. For this purpose the generalized momentum Eq. (5.2) has been expressed as a set of following two coupled convective equations, under the equilibrium condition considered in Eq. (5.5) and perturbation in density Eq. (5.6).

$$\frac{\partial \vec{v}_d}{\partial t} + \vec{v}_d \cdot \nabla \vec{v}_d + \frac{\rho_{d1}}{\rho_d} g = \frac{\vec{\psi}}{\rho_d}, \tag{5.23}$$

$$\frac{\partial \vec{\psi}}{\partial t} + \vec{v}_d \cdot \nabla \vec{\psi} = \frac{\eta}{\tau_m}\nabla^2 \vec{v}_d - \frac{\vec{\psi}}{\tau_m}. \tag{5.24}$$

Taking curl of Eq. (5.23) the evolution of vorticity under the Boussinesq approximation the coupled set of Eqs. (5.23)-(5.24) have been recast as:

$$\frac{\partial \vec{\xi}}{\partial t} + \left(\vec{v}_d \cdot \vec{\nabla}\right)\vec{\xi} = -\frac{g}{\rho_{d0}}\frac{\partial \rho_{d1}}{\partial x} + \frac{\partial}{\partial x}\left(\frac{\psi_y}{\rho_d}\right) - \frac{\partial}{\partial y}\left(\frac{\psi_x}{\rho_d}\right), \tag{5.25}$$

$$\frac{\partial \vec{\psi}}{\partial t} + \left(\vec{v}_d \cdot \vec{\nabla}\right) \vec{\psi} = \frac{\eta}{\tau_m} \nabla^2 \vec{v}_d - \frac{\vec{\psi}}{\tau_m}, \tag{5.26}$$

and continuity equation

$$\frac{\partial \rho_d}{\partial t} + \left(\vec{v}_d \cdot \nabla\right) \rho_d = 0. \tag{5.27}$$

Here, $\vec{\xi} = \vec{\nabla} \times \vec{v}_d$ (here $\vec{\xi}$ is normalised with dust plasma frequency) is the vorticity. The velocity at each time step is updated by using the Poisson's equation $\nabla^2 \vec{v}_d = -\vec{\nabla} \times \vec{\xi}$ to be used as input to other equations for convection.

We have used the flux corrected scheme (Boris *et al.* [31]) to evolve the coupled set of Eqs.(5.27), (5.25) and (5.26) for various kinds of density profiles.

5.4 Gravitational and buoyancy-driven instabilities

In this section, we present the results of the numerical simulation of gravity-driven instabilities and show numerically that the growth rate of instabilities gets suppressed with increasing coupling strength as expected analytically in Eqs. (5.19)-(5.21).

5.4.1 Rayleigh-Taylor instability

We consider two types of density inhomogeneity profiles, namely (A) with sharp interface between two different densities, where heavier fluid ρ_{d02} (upper) is supported by lighter one ρ_{d01} (lower) as shown in Fig. 5.1(a) and (B) with gradually increasing density gradient along y axis as shown in Fig. 5.1(b). In colorbar, letter **H** is the acronym of the heavy density regime and **L** stands for lighter density regime.

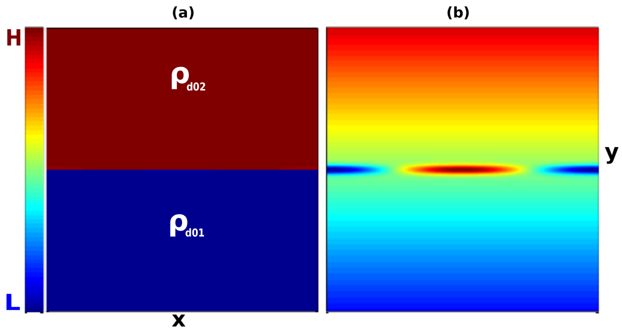

Figure 5.1: Initial density profiles for R-T instability at time t=0 (a) sharp density interface profile and (b) gradually increasing density gradient along vertical y axis; where **H** stands for heavy density and **L** for lighter one.

For both cases A and B, system length is $lx = ly = 2\pi$ and density gradient is chosen along vertical y axis opposite to gravitational acceleration $g(= 10)$. Boundary condition is taken periodic along horizontal direction (X-axis) and non-periodic along vertical direction (Y-axis). A sufficient electric field is provided for equilibrium balance against gravity for the dust particles to levitate, we had a discussion about it in earlier Section 5.2.

5.4.1.1 Sharp interface

For case A (Fig. 5.1(a)), we consider a system consists of two incompressible fluids of constant densities ρ_{d01}=1 for $-\pi \leq y \leq 0$ and ρ_{d02}=2 for $0 = y \leq \pi$ with the denser fluid ρ_{d02} placed above the less dense ρ_{d01}. This equilibrium configuration remains stable in absence of gravity. To hasten the evolution (R-T instability) of our considered equilibrated system under gravity, we impose a small amplitude ϕ_0 sinusoidal perturbation on the interface $(y = 0)$ separating the two different density profiles i.e.

$$\rho_{d1} = \phi_0 cos(\mathrm{k}_x x) exp(-y^2/\epsilon^2). \tag{5.28}$$

Here k_x is the wavelength of the perturbation mode which governs the growth of instability. The thickness of perturbation mode is defined by the value of ϵ. The values of these parameters taken in the present case are $\phi_0 = 0.01$, $\epsilon = 0.1$ and $\mathrm{k}_x = 1$. The total density is $\rho_d = \rho_{d0} + \rho_{d1}$, where $\rho_{d0} = \rho_{d01} + \rho_{d02}$

The R-T instability for the hydrodynamic fluid (HD) of sharp density gradient profile shown in Fig. 5.2 is reproduced by our numerical code. Here, the initial perturbation on the interface was given at $k_x = 1$ which is observed. At the initial stage, the growth is linear until instability amplitudes grow to the order of 0.1λ to 0.4λ, where λ is the perturbation wavelength. As the time elapses, the instability reaches a nonlinear regime. The heavy fluid penetrates into the light fluid as spike. At same time, the lighter one start to move into the heavy fluid along the two sides of the spike and roll-up forming bubbles (as the 'cat-eye'). Bubbles start to grow in size with time. This demonstrates the evolution (Fig. 5.2) of the sharp density gradient stratified against gravity, a well known result for hydrodynamic fluid, substantiating our numerical work.

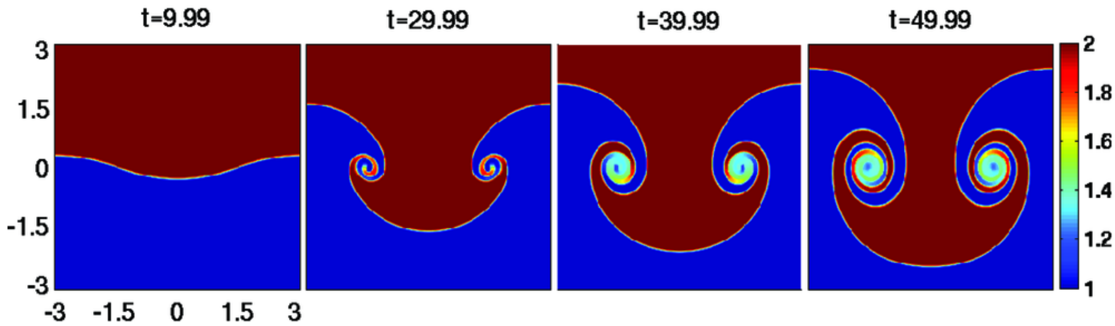

Figure 5.2: Evolution of sharp density profile in time for inviscid hydrodynamic fluid.

We now study the role of strong coupling effect on this instability by choosing a finite value of η/τ_m in our simulations. The subplots of Fig. 5.3 shows the evolution of the interface for a visco-elastic fluid with η= 0.1, τ_m=20, η/τ_m =0.005. The initial linear growth is followed up by nonlinear stage where rolls form. The trend is thus similar to that of the hydrodynamic fluid. However, a comparison of cases with different values of η/τ_m shows that there is a reduction in growth rate with increasing value of the coupling as expected analytically.

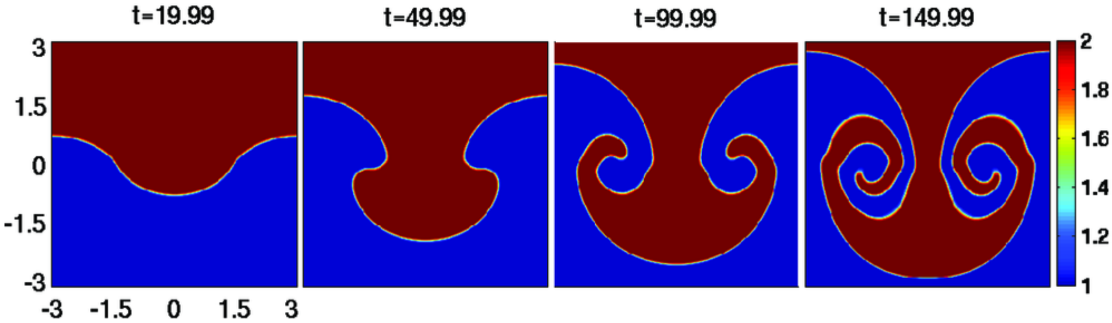

Figure 5.3: Evolution of sharp density profile in time for strongly coupled dusty plasma medium for the η= 0.1; τ_m=20.

In Fig. 5.4, we have compared two different cases of GHD simulation, with different values of η and τ_m parameters ($\eta = 0.1, \tau_m = 5, \eta/\tau_m$=0.02 for Fig. 5.4(a) and $\eta = 1, \tau_m = 20, \eta/\tau_m$=0.05 for Fig. 5.4(b)). From the comparison of Fig. 5.3, Fig. 5.4(a) and Fig. 5.4 (b) it is clear that at each time step, the evolution/growth of perturbation/instability gets weaker with increasing coupling strength i.e. η/τ_m.

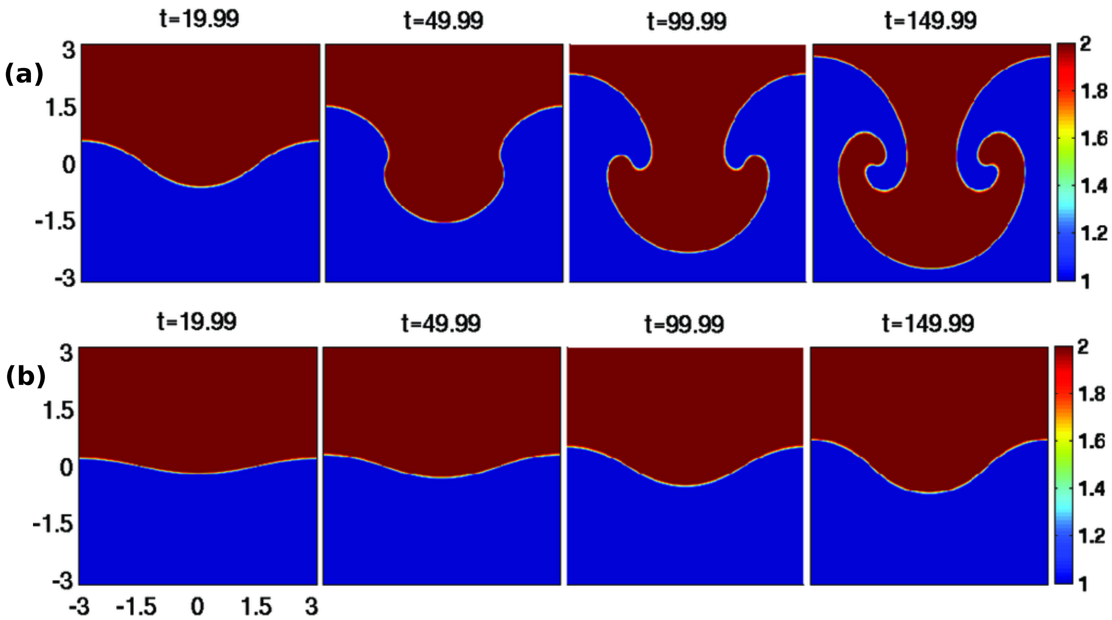

Figure 5.4: Evolution of sharp density profile in time for strongly coupled dusty plasma medium for the cases (a) η= 0.1; τ_m=5 and (b) η= 1; τ_m=20.

Thus, all these stages show that the R-T instability in the dust fluid phenomenologically/trend similar to the hydrodynamic case (Fig. 5.2) as observed experimentally by Pacha *et al.* [122] in their experiment of dusty plasma.

5.4.1.2 Gradually density gradient in counter direction of gravity

Apart from the sharp interface separating the two fluids (Fig. 5.1(a)), the R-T instability can also be observed where the density gradient gradually increases with gravity/accelerating force. Fig. 5.1(b) shows the density profile with gradually increasing in vertical direction along y axis is given as:

$$\rho_d = \rho_{d0} + \phi_0 exp(\sigma y) + \rho_{d1}. \tag{5.29}$$

Here ρ_{d0} is constant background density. The value of parameters taken for present case are ρ_{d0}=5, amplitude of inhomogeneity ϕ_0=0.1, to evolve the coupled and σ=0.025 decide the ramp of inhomogeneity in background density. The sinusoidal perturbation ρ_{d1} (see Eq. 5.28) is imposed at y = 0, which can be clearly seen in Fig. 5.1(b).

In Fig. 5.5, we have compared three different cases of GHD simulation, with different values of η and τ_m parameter ($\eta = 0.1, \tau_m = 20, \eta/\tau_m$=0.005 for Fig. 5.5(a), ($\eta = 0.1, \tau_m = 5, \eta/\tau_m$=0.02 for Fig. 5.5(b) and $\eta = 1, \tau_m = 20, \eta/\tau_m$=0.05 for Fig. 5.5(c)). From the comparison of Fig. 5.5(a,b,c), it is clear that at each time step, the evolution/growth of perturbation/instability gets weaker with increasing coupling strength i.e. η/τ_m.

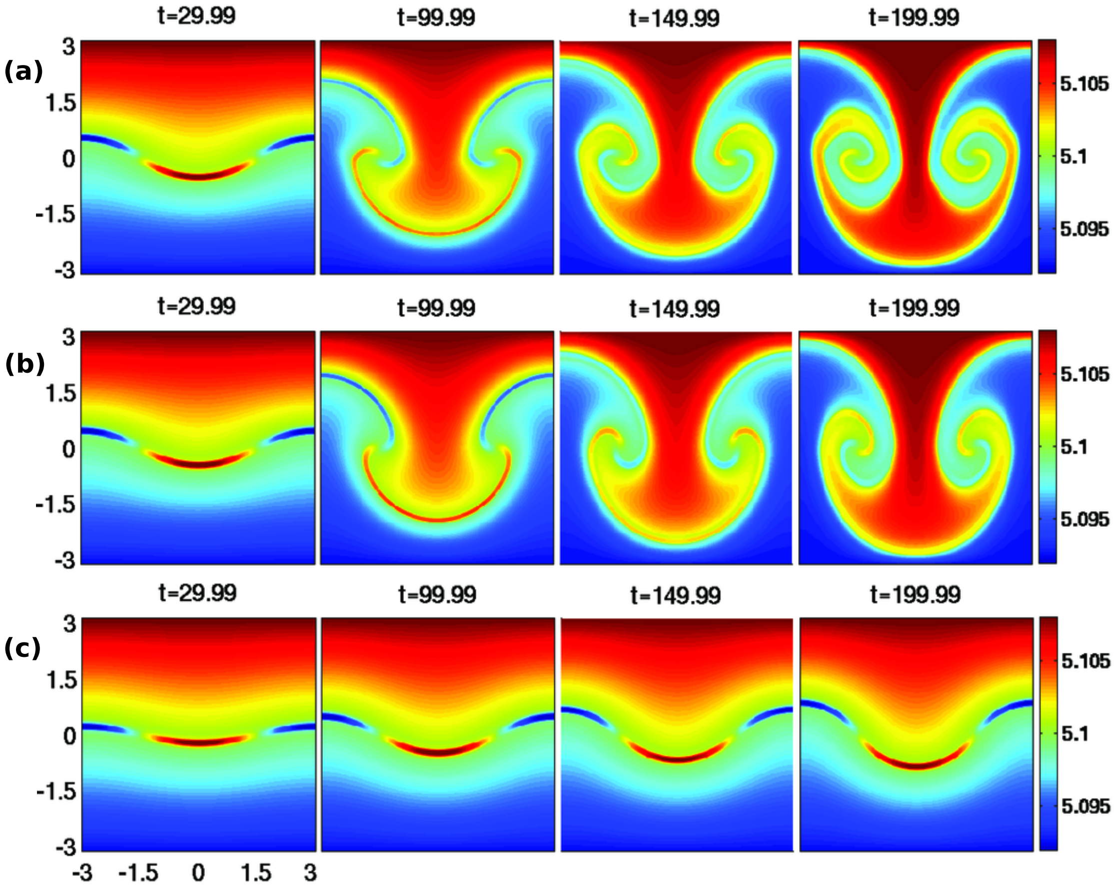

Figure 5.5: Evolution of gradually density profile in time for strongly coupled dusty plasma medium for the cases (a) η=0.1; τ_m=20, (b) η=0.1; τ_m=5 and (c) η=1; τ_m=20.

One can see that the growth rate is found to decrease with the increasing value of η/τ_m and finally gets saturated.

5.4.2 Buoyancy-driven evolution

We now consider the evolution of localized low/high density bubbles/droplets in the medium. Under the influence of gravity, the less dense regions (bubble) have a tendency to float upwards, whereas the higher density (droplet) sink against the background low density fluid. A detailed numerical simulation is carried out to study a rising bubble and a falling droplet for the visco-elastic medium. The prime concern here is to specifically understand the role of TS waves on the evolution of a bubble and a droplet in the i-GHD medium.

5.4.2.1 Rising bubble and falling droplet

We consider the two types of density inhomogeneity profiles, namely (A) an initially static and circular bubble whose density is less than that of the surrounding quiescent Newtonian/visco-elastic fluid as shown in Fig. 5.6(a) and (B) initially static and a circular droplet whose density is higher than that of the surrounding medium as shown in Fig. 5.6(b). In both the cases the variation in density is symmetric about the axis which is perpendicular to simulation plane.

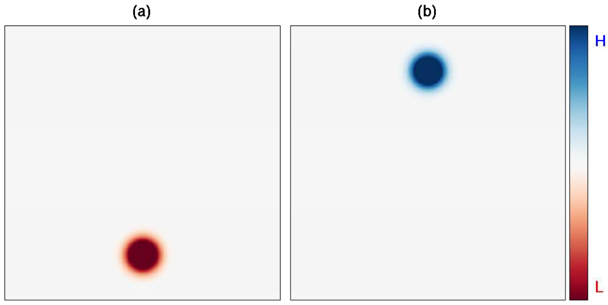

Figure 5.6: Initial densities' profiles at time t=0 (a) bubble of less density inside the heavier fluid and (b) droplet of less density inside the heavier fluid.

For both cases, we have considered a system of length $lx = ly = 12\pi$, approximating the gravitational acceleration as $g = 10$. Boundary condition is periodic along horizontal direction (X-axis) and non-periodic along vertical direction (Y-axis).

5.4.2.2 Rising bubble

In order to simulate the case of rising bubble (i.e. case A), we have considered a Gaussian density profile given by

$$\rho_{d1} = \rho_0' exp\left(\frac{-\left((x-x_c)^2 + (y-y_c)^2\right)}{a_c^2}\right), \tag{5.30}$$

where a_c is the bubble core radius and the numerical simulation has been carried out for a_c=2.0, $\rho_0' = -0.5$ and $x_c = 0$, $y_c = -4\pi$. We took the homogeneous background density as $\rho_{d0} = 5$. The total density is $\rho_d = \rho_{d0} + \rho_{d1}$.

Figure 5.7 displays the density profile of a bubble at various times. Initially at time $t = 0$, the bubble is axisymmetric (Fig. 5.6(a)) and as the system evolves, the bubble simply rises without any significant change in shape for a short period of time. At a later stage, the initially circular profile assumes a crescent shape as evident from the first subplot of Fig. 5.7. Further, as time progresses, a mushroom-like structure which is characteristic of R-T instability begins to appear along with rolling and mixing at the edge of bubble. This mushroom-like structure then breaks into two distinct elliptical lobes as evident from the figure. These lobes propagate forward as a single entity leaving behind wake-like structure in background fluid.

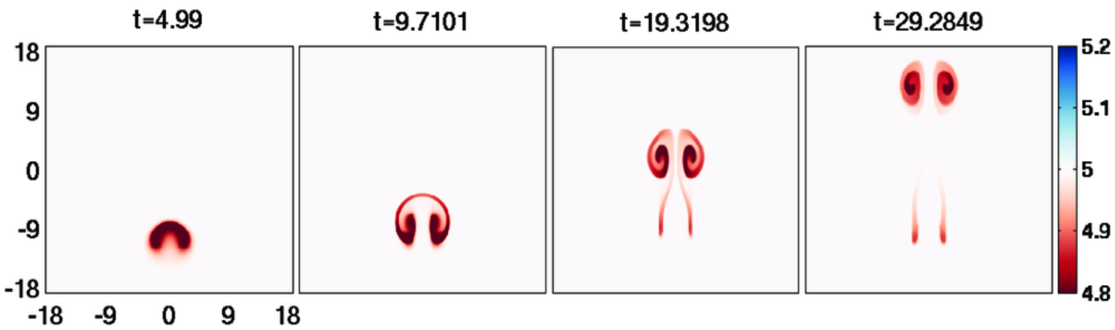

Figure 5.7: Evolution of bubble density profile in time for inviscid hydrodynamic fluid

We now show the simulation of this density configuration for the visco-elastic case and compare it with the simulation for hydrodynamic case described above. In Fig. 5.8, we demonstrate the different stages of GHD simulation, with values of $\eta = 2.5, \tau_m = 20$ i.e. η/τ_m=0.125. From the comparative observations between Fig. 5.7 and Fig. 5.8, it is interesting to notice that the vertically rising rate of bubble decreases in GHD. The appearing rolled-up lobes also seem to be comparatively much more displaced sidewards. Thus the structures are broader and the upward movement is constraint in the visco-elastic case. The wake is also found to be weaker in this case.

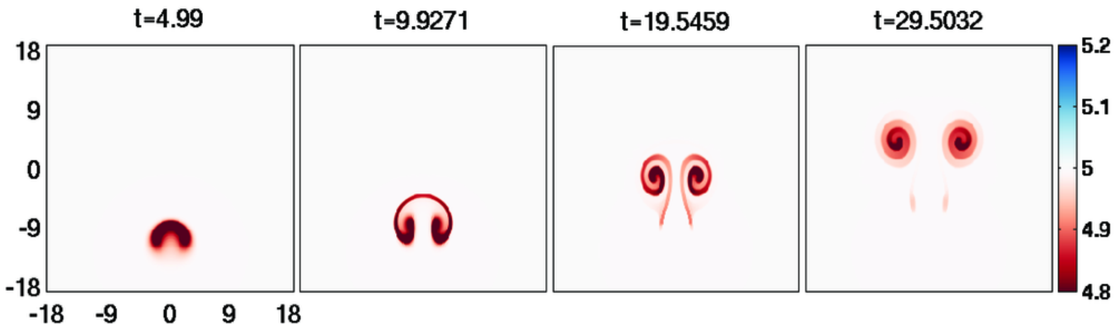

Figure 5.8: Evolution of bubble density profile in time for the strongly coupled dusty plasma medium, η= 2.5; τ_m=20.

To envisage the effect of strong coupling, we compare this GHD simulation (Fig. 5.8) with another GHD system (Fig. 5.9) having higher coupling strength i.e. η=10, τ_m=20, η/τ_m=0.5. We observe that with increasing coupling strength the vertically rising rate of bubble decreases. Also, the elliptical lobes start moving apart in horizontal direction earlier in stronger coupled medium. At the same time, the rolling rate of lobes increases causing the expansion of lobes and disappearance of the dragging tail. This horizontal motion commences earlier in the medium with stronger coupling.

Figure 5.9: Evolution of bubble density profile in time for the strongly coupled dusty plasma medium, η= 10; τ_m=20.

In Fig. 5.10, the vorticity subplots in first and second row correspond to the density profiles shown in Fig. 5.8 and Fig. 5.9, respectively. This figure clearly elucidates the role of TS waves (coupling strength i.e η/τ_m) in evolution of the bubble in GHD medium.

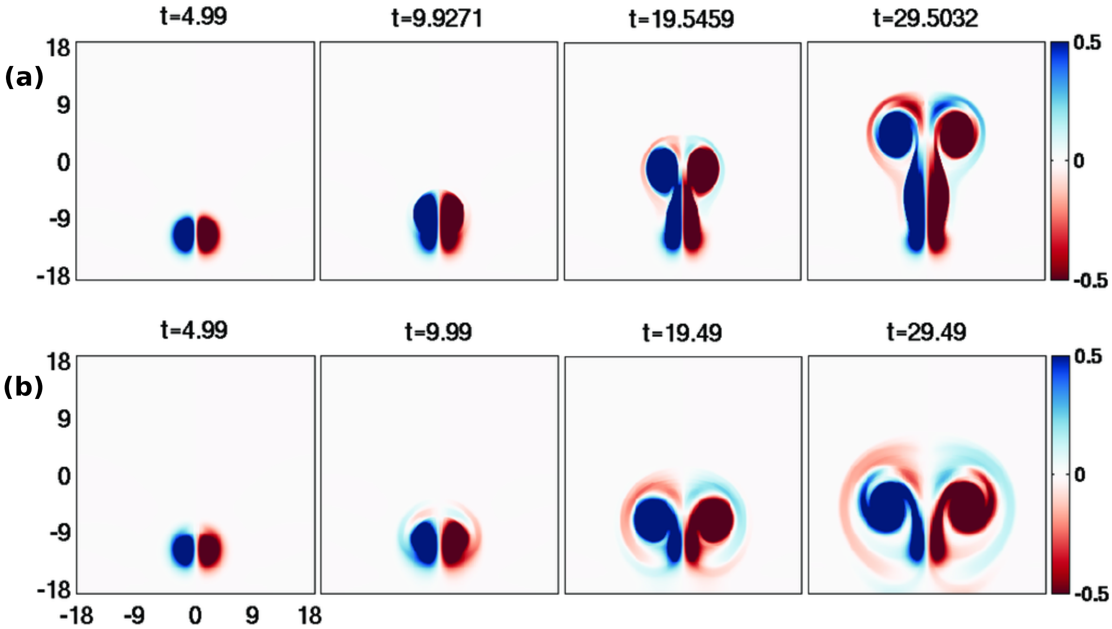

Figure 5.10: Evolution of bubble vorticity profile in time for strongly coupled dusty plasma medium for the cases (a) η= 2.5; τ_m=20, and (b) η= 10; τ_m=20.

As discussed earlier, the GHD medium supports transverse waves and they traverse with the phase velocity $v_p = \sqrt{\eta/\tau_m}$. It is evident from Fig. 5.10 that there is emission of TS waves surrounding the vorticity lobes for visco-elastic fluids and no such TS waves exist for hydrodynamic fluid (Fig. 5.11). Further, the TS waves propagate with velocity v_p=0.158 and v_p=0.316 for the coupling parameters η= 2.5; τ_m=20 and η= 10; τ_m=20, respectively. This implies that the TS enclosure should be larger for the second case. The relative observations of Fig. 5.10(a) and Fig. 5.10(b) clearly reflect the aforementioned fact. The emission of TS wave from each of the lobes of the vorticity structure has profound effect on its evolution. The wave from either lobe pushes the other lobe in the direction perpendicular to direction of propagation of the entire structure and as a result the lobes get well separated with time. Besides this lobe separation, the emission of TS wave significantly reduced the strength of dipole thereby impeding the dipole propagation. From the discussion thus far it is expected that the propagation speed of the dipole should reduce and the separation between the lobes should increase with the increase in the coupling strength of the medium. These features of the dipole propagation can be well identified in Fig. 5.10.

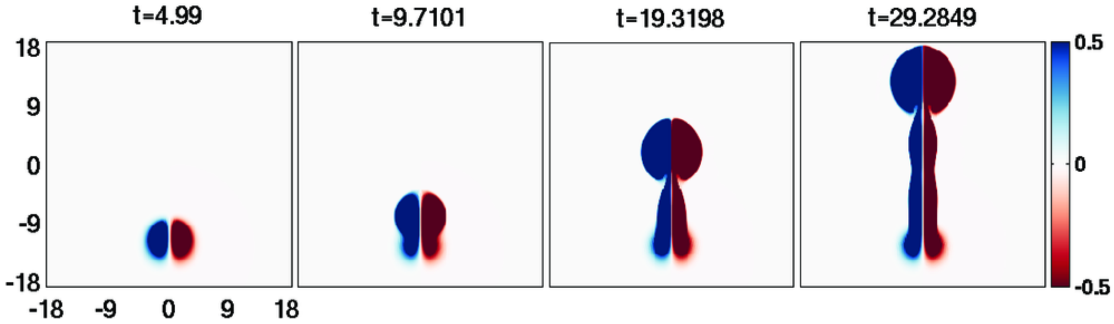

Figure 5.11: Evolution of bubble vorticity profile in time for hydrodynamic fluid

5.4.2.3 Falling droplet

For case B (Fig. 5.6(b)), the density profile of droplet is given as

$$\rho_{d1} = \rho_0' exp\left(\frac{-(x-x_c)^2-(y-y_c)^2}{a_c^2}\right), \tag{5.31}$$

where a_c is the droplet core radius, the numerical simulation has been carried out for a_c=2.0, $\rho_0' = 0.5$ and $x_c = 0$, $y_c = 4\pi$. We considered the homogeneous background density as $\rho_{d0} = 5$. The total density is $\rho_d = \rho_{d0} + \rho_{d1}$.

Figure 5.12 shows the dynamics of the droplet, falling in tranquil hydrodynamic fluid. The suspended drop starts to fall. As time passes, the drop breaks up forming first a semicircular structure then a two lobes similar to the case of bubble.

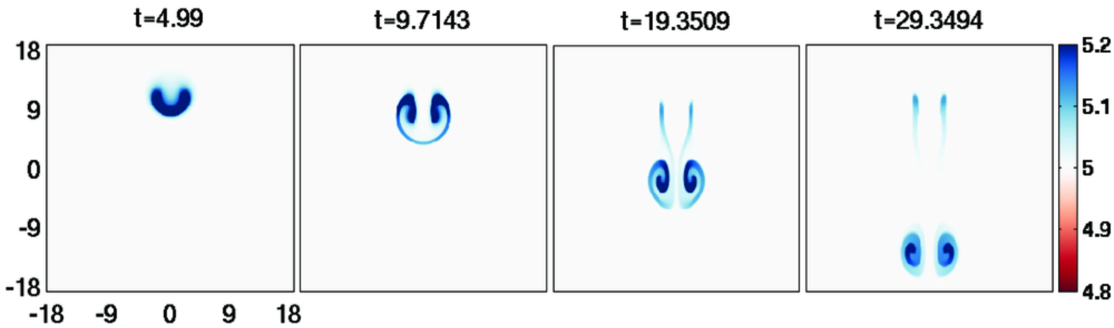

Figure 5.12: Evolution of droplet density profile in time for inviscid hydrodynamic fluid.

Figure 5.13 reveals the different stages of droplet for GHD simulation with values of $\eta = 2.5, \tau_m = 20$. As done for rising bubble, we shall now compare

Fig. 5.12 and Fig. 5.13. It is evident that the vertically falling rate of droplet decreases for the GHD case. In addition to the slowing down of the falling rate (Fig. 5.13), the two lobes start separating apart horizontally. The dragging tail from the structure can also be observed which decreases in size in GHD.

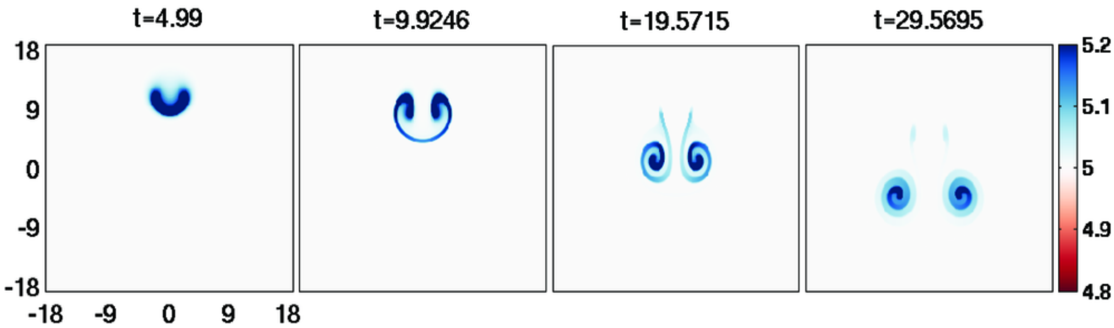

Figure 5.13: Evolution of droplet density profile in time for strongly coupled dusty plasma medium for the case η= 2.5; τ_m=20.

For a higher coupling strength ($\eta = 10, \tau_m = 20$ i.e. η/τ_m=0.5) shown in Fig. 5.14, the downward motion is even slower. The transverse dimension is even larger and the dragging tail does not seem to appear at all.

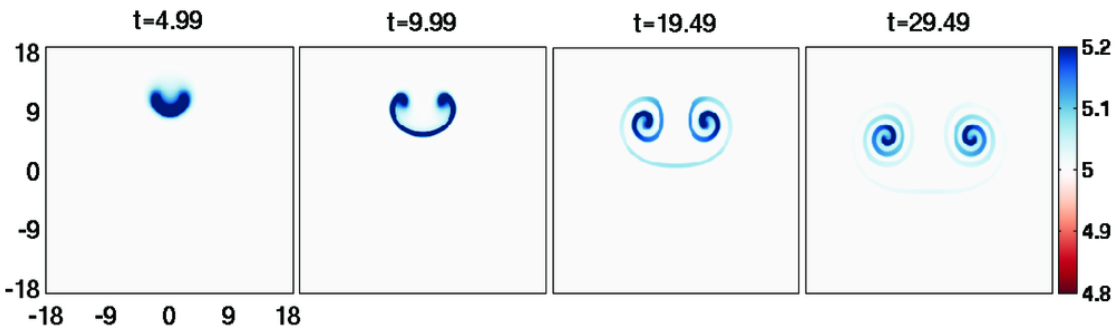

Figure 5.14: Evolution of droplet density profile in time for strongly coupled dusty plasma medium for the case η= 10; τ_m=20.

Again, similar to the case of bubbles, the vorticity plots are provided for observing a clear role of TS waves i.e. pushing the two lobes apart, as seen in Fig. 5.15.

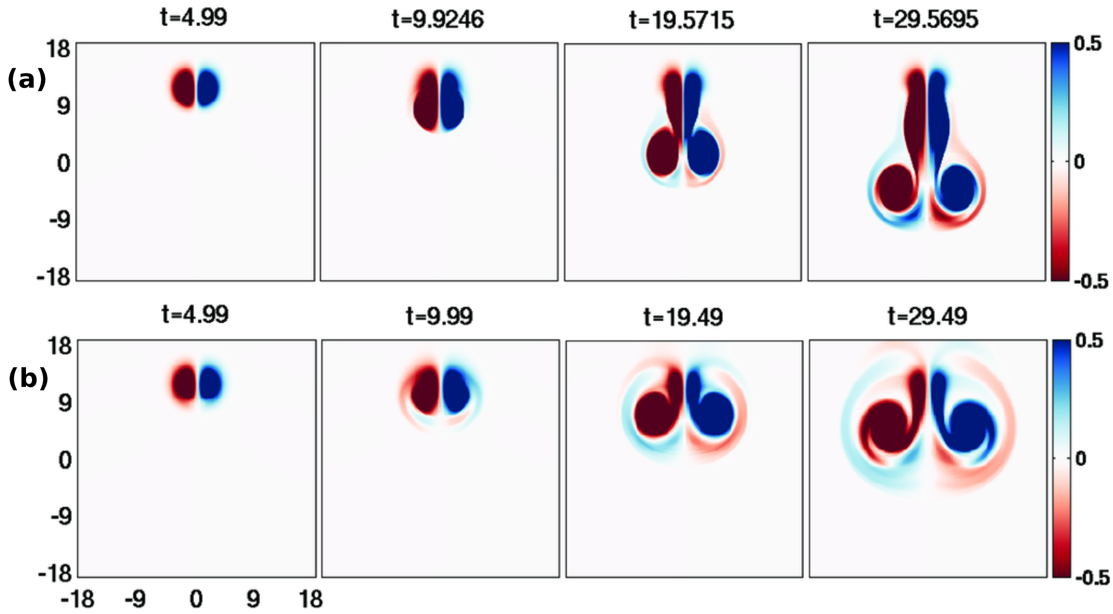

Figure 5.15: Evolution of droplet vorticity profile in time for strongly coupled dusty plasma medium for the cases (a) η= 2.5; τ_m=20, and (b) η= 10; τ_m=20

For hydrodynamic fluid the corresponding vorticity subplots (Fig. 5.16) to the mentioned density profile (Fig. 5.12), no such wave which can constraint the falling rate, were observed.

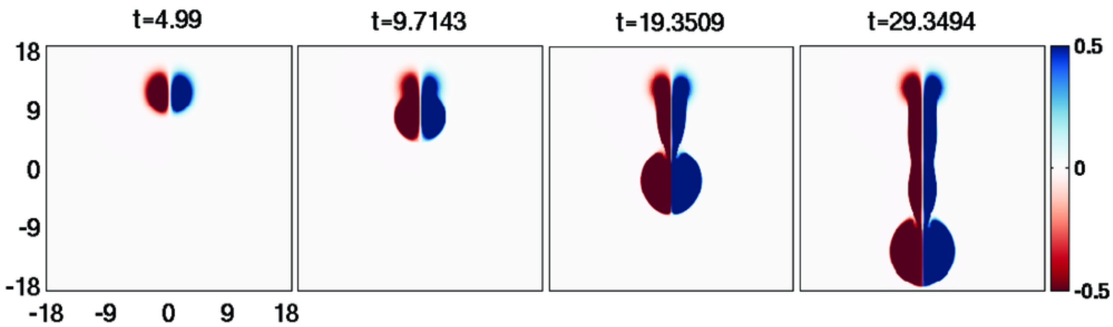

Figure 5.16: Evolution of droplet vorticity profile in time for hydrodynamic fluid.

Thus, we conclude that the increase of phase velocity of TS waves with coupling strength suppresses the buoyant nature of a bubble and a droplet.

5.4.2.4 Interaction of a bubble and a droplet

The focus of this subsection is to study the interaction between a bubble and a droplet. Here, we have considered two cases as shown in Fig. 5.17.

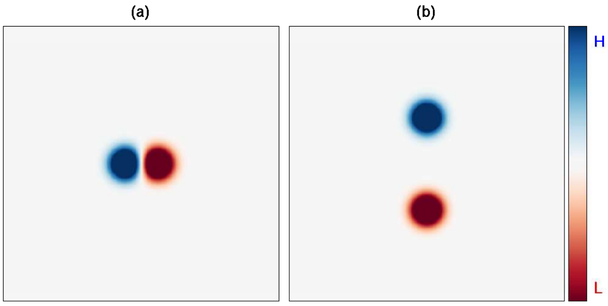

Figure 5.17: Initial density profiles at time t=0 (a) the droplet (left) and the bubble (right) are placed at the same height and (b) the droplet and the bubble are aligned vertically with the droplet placed above the bubble

The density inhomogeneity (droplet and bubble) for the present case is given by

$$\rho_{d1} = \rho'_{d1} + \rho'_{d2}, \tag{5.32}$$

with the background density $\rho_{d0} = 5$ for the both cases. The density profile for the droplet is

$$\rho'_{d1} = \rho'_{01} exp\left(\frac{-(x - x_{c1})^2 - (y - y_{c1})^2}{a_{c1}^2}\right), \tag{5.33}$$

and the density profile for the bubble is

$$\rho'_{d2} = -\rho'_{02} exp\left(\frac{-(x - x_{c2})^2 - (y - y_{c2})^2}{a_{c2}^2}\right). \tag{5.34}$$

Here, ρ'_{01}=ρ'_{02}=0.5. The total density is $\rho_d = \rho_{d0} + \rho_{d1}$.

In the first case (A), the droplet and the bubble are placed at the same height. For the droplet, the values of the parameters a_{c1}, x_{c1}, and y_{c1} are 2.0, 2.2 and 0.0, respectively and for the bubble, the values of the parameters a_{c2}, x_{c2}, and y_{c2} are 2.0, -2.2 and 0.0, respectively.

It is worth noting at this point that if the bubble and the drop were well separated, there would be no interaction between them and their evolution would be same as discussed earlier. To include the interaction effects, the bubble and droplet are closely spaced for the present case. This horizontal configuration of droplet and bubble induces initial counterclockwise rotation of the combined structure about a common center of rotation. Owing to gravity, the two density lobes gradually take a crescent shape as they rotate. The combined effect of gravity and rotation transforms the crescent-shaped lobes into thin intertwining spirals. Up to this stage, there is no significant difference in density profiles for HD and GHD cases and the common evolution features can be clearly seen in the first rows of Figs. 5.18, 5.19 and 5.20.

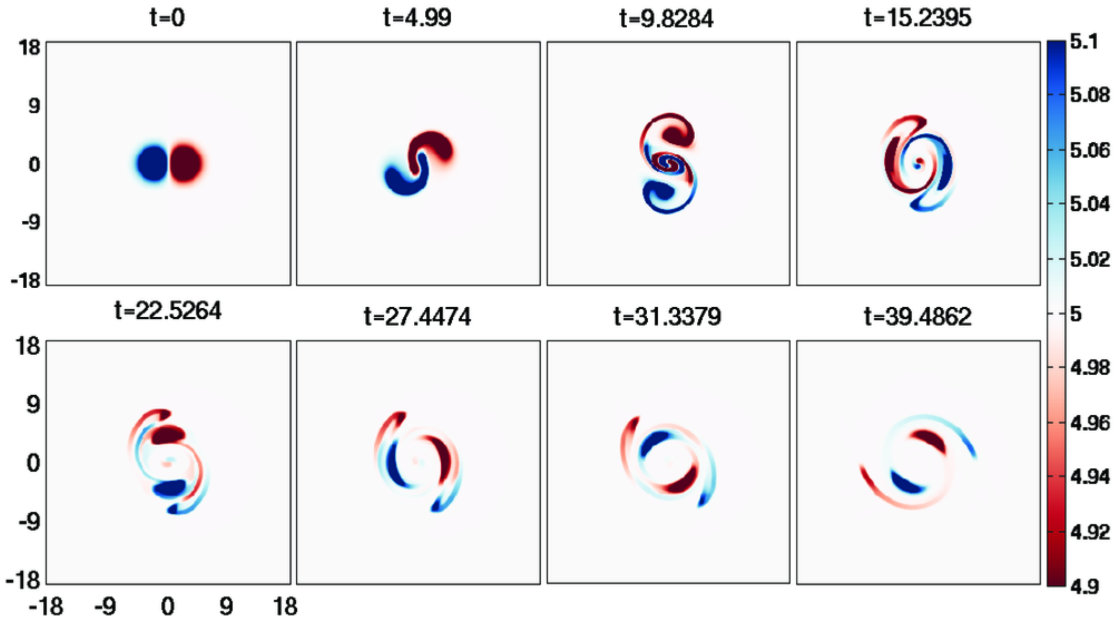

Figure 5.18: Evolution of combine bubble and drop density in time for hydrodynamic fluid.

At later stage, the density configuration evolves quite differently for HD and GHD cases. In case of HD we observe two persistently rotating prominent crescent structures along with faint spirals. However, for the GHD cases the crescent structure is completely absent and the whole structure evolves into spirals.

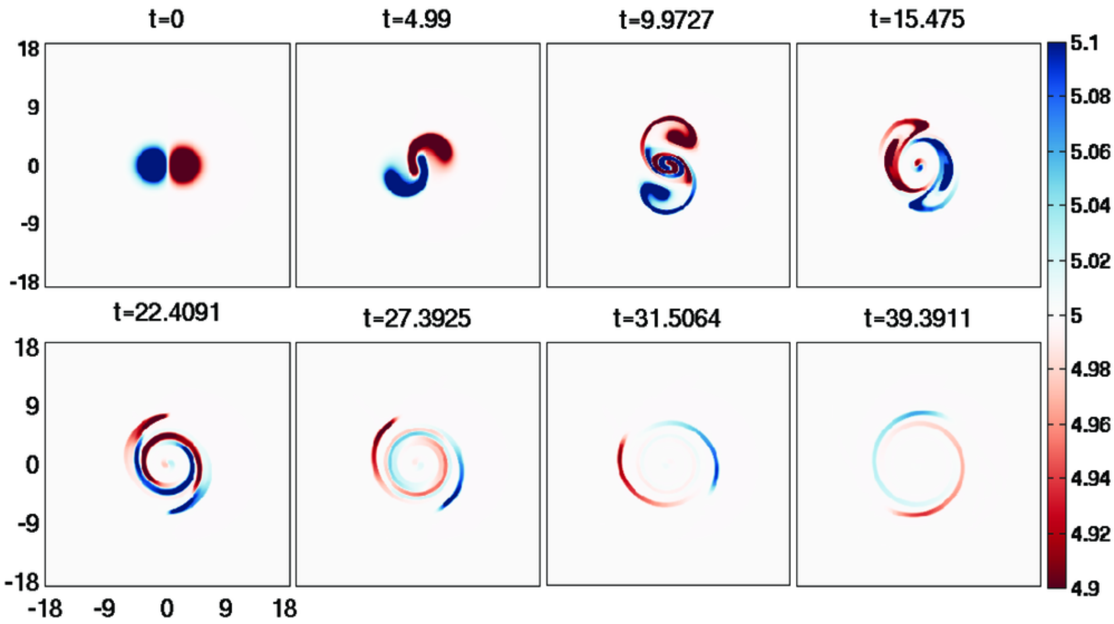

Figure 5.19: Evolution of rotating density profile in time for strongly coupled dusty plasma medium for η= 2.5; τ_m=20.

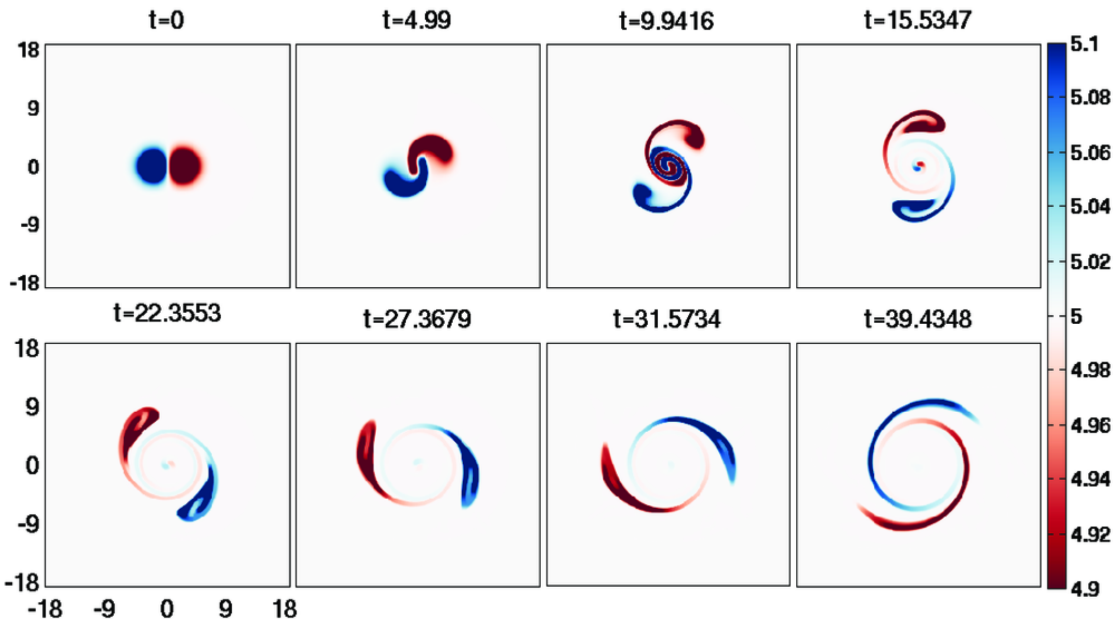

Figure 5.20: Evolution of rotating density profile in time for strongly coupled dusty plasma medium for the η= 10; τ_m=20.

The evolution of the spirals in GHD medium is significantly affected by the coupling strength. As the coupling strength increases, the emission of TS wave from the spirals become dominant. This TS wave then drives the spiral arms outward away from the center of rotation. Comparison of second row from Fig. 5.19 (η= 2.5; τ_m = 20) and Fig. 5.20 (η= 10; τ_m = 20) clearly displays the aforementioned effects of the coupling strength on the evolution of the spirals.

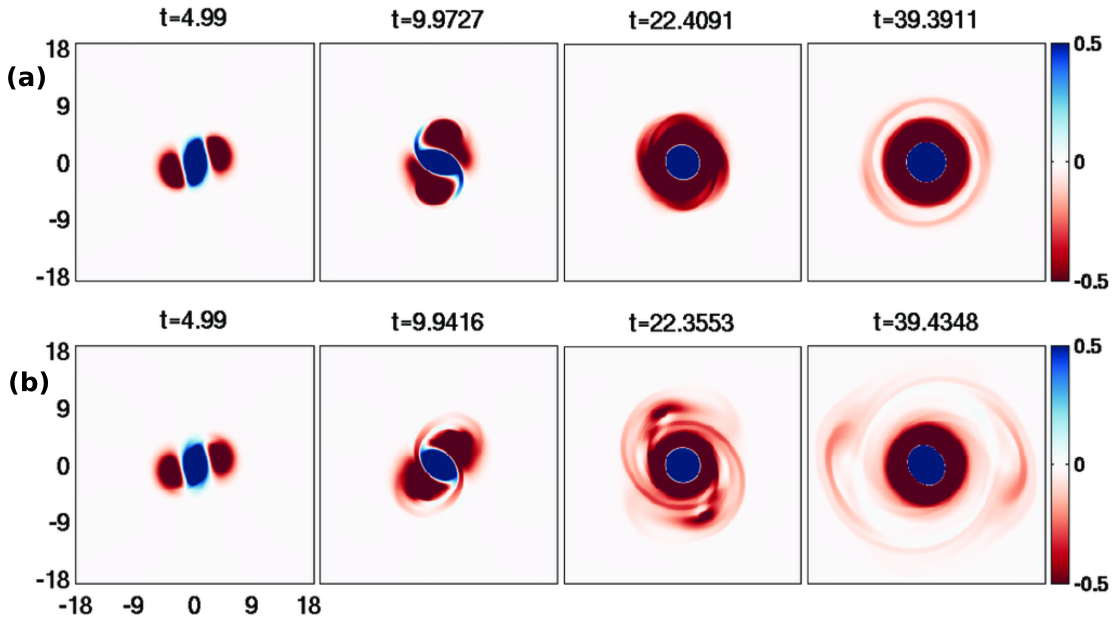

Figure 5.21: Evolution of vorticity profiles in time for strongly coupled dusty plasma medium corresponding to the rotating density profiles for the cases (a) η= 2.5; τ_m=20, and (b) η= 10; τ_m=20.

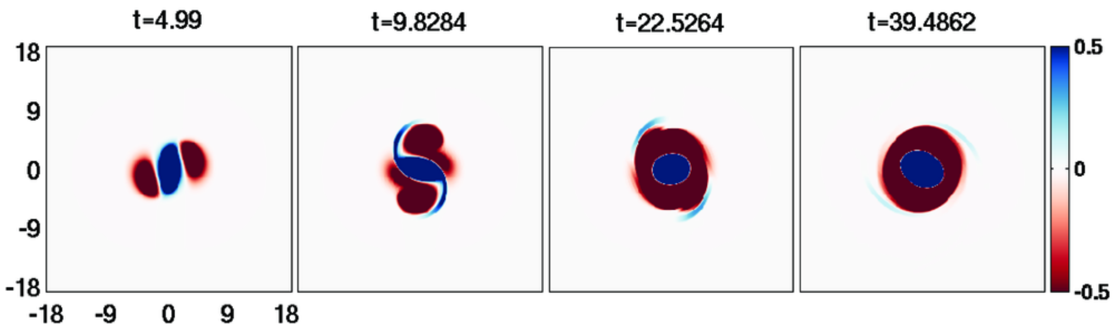

Figure 5.22: Evolution of vorticity profile in time for hydrodynamic fluid.

The presence of TS wave could be understood well by comparing vorticity contour plots for GHD mediums with different coupling strengths as shown in

Fig. 5.21(a) (η=2.5; τ_m=20, η/τ_m=0.125) and Fig. 5.21(b) (η= 10; τ_m=20, i.e. η/τ_m=0.5). Corresponding subplots for HD case in Fig. 5.22 show absence of TS waves.

We now consider the second case (B) where the droplet and the bubble are aligned vertically. For this case the values of the parameters a_c, x_c, y_c, ρ' for the droplet and the bubble are 2.0, 0.0, 4π, 0.5 and 2.0, 0.0, -4π, 0.5, respectively. For this configuration the droplet lies above the bubble (Fig. 5.17(b)) and contrary to the previous case Fig. 5.17(a), there is no rotation of the bubble and the drop. Here, the falling droplet and the rising bubble simply collide with each other during the course of evolution.

Figure 5.23 displays the evolution of this density configuration for the hydrodynamic case. It is evident from the figure that as these two structures evolve, they hit each other and their lobes get separated. One lobe from the bubble and one lobe from the droplet pair with each other and move horizontally subsequently.

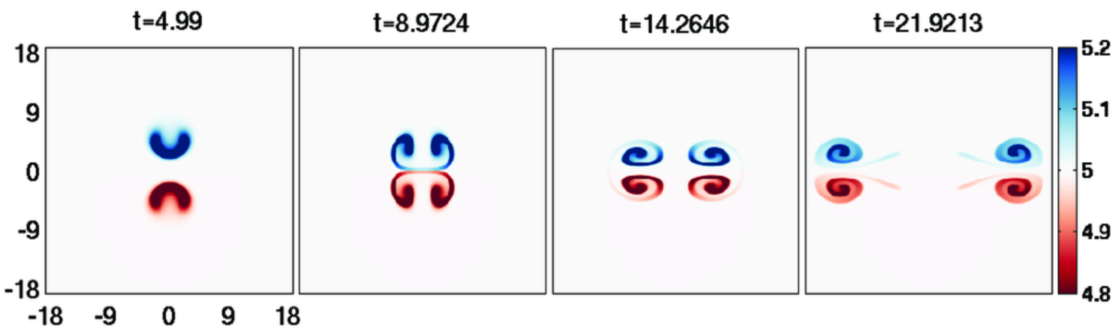

Figure 5.23: Evolution of density profile of colliding bubble and droplet in time for hydrodynamic fluid.

Figure 5.24(a) (η= 2.5; τ_m=20) and Fig. 5.24(b) (η= 10; τ_m=20) show the evolution of same density configuration for GHD case. It is evident from figures that in comparison to the HD case, the horizontal movement of the structures is slower for the GHD case. The horizontal movement further gets slower with increasing coupling strength of the medium.

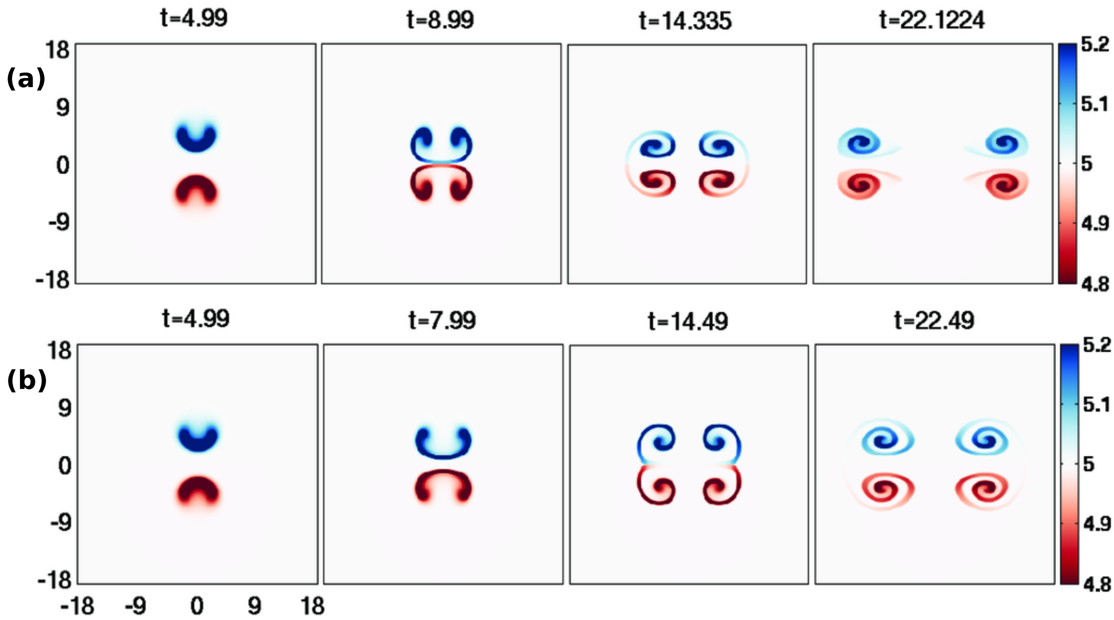

Figure 5.24: Evolution of density profile of colliding bubble and droplet in time for strongly coupled dusty plasma medium for the cases (a) η= 2.5; τ_m=20, and (b) η= 10; τ_m=20.

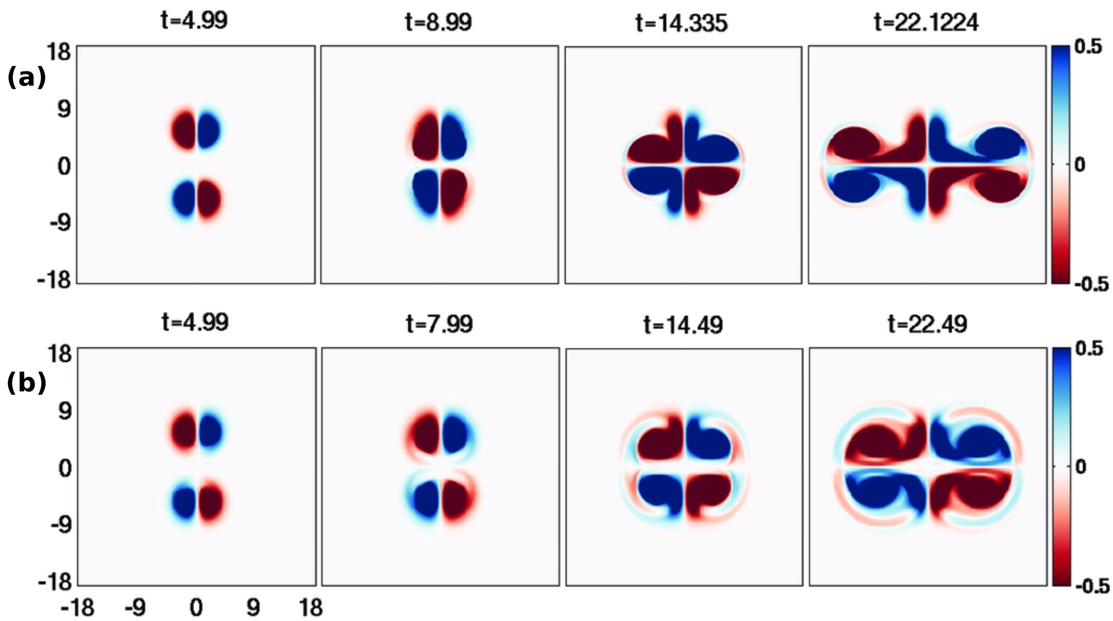

Figure 5.25: Evolution of vorticity profile of colliding bubble and droplet in time for strongly coupled dusty plasma medium for the cases (a) η= 2.5; τ_m=20 and (b) η= 10; τ_m=20.

Figure 5.25 shows the vorticity plots for the GHD case. TS waves surrounding the vorticity lobes are clearly visible for visco-elastic fluids while there is no such waves for HD (Fig. 5.26).

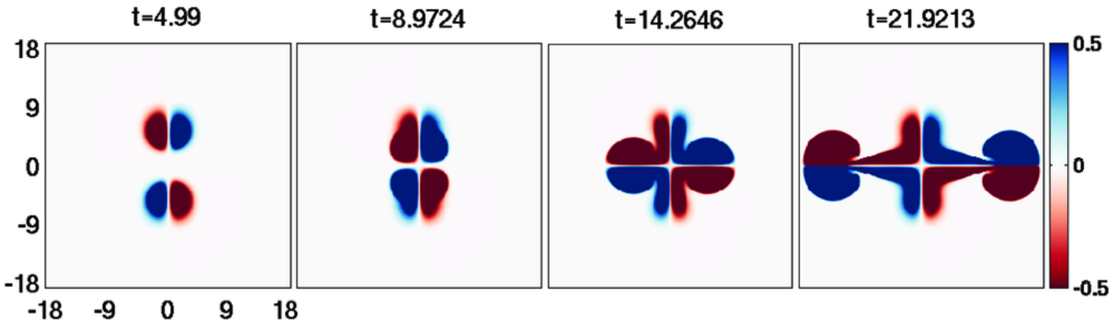

Figure 5.26: Evolution of vorticity profile of colliding bubble and droplet in time for hydrodynamic fluid.

As discussed earlier, the continuous emission of transverse wave saps the dipole strength, thereby reducing its propagation speed. This effect is also observed for the present case, as shown in Fig. 5.25.

5.5 Summary

Our studies show that both R-T instability and buoyancy driven motion get suppressed as one moves from weakly coupled to strongly coupled regime. This has been shown analytically by using the GHD description and also by numerically simulating the system.

The bubble and droplet evolution in the strongly coupled medium as well as their interaction is also studied extensively by numerical simulations. In all these cases a major role of the TS waves in the evolution is shown.

6

Conclusions and Future Work

This chapter summarizes the important findings of our research work and gives an overview of the prospective problems concerning this subject that have not been addressed in this thesis. The present thesis is focussed on the study of dusty plasma system. The dusty plasma system has an important role to play in the context of understanding the physics of strongly coupled systems. The Generalized Hydrodynamic model is a simplified phenomenological model for depicting visco-elastic fluid behaviour. The model has been used for the present studies on strongly coupled dusty plasma behaviour.

The main results of research are summarized in Section 6.1. A brief discussion on the future scope of the work presented in the thesis has been given in Section 6.3.

6.1 Feature points of the thesis

This doctoral thesis reports the collective behavior of the strongly coupled dusty plasma medium using the formalism of Generalized Hydrodynamic (GHD) fluid model. This model accounts for the strong coupling behaviour of the medium by considering the medium to retain memory, as in elastic systems, for a certain duration - known as the memory relaxation time. The system is thus modelled as a visco-elastic fluid. The GHD model in addition to supporting compressible acoustic perturbations also supports transverse shear (TS) wave which are unique to this medium. Our present work is dedicated to an extensive study of the evolution of coherent structures, transport and mixing of the fluid, instability development etc., in the medium using this model prescription and specifically understand the role of TS waves in it. We, have therefore, chosen to completely eliminate the compressible acoustic perturbations from the system by considering the incompressible limit of the GHD equations. This is a valid description when the acoustic velocity is very high. Detailed numerical simulation studies have been carried out for this purpose and the salient features are summarized below:

6.1.1 Incompressible limit of GHD (i-GHD) model

GHD model depicts the existence of both incompressible transverse shear and compressible longitudinal modes. In this thesis only the incompressible limit of the GHD equations for the dusty plasma medium has been considered, which we refer to as the i-GHD model.

In the incompressible limit the Poisson's equation is replaced by the quasi-neutrality condition and charge density fluctuations are ignored. This results in a coupled set of convective equations which are evolved using the flux corrected scheme. In this limit, however, the equations are applicable to any incompressible visco-elastic system and not merely restricted to the strongly coupled dusty plasma (SCDP) system alone. However, the SCDP system may be one of the most convenient system to prepare and conduct experimental studies on visco-elastic traits of a medium.

We have in our studies considered the evolution of a variety of both smooth and sharp coherent vortex structures. The former being smooth is stable to K-H instability whereas the latter suffers from the K-H destabilization also at the edges where vorticity changes sharply and a strong velocity shear exists. A comparison of transport and mixing properties of the HD and i-GHD systems have been provided. A prominent fluid instability, namely the Rayleigh-Taylor instability occurring in the gravitationally stratified system has also been studied in detail.

The main results of the thesis are identified below.

6.1.2 Evolution of smooth coherent structures

The structures being smooth the K-H destabilization is absent. For the i-GHD model these structures emit transverse shear waves.

- **Numerically observation of TS waves : Code validation**
  A smooth circular patch of rotating vortices are observed to emit radially propagating transverse shear waves. The radial phase velocity $\sqrt{\eta/\tau_m}$ was observed as per the analytical predictions made by Kaw *et al.* [48] for GHD model. The $1/\sqrt{r}$ fall in the intensity as expected for radial emission in 2-D is also confirmed numerically

- **Interaction between distinct vortex structures in presence of TS waves**
  In HD fluids the like-signed vortices are observed to merge with time. In i-GHD, however, one of the prominent feature being the emission of TS waves the merging does not lead to a coherent final form like hydrodynamic fluids. Instead a continuous emission of TS waves dominate over the merging process.

  In HD case when two unlike-signed vortices are brought together, they form dipoles which propagate with an axial velocity which depends on the strength of the vorticities and also on the closeness of the two structures. We observe additional features in the case of i-GHD. The axial propagation speed can be chosen to be either faster/slower than the phase velocity of the emitted TS wave. In the case of former which we term as the super-luminar dipoles the emission of TS waves forms a wake behind the dipole and the structure moves axially ahead and displays all other features which are more or less similar to the HD case. However, when the axial propagation speed is slower than the TS wave, it gets entirely engulfed in the emitted waves and pretty soon looses its identity. A detail study of collisional interaction amidst sub- and super-luminar dipoles etc., has also been carried out by us and forms a part of Chapter 2

6.1.3 The conservation theorem

The continuous emission of TS waves from the vortex structures depletes the strength of the structures. Keeping in view the transverse nature of the emitted waves, we take cue from the electromagnetic waves which satisfy Poynting theorem. A Poynting-like conservation theorem is constructed for the 2-D i-GHD model equations. The rate of change of a generalized enstrophy-like quantity (sum of square integrals of vorticity and the velocity strain) is shown to be controlled by radiative, convection and dissipative effects. The radiation term corresponds to the TS waves and shows a striking similarity with electromagnetic waves. The equation also indicates that convection and viscous dissipation are other important mechanism that could significantly change the conserved quantity.

The conservation law was then illustrated by considering the emission of TS waves radiation for various cases e.g. rotating monopole vortex patterns, propagating and colliding dipole structures for the dusty plasma medium. The demonstration of the utility of the method in understanding dipole vorticity patches moving slower and faster than the TS waves provides a comprehensive view on the topic. These conclusions are likely to be generic and applicable to all strongly coupled media.

6.1.4 Sharp vorticity structures: Role in transport and mixing

The sharpness of shear velocity flow leads to K-H destabilization which is an important well known mechanism of mixing and transport in normal HD fluids. In i-GHD the K-H unstable structures are also coupled with TS waves emision which is shown to aid the process of mixing. This has been quantified by carrying out extensive study on the diffusion of passive tracer particles in the medium.

- **Interplay between TS waves and K-H instability**
  We considered various types of sharp rotating vorticity profiles. We observed that each interfaces acts as a source of two (inward and outward moving) wavefront of TS waves along with K-H instability. We find that the TS waves helps in efficient mixing of the fluids entrained inside the vortex structure with that outside in the stagnant medium.

  We also considered the evolution of a multi-circulation vortex structures. At intermediate time range, it provides a complete picture of a turbulent flow which is collection of small vortices and waves. When the system is left for a very long time, it is seen that the presence of TS waves leads to this turbulent state to relax towards a single vortex form much faster than hydrodynamic fluid. Furthermore, it was also confirmed that the relaxation rate of the turbulent medium increases with increasing η/τ_m a signature of the coupling strength.

- **Particle Tracing**
  The observations were quantified by considering the passive test particle simulation. The diffusion and clustering of these particles are directly related to the mixing characteristic of a medium. We considered particles with various values of inertia which dictates there response times. We evaluated the mean square displacement of these particles to find out the diffusivity of the system, which is comparatively higher in i-GHD than HD. We also showed that often these passive particles organize themselves in a spatially inhomogeneous distribution. Phenomena of clustering amongst these particles is clearly evident from the simulations.

6.1.5 Rayleigh-Taylor Instability

Kelvin-Helmholtz and the Rayleigh-Taylor instability are two very prominent fluid instability in a fluid system. While the K-H instability has been recently studied extensively for the GHD system, the R-T instability has not been studied so extensively. We have in this thesis studied the R-T instability and have also considered the dynamics of bubbles and droplets, structures lighter and heavier than the background medium, in the presence of gravity. Our observations about the R-T instability are summarized below:

- **R-T instability**
  We consider the two types of density inhomogeneity profiles, sharp density interface density profile, gradually increasing density profile in opposite direction of gravity force. We observed analytically as well numerically that the growth of R-T instability gets suppressed as one increases the value of η/τ_m which signifies the increase in the strong coupling behaviour. The other trends (e.g. dependence on Atwood's number and wave lenght etc.,) of R-T instability in visco-elastic fluids is similar as in hydrodynamic fluids.

- **Rising bubble and falling drop**
  We have also considered evolution of bubbles/droplets (structures with lower/higher

density than the background medium) in the presence of gravity. The rising/falling rate of bubble/droplet are seen to be significantly reduced as compared to the HD case with increasing η/τ_m. The combined system of bubble and droplet and their interaction has also been studied in extensive detail.

6.2 Future prospects

We provide below a list of studies which can be carried out as an extension to our work here and which would be instrumental for furthering our understanding of visco-elastic fluids.

- **Comparison with Molecular Dynamics (MD) simulations**
  We adopted the GHD model description for the study of the behaviour of strongly coupled dusty plasma medium. A comparison with MD simulations, wherein the dust particles are assumed to interact by the screened Yukawa potential, needs to be carried out

- **Extension to 3-D**
  We have concentrated here on 2-D studies only, where the vorticity is a scalar field. Also the 2-D does not have the vortex stretching term. (The term $\vec{\xi} \cdot \nabla \vec{v}_d$ represents the vortex stretching. In 2-D flow $\vec{\xi} \cdot \nabla \vec{v}_d$=0 i.e. there are no velocity gradients parallel to the vorticity vector.) An extension to 3-D case with vector vorticity fields along with the vortex stretching term would shed more light on the character of TS wave and its emission and interaction with the vorticity. This would be a realistic scenario under microgravity conditions where 2-D dust layers would not form.

- **Evolution of coherent structures in an inhomogeneous medium**
  It is well known that the dipoles propagate with uniform velocity in a HD fluid. In GHD they would slow down subsequently as a result of constant loss by the emission of TS waves. It would be interesting to study the propagation of dipolar structures in an inhomogeneous dusty plasma medium

- **Magnetized dusty plasma**
  In this thesis, we have focussed on the studies of strongly coupled unmag-

netized dusty plasma system depicted by the visco-elastic GHD fluid model. with the availability of strong magnetic fields in laboratory, it would be possible to do experiments wherein the dust species is magnetized. This will open up an entirely new regime of exploration for strongly coupled magnetized media. There is thus a need to develop the GHD model description for magnetized dusty plasmas and carry out simulations and comparison with MD and experimental studies.

These are thus some problems which can be immediately looked upon.

6.3 Final remarks

The simplicity with which the dusty plasma medium experiments can be carried out and diagnosed and the fact that it can be pushed easily in the strong coupling regime, the dusty plasma medium can prove to be an ideal system to explore matter in strong coupling regime. Furthermore, since each particles here can be visualized and the time evolution can also be easily tracked the emergence of macroscopic complexity through underlying simplicity of microscopic interactions can be easily tracked. Hence it is necessary that the properties of this medium be explored and modelled suitably by simplified description. The GHD fluid model is a step in that direction.

Bibliography

[1] C. K. Goertz. Dusty plasmas in the solar system. *Reviews of Geophysics*, 27(2):271–292, 1989.

[2] T. G. Northrop. Dusty plasmas. *Physica Scripta*, 45(5):475, 1992.

[3] J. H. Chu and Lin I. Direct observation of coulomb crystals and liquids in strongly coupled rf dusty plasmas. *Phys. Rev. Lett.*, 72:4009–4012, Jun 1994.

[4] M. H. Thoma, M. Kretschmer, H. Rothermel, H. M. Thomas, and G. E. Morfill. The plasma crystal. *American journal of physics*, 73(5):420–424, 2005.

[5] P. K. Shukla and A. A. Mamun. *Introduction to dusty plasma physics*. CRC Press, 2010.

[6] G. S. Selwyn, J. Singh, and R. S. Bennett. I n s i t u laser diagnostic studies of plasma-generated particulate contamination. *Journal of Vacuum Science and Technology A*, 7(4):2758–2765, 1989.

[7] G. S. Selwyn, J. S. McKillop, Kurt L. Haller, and J. J. Wu. I n s i t u plasma contamination measurements by hene laser light scattering: A case study. *Journal of Vacuum Science Technology A: Vacuum, Surfaces, and Films*, 8(3):1726–1731, May 1990.

[8] N. N. Rao, P. K. Shukla, and M. Y. Yu. Dust-acoustic waves in dusty plasmas. *Planetary and Space Science*, 38(4):543 – 546, 1990.

[9] F. Verheest. Nonlinear dust-acoustic waves in multispecies dusty plasmas. *Planetary and Space Science*, 40(1):1–6, 1992.

[10] N. D'Angelo. Coulomb solids and low-frequency fluctuations in rf dusty plasmas. *Journal of Physics D: Applied Physics*, 28(5):1009, 1995.

[11] A. Barkan, R. L. Merlino, and N. D'angelo. Laboratory observation of the dust-acoustic wave mode. *Physics of Plasmas*, 2(10):3563–3565, 1995.

[12] C. Thompson, A. Barkan, R. L. Merlino, and N. D'Angelo. Video imaging of dust acoustic waves. *IEEE transactions on plasma science*, 27(1):146–147, 1999.

[13] B. S. Xie and M. Y. Yu. Dust acoustic waves in strongly coupled dissipative plasmas. *Phys. Rev. E*, 62:8501–8507, Dec 2000.

[14] B. Eliasson and P. K. Shukla. Dust acoustic shock waves. *Phys. Rev. E*, 69:067401, Jun 2004.

[15] J. Heinrich, S. H. Kim, and R. L. Merlino. Laboratory observations of self-excited dust acoustic shocks. *Phys. Rev. Lett.*, 103:115002, Sep 2009.

[16] D. Samsonov, G. Morfill, H. Thomas, T. Hagl, H. Rothermel, V. Fortov, A. Lipaev, V. Molotkov, A. Nefedov, O. Petrov, A. Ivanov, and S. Krikalev. Kinetic measurements of shock wave propagation in a three-dimensional complex (dusty) plasma. *Phys. Rev. E*, 67:036404, Mar 2003.

[17] D. Samsonov, S. K. Zhdanov, R. A. Quinn, S. I. Popel, and G. E. Morfill. Shock melting of a two-dimensional complex (dusty) plasma. *Phys. Rev. Lett.*, 92:255004, Jun 2004.

[18] P. Bandyopadhyay, G. Prasad, A. Sen, and P. K. Kaw. Experimental study of nonlinear dust acoustic solitary waves in a dusty plasma. *Physical review letters*, 101(6):065006, 2008.

[19] P. K. Shukla and V. P. Silin. Dust ion-acoustic wave. *Physica Scripta*, 45(5):508, 1992.

[20] A. Barkan, N. D'Angelo, and R. L. Merlino. Experiments on ion-acoustic waves in dusty plasmas. *Planetary and Space Science*, 44(3):239–242, 1996.

[21] R. L. Merlino, A. Barkan, C. Thompson, and N. D'angelo. Laboratory studies of waves and instabilities in dusty plasmas. *Physics of Plasmas*, 5(5):1607–1614, 1998.

[22] Y. Nakamura, H. Bailung, and P. K. Shukla. Observation of ion-acoustic shocks in a dusty plasma. *Phys. Rev. Lett.*, 83:1602–1605, Aug 1999.

[23] Y. Nakamura. Experiments on ion-acoustic shock waves in a dusty plasma. *Physics of Plasmas*, 9(2):440–445, 2002.

[24] Y. Nakamura and A. Sarma. Observation of ion-acoustic solitary waves in a dusty plasma. *Physics of Plasmas*, 8(9):3921–3926, 2001.

[25] F. Melandso. Lattice waves in dust plasma crystals. *Physics of Plasmas*, 3(11):3890–3901, 1996.

[26] A. Homann, A. Melzer, S. Peters, R. Madani, and A. Piel. Laser-excited dust lattice waves in plasma crystals. *Physics Letters A*, 242(3):173–180, 1998.

[27] B. Farokhi, P. K. Shukla, N. L. Tsintsadze, and D. D. Tskhakaya. Linear and nonlinear dust lattice waves in plasma crystals. *Physics Letters A*, 264(4):318–323, 1999.

[28] H. Ikezi. Coulomb solid of small particles in plasmas. *Physics of Fluids*, 29(6), 1986.

[29] H. Thomas, G. E. Morfill, V. Demmel, J. Goree, B. Feuerbacher, and D. Möhlmann. Plasma crystal: Coulomb crystallization in a dusty plasma. *Phys. Rev. Lett.*, 73:652–655, Aug 1994.

[30] J. Frenkel. *Kinetic Theory Of Liquids*. Dover Publications, 1955.

[31] J. P. Boris, A. M. Landsberg, E. S. Oran, and J. H. Gardner. *LCPFCT A flux-corrected transport algorithm for solving generalized continuity equations*. Technical Report NRL Memorandum Report 93-7192, Naval Research Laboratory, 1993.

[32] G. Kalman and K. I. Golden. Response function and plasmon dispersion for strongly coupled coulomb liquids. *Phys. Rev. A*, 41:5516–5527, May 1990.

[33] K. I. Golden and G. J. Kalman. Erratum: Quasilocalized charge approximation in strongly coupled plasma physics [phys. plasmas 7, 14 (2000)]. *Physics of Plasmas*, 8(11), 2001.

[34] Z. Donkó, P. Hartmann, and G. J. Kalman. Molecular dynamics simulations of strongly coupled plasmas: Localization and microscopic dynamics. *Physics of Plasmas*, 10(5):1563–1568, 2003.

[35] M. Rosenberg and G. Kalman. Dust acoustic waves in strongly coupled dusty plasmas. *Phys. Rev. E*, 56:7166–7173, Dec 1997.

[36] M. Rosenberg, G. J. Kalman, P. Hartmann, and J. Goree. Effect of strong coupling on the dust acoustic instability. *Phys. Rev. E*, 89:013103, Jan 2014.

[37] G. Kalman, M. Rosenberg, and H. E. DeWitt. Collective modes in strongly correlated yukawa liquids: Waves in dusty plasmas. *Phys. Rev. Lett.*, 84:6030–6033, Jun 2000.

[38] H. Ohta and S. Hamaguchi. Wave dispersion relations in yukawa fluids. *Phys. Rev. Lett.*, 84:6026–6029, Jun 2000.

[39] G. J. Kalman, P. Hartmann, Z. Donkó, and M. Rosenberg. Two-dimensional yukawa liquids: Correlation and dynamics. *Phys. Rev. Lett.*, 92:065001, Feb 2004.

[40] Z. Donko, G. J. Kalman, and P. Hartmann. Dynamical correlations and collective excitations of yukawa liquids. *Journal of Physics: Condensed Matter*, 20(41):413101, 2008.

[41] T. Ott, D. A. Baiko, H. Kählert, and M. Bonitz. Wave spectra of a strongly coupled magnetized one-component plasma: Quasilocalized charge approximation versus harmonic lattice theory and molecular dynamics. *Phys. Rev. E*, 87:043102, Apr 2013.

[42] K. I. Golden, G. J. Kalman, Z. Donkó, and P. Hartmann. Acoustic dispersion in a two-dimensional dipole system. *Phys. Rev. B*, 78:045304, Jul 2008.

[43] K. I. Golden, G. J. Kalman, Z. Donkó, and P. Hartmann. Collective excitations in a two-dimensional dipole system. *Journal of Physics A: Mathematical and Theoretical*, 42(21):214017, 2009.

[44] K. I. Golden, G. J. Kalman, P. Hartmann, and Z. Donkó. Dynamics of two-dimensional dipole systems. *Phys. Rev. E*, 82:036402, Sep 2010.

[45] P. Hartmann, Z. Donkó, M. Rosenberg, and G. J. Kalman. Waves in two-dimensional superparamagnetic dusty plasma liquids. *Phys. Rev. E*, 89:043102, Apr 2014.

[46] S. Ichimaru. Strongly coupled plasmas: high-density classical plasmas and degenerate electron liquids. *Rev. Mod. Phys.*, 54:1017–1059, Oct 1982.

[47] M. S. Murillo. Static local field correction description of acoustic waves in strongly coupling dusty plasmas. *Physics of Plasmas*, 5(9):3116–3121, 1998.

[48] P. K. Kaw and A. Sen. Low frequency modes in strongly coupled dusty plasmas. *Physics of Plasmas*, 5(10):3552–3559, 1998.

[49] M. A. Berkovsky. Spectrum of low frequency modes in strongly coupled plasmas. *Physics Letters A*, 166(5):365–368, 1992.

[50] S. Ichimaru, H. Iyetomi, and S. Tanaka. Statistical physics of dense plasmas: Thermodynamics, transport coefficients and dynamic correlations. *Physics Reports*, 149(2-3):91–205, 1987.

[51] A. Diaw and M. S. Murillo. Generalized hydrodynamics model for strongly coupled plasmas. *Phys. Rev. E*, 92:013107, Jul 2015.

[52] H. Ohta and S. Hamaguchi. Molecular dynamics evaluation of self-diffusion in yukawa systems. *Physics of Plasmas*, 7(11):4506–4514, 2000.

[53] B. Liu and J. Goree. Superdiffusion in two-dimensional yukawa liquids. *Physical Review E*, 75(1):016405, 2007.

[54] O. S. Vaulina, X. G. Adamovich, O. F. Petrov, and V. E. Fortov. Evolution of the mass-transfer processes in nonideal dissipative systems ii: Experiments in dusty plasma. *Physical Review E*, 77(6):066404, 2008.

[55] Y. Feng, J. Goree, B. Liu, T. P. Intrator, and M. S. Murillo. Superdiffusion of two-dimensional yukawa liquids due to a perpendicular magnetic field. *Phys. Rev. E*, 90:013105, Jul 2014.

[56] Z. Donkó and B. Nyiri. Molecular dynamics calculation of the thermal conductivity and shear viscosity of the classical one-component plasma. *Physics of Plasmas*, 7(1):45, 2000.

[57] T. Saigo and S. Hamaguchi. Shear viscosity of strongly coupled yukawa systems. *Physics of Plasmas*, 9(4):1210–1216, 2002.

[58] V. Nosenko and J. Goree. Shear flows and shear viscosity in a two-dimensional yukawa system (dusty plasma). *Phys. Rev. Lett.*, 93:155004, Oct 2004.

[59] M. S. Murillo. Viscosity estimates of liquid metals and warm dense matter using the yukawa reference system. *High Energy Density Physics*, 4(1-2):49–57, 2008.

[60] Z. Donkó, J. Goree, and P. Hartmann. Viscoelastic response of yukawa liquids. *Phys. Rev. E*, 81:056404, May 2010.

[61] P. Hartmann, M. C. Sándor, A. Kovács, and Z. Donkó. Static and dynamic shear viscosity of a single-layer complex plasma. *Physical Review E*, 84(1):016404, 2011.

[62] A. Shahzad and M. He. Shear viscosity and diffusion motion of two-dimensional dusty plasma liquids. *Physica Scripta*, 86(1):015502, 2012.

[63] F. F. Munarin, K. Nelissen, W. P. Ferreira, G. A. Farias, and F. M. Peeters. Hysteresis and reentrant melting of a self-organized system of classical particles confined in a parabolic trap. *Phys. Rev. E*, 77:031608, Mar 2008.

[64] C. J. Olson Reichhardt, C. Reichhardt, and A. R. Bishop. Structural transitions, melting, and intermediate phases for stripe- and clump-forming systems. *Phys. Rev. E*, 82:041502, Oct 2010.

[65] A. Joy and R. Ganesh. Coherent vortices in strongly coupled liquids. *Phys. Rev. Lett.*, 106:135001, Mar 2011.

[66] K. Kadau, T. C. Germann, N. G. Hadjiconstantinou, P. S. Lomdahl, G. Dimonte, B. L. Holian, and B. J. Alder. Nanohydrodynamics simulations: An atomistic view of the rayleigh-taylor instability. *Proceedings of the National Academy of Sciences of the United States of America*, 101(16):5851–5855, 2004.

[67] A. Joy and R. Ganesh. Kelvin helmholtz instability in strongly coupled yukawa liquids. *Phys. Rev. Lett.*, 104:215003, May 2010.

[68] S. K. Tiwari, V. S. Dharodi, A. Das, P. K. Kaw, and A. Sen. Kelvin-helmholtz instability in dusty plasma medium: Fluid and particle approach. *Journal of Plasma Physics*, 80:817–823, 12 2014.

[69] D. Winske, M. S. Murillo, and M. Rosenberg. Numerical simulation of dust-acoustic waves. *Phys. Rev. E*, 59:2263–2272, Feb 1999.

[70] D. Winske, W. S. Daughton, D. S. Lemons, M. S. Murillo, and W. R. Shanahan. Dust wake in a collisional plasma. In Y. Nakamura, T. Yokota, and P. K. Shukla, editors, *Frontiers in Dusty Plasmas*, pages 513–516. Elsevier Science B. V., Amsterdam, 2000.

[71] W. L. Slattery, G. D. Doolen, and H. E. DeWitt. Improved equation of state for the classical one-component plasma. *Phys. Rev. A*, 21:2087–2095, Jun 1980.

[72] Y. Hayashi and K. Tachibana. Observation of coulomb-crystal formation from carbon particles grown in a methane plasma. *Japanese journal of applied physics*, 33(6A):L804, 1994.

[73] A. Melzer, T. Trottenberg, and A. Piel. Experimental determination of the charge on dust particles forming. *Physics Letters A*, 191(3-4):301–308, 1994.

[74] H. M. Thomas, G. E. Morfill, and E. Gregor. Melting dynamics of a plasma crystal. *Nature Publishing Group*, 379:806–809, Feb 1996.

[75] J. B. Pieper, J. Goree, and R. A. Quinn. Three-dimensional structure in a crystallized dusty plasma. *Physical Review E*, 54(5):5636, 1996.

[76] G. E. Morfill, H. M. Thomas, U. Konopka, and M. Zuzic. The plasma condensation: Liquid and crystalline plasmas. *Physics of Plasmas*, 6(5):1769–1780, 1999.

[77] P. K. Kaw. Collective modes in a strongly coupled dusty plasma. *Physics of Plasmas*, 8(5):1870–1878, 2001.

[78] J. Pramanik, G. Prasad, A. Sen, and P. K. Kaw. Experimental observations of transverse shear waves in strongly coupled dusty plasmas. *Phys. Rev. Lett.*, 88:175001, Apr 2002.

[79] S. K. Tiwari, V. S. Dharodi, A. Das, B. G. Patel, and P. K. Kaw. Evolution of sheared flow structure in visco-elastic fluids. *AIP Conference Proceedings*, 1582(1), 2014.

[80] S. K. Tiwari, A. Das, P. K. Kaw, and A. Sen. Longitudinal singular response of dusty plasma medium in weak and strong coupling limits. *Physics of Plasmas*, 19(1), 2012.

[81] S. K. Tiwari, A. Das, P. K. Kaw, and A. Sen. Observation of sharply peaked solitons in dusty plasma simulations. *New Journal of Physics*, 14(6):063008, 2012.

[82] S. K. Tiwari, A. Das, P. K. Kaw, and A. Sen. Kelvin-helmholtz instability in a weakly coupled dust fluid. *Physics of Plasmas*, 19(2), 2012.

[83] S. K. Tiwari, A. Das, D. Angom, B. G. Patel, and P. K. Kaw. Kelvin-helmholtz instability in a strongly coupled dusty plasma medium. *Physics of Plasmas*, 19(7), 2012.

[84] S. K. Tiwari, V. S. Dharodi, A. Das, B. G. Patel, and P. K. Kaw. Turbulence in strongly coupled dusty plasmas using generalized hydrodynamic description. *Physics of Plasmas*, 22(2):023710, 2015.

[85] M. S. Janaki, N. Chakrabarti, and D. Banerjee. Jeans instability in a viscoelastic fluid. *Physics of Plasmas*, 18(1), 2011.

[86] D. Banerjee, J. S. Mylavarapu, and N. Chakrabarti. Viscoelastic modes in a strongly coupled, cold, magnetized dusty plasma. *Physics of Plasmas*, 17(11), 2010.

[87] S. Ghosh, M. R. Gupta, N. Chakrabarti, and M. Chaudhuri. Nonlinear wave propagation in a strongly coupled collisional dusty plasma. *Phys. Rev. E*, 83:066406, Jun 2011.

[88] D. Banerjee, M. S. Janaki, N. Chakrabarti, and M. Chaudhuri. Viscosity gradient-driven instability of'shear mode'in a strongly coupled plasma. *New Journal of Physics*, 12(12):123031, 2010.

[89] M. S. Janaki and N. Chakrabarti. Shear wave vortex solution in a strongly coupled dusty plasma. *Physics of Plasmas*, 17(5), 2010.

[90] P. K. Shukla and A. A. Mamun. Dust-acoustic shocks in a strongly coupled dusty plasma. *Plasma Science, IEEE Transactions on*, 29(2):221–225, 2001.

[91] F. M. Peeters and X. Wu. Wigner crystal of a screened-coulomb-interaction colloidal system in two dimensions. *Physical Review A*, 35(7):3109, 1987.

[92] S. V. Vladimirov, P. V. Shevchenko, and N. F. Cramer. Vibrational modes in the dust-plasma crystal. *Physical Review E*, 56(1):R74, 1997.

[93] X. Wang, A. Bhattacharjee, and S. Hu. Longitudinal and transverse waves in yukawa crystals. *Physical review letters*, 86(12):2569, 2001.

[94] P. Schmidt, G. Zwicknagel, P.-G. Reinhard, and C. Toepffer. Longitudinal and transversal collective modes in strongly correlated plasmas. *Physical Review E*, 56(6):7310, 1997.

[95] S. Nunomura, D. Samsonov, and J. Goree. Transverse Waves in a Two-Dimensional Screened-Coulomb Crystal (Dusty Plasma). *Phys. Rev. Lett.*, 84:5141–5144, 2000.

[96] D. A. Law, W. H. Steel, B. M. Annaratone, and J. E. Allen. Probe-induced particle circulation in a plasma crystal. *Phys. Rev. Lett.*, 80:4189–4192, May 1998.

[97] G. E. Morfill, H. M. Thomas, U. Konopka, H. Rothermel, M. Zuzic, A. Ivlev, and J. Goree. Condensed plasmas under microgravity. *Phys. Rev. Lett.*, 83:1598–1601, Aug 1999.

[98] M. Klindworth, A. Melzer, A. Piel, and V. A. Schweigert. Laser-excited intershell rotation of finite coulomb clusters in a dusty plasma. *Phys. Rev. B*, 61:8404–8410, Mar 2000.

[99] P. K. Kaw, K. Nishikawa, and N. Sato. Rotation in collisional strongly coupled dusty plasmas in a magnetic field. *Physics of Plasmas*, 9(2):387–390, 2002.

[100] P. K. Shukla. Nonlinear waves and structures in dusty plasmas. *Physics of Plasmas*, 10(5):1619–1627, 2003.

[101] G. E. Morfill, M. Rubin-Zuzic, H. Rothermel, A. V. Ivlev, B. A. Klumov, H. M. Thomas, U. Konopka, and V. Steinberg. Highly resolved fluid flows: “liquid plasmas” at the kinetic level. *Phys. Rev. Lett.*, 92:175004, Apr 2004.

[102] Y. Saitou and O. Ishihara. Dynamic circulation in a complex plasma. *Phys. Rev. Lett.*, 111:185003, Nov 2013.

[103] U. Konopka, D. Samsonov, A. V. Ivlev, J. Goree, V. Steinberg, and G. E. Morfill. Rigid and differential plasma crystal rotation induced by magnetic fields. *Physical Review E*, 61(2):1890, 2000.

[104] M. Schwabe, U. Konopka, P. Bandyopadhyay, and G. E. Morfill. Pattern formation in a complex plasma in high magnetic fields. *Phys. Rev. Lett.*, 106:215004, May 2011.

[105] J. Vranješ, G. Marić, and P. K. Shukla. Tripolar vortices and vortex chains in dusty plasma. *Physics Letters A*, 258(4):317–322, 1999.

[106] M. L. Norman, L. Smarr, M. D. Smith, and J. R. Wilson. Hydrodynamic formation of twin-exhaust jets. *Astrophysical*, 247:52–58, 1981.

[107] W. D. Arnett, J. N. Bahcall, R. P. Kirshner, and S. E. Woosley. Supernova 1987a. *Annual Review of Astronomy and Astrophysics*, 27:629–700, 1989.

[108] J. C. Beale and R. D. Reitz. Modeling spray atomization with the kelvin-helmholtz/rayleigh-taylor hybrid model. *Atomization and sprays*, 9(6), 1999.

[109] S. C. Kong, P. K. Senecal, and R. D. Reitz. Developments in spray modeling in diesel and direct-injection gasoline engines. *Oil & Gas Science and Technology*, 54(2):197–204, 1999.

[110] M. Chertkov. Phenomenology of rayleigh-taylor turbulence. *Phys. Rev. Lett.*, 91:115001, Sep 2003.

[111] G. A. Hoshoudy. Quantum effects on the rayleigh-taylor instability of viscoelastic plasma model through a porous medium. *Journal of Modern Physics*, 2(10), 2011.

[112] B. Srinivasan and X.-Z. Tang. The mitigating effect of magnetic fields on rayleigh-taylor unstable inertial confinement fusion plasmas. *Physics of Plasmas*, 20(5), 2013.

[113] S. I. Abarzhi. Review of theoretical modelling approaches of rayleigh–taylor instabilities and turbulent mixing. *Philosophical Transactions of the Royal Society of London A: Mathematical, Physical and Engineering Sciences*, 368(1916):1809–1828, 2010.

[114] S. I. Abarzhi. Coherent structures and pattern formation in the rayleigh-taylor turbulent mixing. *Phys. Scr.*, 78(1), 2008.

[115] S. I. Abarzhi and R. Rosner. Comparative study of approaches for modeling rayleigh-taylor turbulent mixing. *Phys. Scr.*, T142:1, 2010.

[116] M. Zuzic, A. V. Ivlev, J. Goree, G. E. Morfill, H. M. Thomas, H. Rothermel, U. Konopka, R. Sütterlin, and D. D. Goldbeck. Three-dimensional strongly coupled plasma crystal under gravity conditions. *Phys. Rev. Lett.*, 85:4064–4067, Nov 2000.

[117] V. E. Fortov, O. S. Vaulina, O. F. Petrov, V. I. Molotkov, A. M. Lipaev, V. M. Torchinsky, H. M. Thomas, G. E. Morfill, S. A. Khrapak, Yu. P. Semenov, A. I. Ivanov, S. K. Krikalev, A. Yu. Kalery, S. V. Zaletin, and Yu. P. Gidzenko. Transport of microparticles in weakly ionized gas-discharge plasmas under microgravity conditions. *Phys. Rev. Lett.*, 90:245005, Jun 2003.

[118] M. Kretschmer, S. A. Khrapak, S. K. Zhdanov, H. M. Thomas, G. E. Morfill, V. E. Fortov, A. M. Lipaev, V. I. Molotkov, A. I. Ivanov, and M. V. Turin. Force field inside the void in complex plasmas under microgravity conditions. *Phys. Rev. E*, 71:056401, May 2005.

[119] J. Beckers, D. J. M. Trienekens, and G. M. W. Kroesen. Absolute measurement of the total ion-drag force on a single plasma-confined microparticle at the void edge under microgravity conditions. *Phys. Rev. E*, 88:055101, Nov 2013.

[120] N. D'Angelo. The rayleigh-taylor instability in dusty plasmas. *Planetary and space science*, 41(6):469–474, 1993.

[121] B. M. Veeresha, A. Das, and A. Sen. Rayleigh-taylor instability driven nonlinear vortices in dusty plasmas. *Physics of Plasmas*, 12(4), 2005.

[122] K. A. Pacha, J. R. Heinrich, S.-H. Kim, and R. L. Merlino. Observation of the taylor instability in a dusty plasma. *Physics of Plasmas*, 19(1), 2012.

[123] A. Das and P. Kaw. Suppression of rayleigh-taylor instability in strongly coupled plasmas. *Physics of Plasmas*, 21(6), 2014.

[124] K. Avinash and A. Sen. Rayleigh-taylor instability in dusty plasma experiment. *Physics of Plasmas*, 22(8):083707, 2015.

[125] N. d'Angelo and B. Song. The kelvin-helmholtz instability in dusty plasmas. *Planetary and Space Science*, 38(12):1577–1579, 1990.

[126] S. P. S. Rawat and N. N. Rao. Kelvin-helmholtz instability driven by sheared dust flow. *Planetary and space science*, 41(2):137–140, 1993.

[127] B. P. Pandey, S. V. Vladimirov, A. Samarian, et al. Shear driven instabilities in dusty plasmas. 2012.

[128] Q. Z. Luo, N. D'Angelo, and R. L. Merlino. The kelvin-helmholtz instability in a plasma with negatively charged dust. *Physics of Plasmas*, 8(1):31–35, 2001.

[129] S.-I. Han, S. Stapf, and B. Blümich. Nmr imaging of falling water drops. *Phys. Rev. Lett.*, 87:144501, Sep 2001.

[130] A. N. Dingle and H. F. Schulte Jr. A research instrument for the study of raindrop-size spectra. *Journal of Applied Meteorology*, 1(1):48–59, 1962.

[131] J. F. Davidson, D. Harrison, and J. R. F. G. D. Carvalho. On the liquidlike behavior of fluidized beds. *Annual Review of Fluid Mechanics*, 9(1):55–86, 1977.

[132] M. Schwabe, M. Rubin-Zuzic, S. Zhdanov, A. V. Ivlev, H. M. Thomas, and G. E. Morfill. Formation of bubbles, blobs, and surface cusps in complex plasmas. *Physical review letters*, 102(25):255005, 2009.

[133] M. Schwabe. *Dynamical effects in fluid complex plasmas*. PhD thesis, lmu, 2009.

[134] H.-Y. Chu, Y.-K. Chiu, C.-L. Chan, and Lin I. Observation of laser-pulse-induced traveling microbubbles in dusty plasma liquids. *Phys. Rev. Lett.*, 90:075004, Feb 2003.

[135] S. Douady, Y. Couder, and M. E. Brachet. Direct observation of the intermittency of intense vorticity filaments in turbulence. *Physical Review Letters*, 67(8):983, 1991.

[136] J. R. Fessler, J. D. Kulick, and J. K. Eaton. Preferential concentration of heavy particles in a turbulent channel flow. *Physics of Fluids*, 6(11):3742–3749, 1994.

[137] E. Balkovsky, G. Falkovich, and A. Fouxon. Clustering of inertial particles in turbulent flows. *arXiv preprint chao-dyn/9912027*, 1999.

[138] E. Balkovsky, G. Falkovich, and A. Fouxon. Intermittent distribution of inertial particles in turbulent flows. *Physical Review Letters*, 86(13):2790, 2001.

[139] G. Falkovich and A. Pumir. Intermittent distribution of heavy particles in a turbulent flow. *Physics of Fluids*, 16(7):L47–L50, 2004.

[140] L. I. Zaichik, O. Simonin, and V. M. Alipchenkov. Two statistical models for predicting collision rates of inertial particles in homogeneous isotropic turbulence. *Physics of Fluids*, 15(10):2995–3005, 2003.

[141] R. J. Hill. Scaling of acceleration in locally isotropic turbulence. *Journal of Fluid Mechanics*, 452:361–370, 2002.

[142] J. Bec, L. Biferale, G. Boffetta, A. Celani, M. Cencini, A. Lanotte, S. Musacchio, and F. Toschi. Acceleration statistics of heavy particles in turbulence. *Journal of Fluid Mechanics*, 550(1):349–358, 2006.

[143] V. Yakhot and K. R. Sreenivasan. Towards a dynamical theory of multifractals in turbulence. *Physica A: Statistical Mechanics and its Applications*, 343:147–155, 2004.

[144] K. D. Squires and J. K. Eaton. Preferential concentration of particles by turbulence. *Physics of Fluids A: Fluid Dynamics*, 3(5):1169–1178, 1991.

[145] M. Boivin, O. Simonin, and K. D. Squires. Direct numerical simulation of turbulence modulation by particles in isotropic turbulence. *Journal of Fluid Mechanics*, 375:235–263, 1998.

[146] W. C. Reade and L. R. Collins. A numerical study of the particle size distribution of an aerosol undergoing turbulent coagulation. *Journal of Fluid Mechanics*, 415:45–64, 2000.

[147] Y. Zhou, A. S. Wexler, and L.-P. Wang. Modelling turbulent collision of bidisperse inertial particles. *Journal of Fluid Mechanics*, 433:77–104, 2001.

[148] J. Chun, D. L. Koch, S. L. Rani, A. Ahluwalia, and L. R Collins. Clustering of aerosol particles in isotropic turbulence. *Journal of Fluid Mechanics*, 536:219–251, 2005.

[149] L. R. Collins and A. Keswani. Reynolds number scaling of particle clustering in turbulent aerosols. *New Journal of Physics*, 6(1):119, 2004.

[150] L. Biferale, G. Boffetta, A. Celani, A. Lanotte, and F. Toschi. Particle trapping in three-dimensional fully developed turbulence. *Physics of Fluids*, 17(2):021701, 2005.

[151] L. Biferale, G. Boffetta, A. Celani, B. J. Devenish, A. Lanotte, and F. Toschi. Multifractal statistics of lagrangian velocity and acceleration in turbulence. *Physical review letters*, 93(6):064502, 2004.

[152] P. K. Yeung. Lagrangian characteristics of turbulence and scalar transport in direct numerical simulations. *Journal of Fluid Mechanics*, 427:241–274, 2001.

[153] P. K. Yeung. Lagrangian investigations of turbulence. *Annual review of fluid mechanics*, 34(1):115–142, 2002.

[154] T. Ishihara and Y. Kaneda. Relative diffusion of a pair of fluid particles in the inertial subrange of turbulence. *Physics of Fluids*, 14(11):L69–L72, 2002.

[155] M. Cencini, J. Bec, L. Biferale, G. Boffetta, A. Celani, A. S. Lanotte, S. Musacchio, and F. Toschi. Dynamics and statistics of heavy particles in turbulent flows. *Journal of Turbulence*, (7):N36, 2006.

[156] A. La Porta, G. A. Voth, A. M. Crawford, J. Alexander, and E. Bodenschatz. Fluid particle accelerations in fully developed turbulence. *Nature*, 409(6823):1017–1019, 2001.

[157] G. A. Voth, A. la Porta, A. M. Crawford, J. Alexander, and E. Bodenschatz. Measurement of particle accelerations in fully developed turbulence. *Journal of Fluid Mechanics*, 469:121–160, 2002.

[158] S. Ott and J. Mann. An experimental investigation of the relative diffusion of particle pairs in three-dimensional turbulent flow. *Journal of Fluid Mechanics*, 422:207–223, 2000.

[159] N. Mordant, P. Metz, O. Michel, and J.-F. Pinton. Measurement of lagrangian velocity in fully developed turbulence. *Physical Review Letters*, 87(21):214501, 2001.

[160] B. L. Sawford, P. K. Yeung, M. S. Borgas, P. Vedula, A. La Porta, A. M. Crawford, and E. Bodenschatz. Conditional and unconditional acceleration statistics in turbulence. *Physics of Fluids*, 15(11):3478–3489, 2003.

[161] T. G. Mason, K. Ganesan, J. H. van Zanten, D. Wirtz, and S. C. Kuo. Particle tracking microrheology of complex fluids. *Physical Review Letters*, 79(17):3282, 1997.

[162] T. A. Waigh. Microrheology of complex fluids. *Reports on Progress in Physics*, 68(3):685, 2005.

[163] M. Schwabe, S. Zhdanov, C. Räth, D. B. Graves, H. M. Thomas, and G. E. Morfill. Collective effects in vortex movements in complex plasmas. *Phys. Rev. Lett.*, 112:115002, Mar 2014.

[164] P. Meunier, U. Ehrenstein, T. Leweke, and M. Rossi. A merging criterion for two-dimensional co-rotating vortices. *Physics of Fluids*, 14(8):2757–2766, 2002.

[165] P. Meunier, S. Le Dizes, and T. Leweke. Physics of vortex merging. *Comptes Rendus Physique*, 6(4):431–450, 2005.

[166] Ch. Josserand and M. Rossi. The merging of two co-rotating vortices: a numerical study. *European Journal of Mechanics - B/Fluids*, 26(6):779 – 794, 2007.

[167] G. Falkovich, K. Gawędzki, and M. Vergassola. Particles and fields in fluid turbulence. *Rev. Mod. Phys.*, 73:913–975, Nov 2001.

[168] V. S. Dharodi, S. K. Tiwari, and A. Das. Visco-elastic fluid simulations of coherent structures in strongly coupled dusty plasma medium. *Physics of Plasmas*, 21(7), 2014.